REPORT 1238

INVESTIGATIONS AT SUPERSONIC SPEEDS OF 22 TRIANGULAR WINGS REPRESENTING TWO AIRFOIL SECTIONS FOR EACH OF 11 APEX ANGLES [1]

By Eugene S. Love

SUMMARY

Investigations of two series of 11 triangular wings were conducted at Mach numbers of 1.62, 1.92, and 2.40 to determine the effect of leading-edge shape and to compare actual test values with the nonviscous linear theory. The two series of wings had identical plan forms, a constant thickness ratio of 8 percent, a constant maximum-thickness point at 18 percent chord, and a range of apex half-angles from 10° to 45°. The first series had an elliptical leading edge and the second series, a wedge leading edge. Measurements were made of lift, drag, pitching moment, and pressure distribution, the latter being confined to three wings at one Mach number.

The results indicated that the ratio of the lift-curve slope to the theoretical two-dimensional lift-curve slope was, for any given ratio of the tangent of the wing vertex half-angle to the tangent of the Mach angle, relatively independent of Mach number for each series; and in the case of the wedge-leading-edge wings for which the leading edge lies well ahead of the Mach cone, this ratio approached very near 1. For the range of vertex angles in the vicinity of the Mach cone, the theoretical drag was in poor agreement with the test values, the test values being much lower. Except for cases with the Mach cone well behind the leading edge, the elliptical-leading-edge configuration gave lower minimum drag. Any leading-edge suction achieved by the elliptical-leading-edge wings was evidently of such magnitude as to be overshadowed by other effects. The largest value of maximum lift-drag ratio was obtained by the elliptical-leading-edge configuration. Both series of wings showed a forward travel of the center of pressure with increase in aspect ratio. Schlieren photographs, liquid-film tests, and pressure distributions indicated that the shocks arising on the wing surfaces, the boundary-layer transition lines, and the steep adverse pressure gradients were practically coincident.

It was concluded that, for triangular wings of this thickness ratio, the aerodynamic gains experienced by the elliptical-leading-edge wings as compared with the wedge-leading-edge wings were not a result of any appreciable realization of leading-edge suction but of the favorable effect of the gentle or easy curvature of the ridge line common to the elliptical-leading-edge shape.

INTRODUCTION

The wing of triangular plan form has received much attention as a possible efficient wing for supersonic flight. Reference 1 pointed out that L/D ratios of configurations employing sweepback as outlined in reference 2 could be improved upon, provided that the wing lay well within the Mach cone. Later, the theory of small disturbances was applied to the case of finite aspect ratios (refs. 3 and 4) and a theory was developed for computing the L/D ratios for practical configurations. More recently, several different authors have developed methods independently for calculating the lift and drag of triangular and sweptback wings (refs. 5 to 9).

An experimental investigation of triangular wings was undertaken in 1945 in the Langley model supersonic tunnel, forerunner of the present Langley 9-inch supersonic tunnel (ref. 10). These tests were primarily a preliminary investigation of flat-plate triangular wings (thickness ratio, approximately 1½ percent) to determine the limits of Jones' slender-wing theory and to ascertain the highest values of maximum L/D. In the range of low aspect ratios the results confirmed Jones' original theory but the experimental curves exhibited some unusual breaks when the leading edge lay near the Mach cone. In addition, the tests showed that the center of area of the wing and the center of pressure were coincident. Although the absolute values of the drag were in doubt, as stated by the authors, a maximum L/D of about 7 was obtained.

In order to further the study of triangular-wing characteristics at supersonic speeds, a series of tests was conducted on three triangular-wing models at a Mach number of 1.53 in the Ames 1- by 3-foot supersonic tunnel (ref. 11). The models had a thickness ratio of 5 percent and an aspect ratio of 2, and they were designed to study the effects of variation in thickness distribution and camber when the wing apex was both leading and trailing. These tests indicated that, for the apex-forward condition, the highest value of maximum L/D is obtained with the maximum-thickness point well forward and a slightly rounded leading edge. With the maximum-thickness point at 20 percent, maximum L/D was increased from 6.4 for the sharp leading edge to 6.8 for the rounded leading edge, indicating the possible existence of leading-edge suction predicted by theory. The drag relief obtained by rounding the leading edge fell short of that predicted from theoretical considerations.

The present tests were made to determine the effects of giving a generous curvature to the leading edge of a series of triangular wings with the object of realizing a greater pro-

[1] Supersedes recently declassified NACA RM L9D07, 1949.

portion of theoretical leading-edge suction and thereby increasing the wing efficiency. These tests extend the investigations initiated in reference 10 to wings of higher thickness ratio. Two series of 11 triangular wings each were tested in the Langley 9-inch supersonic tunnel at Mach numbers of 1.62, 1.92, and 2.40. Except for leading-edge shape, the first and second series were identical. The thickness ratio of 8 percent was constant for all these wings, as was the maximum-thickness point at 18 percent chord. The apex half-angles ranged from 10° to 45°, covering the range of conditions for the leading edge ahead of and behind the Mach cone for all test Mach numbers. A third series of eight thin flat-plate wings was tested at a Mach number of 1.92.

SYMBOLS

A	aspect ratio, b^2/S
α	free-stream angle of attack
b	wing span
$\beta=\sqrt{M^2-1}$	
c	chord
c_r	wing root chord
$\bar{c}$	mean aerodynamic chord, two-thirds root chord
C_L	lift coefficient, L/qS
C_D	drag coefficient, D/qS
ΔC_D	rise in drag coefficient above minimum, $C_D-C_{D_{min}}$
C_m	pitching-moment coefficient, $\frac{\text{Moment about center of area}}{qSc_r}$
D	drag
E	elliptic integral of second kind for $\sqrt{1-w^2}$
ϵ	wing vertex half-angle
L	lift
μ	Mach angle, $\sin^{-1}\frac{1}{M}$
M	Mach number
P	pressure coefficient
q	dynamic pressure, $\frac{1}{2}\rho V^2$
ρ	stream density
R	Reynolds number based on $\bar{c}$
S	wing area
t	maximum wing thickness
V	free-stream velocity
$w=\frac{\tan\epsilon}{\tan\mu}$	
x	location of maximum thickness in percent chord
y	maximum thickness in percent chord

APPARATUS AND TESTS

WIND TUNNEL AND MODEL SUPPORT

The Langley 9-inch supersonic tunnel is a closed-return, direct-drive tunnel in which the pressure and humidity of the enclosed air may be controlled. Throughout the tests the quantity of water vapor in the tunnel air was kept at sufficiently low values to insure negligible effects of condensation in the supersonic nozzle. The test Mach number is varied by means of interchangeable nozzle blocks forming test sections approximately 9 inches square. A schlieren optical system provides qualitative visual-flow observations. Eleven fine-mesh, turbulence-damping screens are installed in the settling chamber ahead of the nozzles.

The models were mounted from the rear on very slender, tapered stings that passed through the sting windshield with small clearance and were attached to the scales by insertion in the model sting support. (See fig. 1.) It should be noted that the forward edges of the sting windshield lay behind the sting shoulders and thus tended to avoid any impact pressures. The scales are self-balancing beam scales and measure three components, in a horizontal plane, of the total forces on the model and support system.

DESCRIPTION OF MODELS

The geometric characteristics of the model wings are given in figures 2 and 3 and in table I. Photographs of the elliptical- and wedge-leading-edge wings are shown in figure 4. These wings were constructed of highly polished, hard steel and with elliptical leading edges. The wedge-leading-edge wings were obtained from the elliptical-leading-edge wings by grinding to a wedge the region in front of the line of maximum thickness. This grinding caused no appreciable change in thickness ratio, location of maximum thickness, or vertex angle. Mirrors approximately 1/16 inch square were mounted flush in the stings just ahead of the shoulder as a part of the optical angle-of-attack system. (See fig. 1.)

TEST METHODS

Measurements of lift, drag, and pitching moment were made through an angle-of-attack range of approximately ±6°. With the optical system for indicating angle of attack, the indicated angle may be taken as the true value since the load deflection of the wings ahead of the mirror was found to be negligible. Corrections due to the support deflection have been applied to the moment results in calculation of the moment due to drag.

In an effort to obtain the order of magnitude of the tare forces on the sting, force measurements were made of the sting alone at the three Mach numbers. The wedge-shaped gap normally occupied by the wing was filled with metal flush with the sting surfaces. The lift and moment of the sting alone were very small, and any effects of the sting on test results are assumed to be negligible. The drag of the sting alone showed only a very small variation with angle of attack. For the elliptical- or wedge-leading-edge wing having least minimum drag, the drag of the sting alone is approximately 10 percent of the minimum drag. In the wing tests, part of the sting as tested alone is no longer exposed to the airstream and the remainder of the sting is partially immersed in the boundary layer of the wing. For this reason, the contribution of the sting to the total minimum drag is somewhat less than the 10-percent value. For the wings having much larger minimum drag, the contribution of the sting may approach values less than 1 percent. With this in mind, the drag results may be compared quantitatively with theory, although no correction for sting drag has been applied.

There was some doubt as to whether the pressures on either side of the sting within the sting windshield would remain the same if the lips of the windshield were not exactly centered with respect to the sting shoulders. Pressure

measurements showed that, provided the lips of the windshield lay behind the sting shoulders, any offcenter condition produced no differential in pressure between the sides of the sting and therefore contributed no error to lift-scale measurements. A correction was applied to the drag to account for the difference between the free-stream pressure and the pressure in the box enclosing the sting shield and balance.

The estimated probable errors in the aerodynamic quantities for Mach numbers of 1.62, 1.92, and 2.40 are given in the following table:

C_L	±0.0004
C_D	±0.0004
C_m	±0.0018
M	±0.01
α, deg	
Initial	±0.08
Relative	±0.01
R	±20,000

The value of ±0.08° given for angle of attack is a result of error in the initial referencing of each wing with respect to stream direction. The value of ±0.01° is the error that might be incurred in relative-angle-of-attack readings for a given test.

The test values of the Reynolds numbers based on $\bar{c}$ (two-thirds of the root chord) are given in the following table:

Wing	Reynolds number for—		
	M=1.62	M=1.92	M=2.40
1	1.39×10⁶	1.25×10⁶	1.00×10⁶
2	1.39	1.25	1.00
3	1.38	1.23	.99
4	1.20	1.08	.86
5	1.08	.96	.77
6	1.00	.90	.72
7	.94	.84	.67
8	.86	.77	.62
9	.78	.70	.56
10	.74	.66	.53
11	.64	.57	.46

In the course of the present tests, a liquid-film method for observation of boundary-layer transition, similar to that developed in reference 12 and at the Ames Aeronautical Laboratory (ref. 11), was used to supplement the schlieren photographs and pressure distributions. Briefly, the liquid-film method depends upon the fact that the greater shear intensity of turbulent boundary layers vaporizes a film of liquid much more rapidly than the comparatively low shear intensity of laminar regions. The ratio of time for drying of the laminar areas to that of the turbulent areas is approximately 5 to 1 at low Reynolds numbers and is greater at high Reynolds numbers; however, it is quite possible for laminar regions very near the leading edge of an airfoil, where the boundary layer is very thin, to show the same drying rates as turbulent areas because of the initial intensity of the shear at the surface. In any case, the shear intensity and the resulting rate of energy dissipation in the particular region will determine whether the region remains wet or dry and conclusions reached from liquid-film methods are made on this basis. The models were given a mat black finish before applying the liquid-film solution. Upon completion of a run, the models were dusted with powder. Accordingly, the wet regions appear white in the photographs and the dry regions remain black.

All schlieren photographs were taken with the knife edge horizontal. At the time the tests of the elliptical-leading-edge series were conducted, the spark system normally used for the schlieren apparatus was inoperative and a manual shutter was substituted. This explains the poor resolution of unsteady flows evident on the schlieren photographs of these wings, for which the exposure time of 1/100 second was quite large in comparison with the several microseconds for the spark exposures.

RESULTS AND DISCUSSION

The variations of lift, drag, pitching moment, and lift-drag ratio for an angle-of-attack range of approximately −6° to 6° are given for all wings of both the elliptical-leading-edge and wedge-leading-edge series. These characteristics at Mach numbers of 1.62, 1.92, and 2.40 may be seen in figures 5, 6, and 7, respectively, and are summarized in table II. Similarly, the characteristics of eight flat-plate wings, with round and beveled leading edges, tested at a Mach number of 1.92, are presented in figure 8 and are summarized in table III.

LIFT

For the individual wings, the lift generally varies linearly with angle of attack. For this reason, the lift results can be discussed and compared with theory on the basis of lift-curve slope. It has been shown in references 4, 5, and 6 that $\tan \epsilon/\tan \mu$ is a basic parameter in sweptback-wing or triangular-wing theory. Values of $\tan \epsilon/\tan \mu$ greater than 1 represent a wing whose leading edge is ahead of the Mach cone, the converse being true for values of $\tan \epsilon/\tan \mu$ less than 1. References 5, 6, and 8 have pointed out that for triangular wings with leading edges ahead of the Mach cone the lift-curve slope has Ackeret's theoretical two-dimensional value of

$$\left(\frac{dC_L}{d\alpha}\right)_\infty=\frac{4}{\sqrt{M^2-1}} \tag{1}$$

and that for triangular wings with leading edges behind the Mach cone this value becomes

$$\frac{dC_L}{d\alpha}=\frac{2\pi\dfrac{\tan \epsilon}{\tan \mu}}{E\sqrt{M^2-1}} \tag{2}$$

In figure 9 the ratio of the lift-curve slope to the theoretical two-dimensional slope given by equation (1) is plotted against the parameter $\tan \epsilon/\tan \mu$. The ratio of the measured lift-curve slope to the two-dimensional value is, for any given relation of Mach line and leading edge, relatively independent of Mach number, being more so for the wedge- than for the elliptical-leading-edge series. In the lower range of values of $\tan \epsilon/\tan \mu$, 0 to 0.5, the elliptical- and wedge-leading-edge series give approximately the same values of lift-curve-slope ratios, though the values are somewhat higher than those predicted by the linear theory. At values of $\tan \epsilon/\tan \mu$ between 0.5 and 0.6, the curves of both series cross the theoretical curve and give values considerably lower than

the theoretical value in the vicinity of $\frac{\tan \epsilon}{\tan \mu}=1$. As the leading edge becomes coincident with and moves well ahead of the Mach cone, the lift-curve slopes exhibit a tendency to increase. This effect is much more marked for the wedge-leading-edge series and indicates a more rapid lift recovery, due to a more rapid approach to attachment of the shock wave to the wedge leading edge. At a value of $\tan \epsilon/\tan \mu$ of 2.19, the lift-curve slope of the wedge-leading-edge series attains 98 percent of the two-dimensional value. It was noted that the curves of the present tests showed none of the marked breaks in the vicinity of $\frac{\tan \epsilon}{\tan \mu}=1$ that were obtained in the tests of reference 10 on a series of thin, flat-plate triangular wings; and to ascertain whether the thicker nature of the present wing series might possibly have eliminated such breaks, eight flat-plate wings of thickness comparable to those tested in reference 10 were tested at a Mach number of 1.92. Figure 9 shows that no breaks or abrupt changes in lift-curve slopes were obtained from these wings. However, in contrast to the results for the thicker triangular wings, at values of $\tan \epsilon/\tan \mu$ less than 1 the thin wings gave slightly higher lift-curve slopes for the sharp-leading-edge configuration than for the round-leading-edge configuration. Figure 10 is a compilation of several existing results of tests on triangular wings. The faired curves of the present tests are included for comparison. Except for the present tests and the tests of reference 10, the wings were subject to effects of the body on which they were mounted.

DRAG

The minimum drag coefficients for the 8-percent-thick triangular-wing series are presented in figure 11 for the three Mach numbers and compared with the theoretical pressure drag as predicted from linear theory. The pressure drag of the triangular wings of double-wedge section was computed by the method of reference 7 for the three positions of the Mach line, namely, ahead of, between, and behind leading edge and ridge line. The equations used are included in appendix A. Below a value of $\tan \epsilon/\tan \mu$ of approximately 1.6, the elliptical leading edge produces the lower minimum drag. Above this value the converse is true. This effect might be expected in view of the lessening of the adverse pressure gradient behind the ridge line predicted by theory for high values of $\tan \epsilon/\tan \mu$. A similar effect was noted in the lift results (fig. 9) in that the lift-curve slopes of the wedge-leading-edge wings became greater than those of the elliptical-leading-edge wings beyond a value of $\tan \epsilon/\tan \mu$ of approximately 1.6. The unusually low values of minimum drag of wing 7 at all Mach numbers were due to the fact that the thickness of this model was only 97 percent of the specified amount. The curves have been faired through a point corrected for this thickness error. It should be noted that, for wings of this thickness ratio in this range of Reynolds numbers, the linear theory is in poor agreement with the test results. As can be seen by adding a reasonable skin-friction-drag increment to the linear-theory values, the best correlation of actual test values and theory occurs at values of $\tan \epsilon/\tan \mu$ less than 0.7. In any case, it is very doubtful that actual test results will achieve the characteristic peaks indicated by the linear theory as the Mach line successively passes over the ridge line and behind the leading edge; rather, a much smoother curve appears to be the physical result.

DRAG-RISE FACTOR

Reference 4 shows the theoretical value of the drag-rise factor $\Delta C_D/C_L^2$ for triangular wings having a subsonic leading edge (velocity component normal to leading edge is subsonic) and realizing leading-edge suction as

$$\frac{\Delta C_D}{C_L^2}=\frac{1}{\frac{dC_L}{d\alpha}}-\frac{\beta\sqrt{1-w^2}}{4\pi w} \tag{3}$$

where α is in radians.

The last term of this equation accounts for the forward inclination of the resultant force on the wing due to the presence of leading-edge suction. For the case of the triangular wing with supersonic leading edge, this term will vanish and the drag-rise factor becomes merely the reciprocal of the lift-curve slope. The difference between the reciprocal of the lift-curve slope and the value $\Delta C_D/C_L^2$ represents the increment of drag rise due to leading-edge suction. The drag-rise factors for the triangular-wing series are presented in figure 12 for the three Mach numbers and are compared with theory. Experimental values of $\Delta C_D/C_L^2$ were obtained from the parabola which appeared to fit best the variation of ΔC_D with C_L. The test results given by the reciprocal of the individual lift-curve slopes are compared with the experimental values of $\Delta C_D/C_L^2$. For all Mach numbers the experimental $\Delta C_D/C_L^2$ curves were higher than the theory with leading-edge suction; they were lower than, but exhibited the same general trend as, the curves of the reciprocal lift-curve slopes. As previously stated, the difference between the experimental $\Delta C_D/C_L^2$ values and the reciprocal of the lift-curve slopes indicates, according to equation (3), leading edge suction. On this basis, but contrary to expectations, the greater suction is realized by the wedge-leading-edge wings. The extensive change in leading-edge shape probably introduced phenomena other than leading-edge suction and had such a large effect as to mask the effects of the suction. The method of indicating leading-edge suction based on equation (3) is apparently inadequate for the wings tested. Although leading-edge suction would not be expected for thin, uncambered wings of sharp leading edge, it is possible that the wedge-leading-edge wings may realize some leading-edge-suction because of the well-forward location of the maximum-thickness point, the large absolute thickness of the wings, and the resulting large included angle of the wedge leading edge.

The experimental $\Delta C_D/C_L^2$ curves for the wedge-leading-edge wings give a lower value of drag rise, which departs from the elliptical-leading-edge values very noticeably as the Mach cone is swept behind the leading edge. Such an effect might possibly be expected from theoretical drag considerations as the elliptical leading edge creates a stronger bow wave or unattached shock. At Mach numbers of 1.92 and 2.40 the experimental curves of $\Delta C_D/C_L^2$ for the wedge-leading-edge wings show less drag rise at high values

of tan ϵ/tan μ, roughly 1.4 and higher, than that predicted by theory. However, the fact that the theoretical curve assumes no change in the basic form drag and friction drag with angle of attack and does not include viscous effects must, of course, be considered in making any comparison with theory.

LIFT-DRAG RATIO

The maximum values of lift-drag ratio $(L/D)_{max}$ are presented in figure 13 for the three Mach numbers and compared with the linear theory for sharp-leading-edge wings with and without the effect of leading-edge suction. The theoretical $(L/D)_{max}$ for uncambered wings is

$$(L/D)_{max}=\frac{1}{2}\sqrt{\frac{1}{C_{D_{min}}\frac{\Delta C_D}{C_L^2}}} \tag{4}$$

In the theoretical calculations it was assumed that turbulent flow existed over the greater portion of the wing behind the ridge line. Accordingly, a friction-drag coefficient based on turbulent flow and a mean value of the test Reynolds numbers was assumed to be 0.0093. This value was added to the previously calculated pressure-drag values in determining the theoretical $(L/D)_{max}$. No points are indicated on the test curves as it was often necessary to extrapolate the L/D curves of the individual wings to obtain the value of $(L/D)_{max}$ because of the low angle-of-attack range of the tests. The extrapolated values are given in table II. As expected, the highest values of $(L/D)_{max}$ were obtained at low values of tan ϵ/tan μ, the region of low values of minimum drag. In the vicinity of $\frac{\tan\epsilon}{\tan\mu}=1$, the test values are greater than the theoretical because of the abnormally large drag values predicted by theory. At the higher values of tan ϵ/tan μ, the test results are less than the theoretical primarily because the experimental lift-curve slopes are less than the theoretical and the experimental drag is greater than the theoretical. The higher $(L/D)_{max}$ of the elliptical-leading-edge wings at low values of tan ϵ/tan μ may be traced to the smaller minimum drag of these wings rather than to any large realization of leading-edge-suction force. In general, the linear theory gives a fair approximation of maximum L/D for wings of this thickness ratio. It is interesting to note that values of $(L/D)_{max}$ as high as 8.10 were obtained for the thin-plate wings (see table III) as compared with a value of 5.8 for the thick-wing series.

CENTER OF PRESSURE AND PITCHING MOMENT

Pitching-moment-curve slopes $\frac{dC_m}{d\alpha}$ at zero lift are presented in figure 14 as a function of tan ϵ/tan μ and show that the center of area is a good approximation of the center of pressure. Figure 15 gives the actual center-of-pressure location. For both the elliptical- and wedge-leading-edge series, the center of pressure shifts forward with increase in tan ϵ/tan μ, the overall travel being approximately 10 percent. The location of the center of pressure appears relatively independent of Mach number for the wings of a given leading-edge shape. However, the center of pressure of the elliptical-leading-edge wings lies 3 to 4 percent ahead of its location for the wedge-leading-edge wings, probably as a result of the difference in profile and associated differences in shock locations.

LIQUID-FILM AND SCHLIEREN PHOTOGRAPHS

Schlieren photographs were taken of wings 1, 5, and 11. (See figs. 16 to 19.) Wing 1 represents the highly sweptback wing near the center of the Mach cone; wing 5, the condition of the leading edge near the Mach cone; and wing 11, the condition of supersonic leading edge for all test Mach numbers.

In figure 16 (a) plan-form schlieren photographs of wedge-leading-edge wing 1 are shown for 0° and 4° angle of attack at a Mach number of 1.62. The corresponding liquid-film patterns are shown in figure 20 (c), the upper surface being shown for the 4° angle-of-attack condition. In the schlieren photographs a distinct trailing vortex may be seen leaving the trailing edge near the tips at zero angle of attack. At an angle of attack of 4° the vortices are much more intense and exhibit a tendency to form two distinct line vortices from either tip. The liquid-film photographs show similar patterns on the wing surface. The dry regions obviously are due to the large shear intensity through momentum transfer along the lines of vorticity. It appears that the outer line of vorticity approaches coincidence with the position just behind the ridge line where the adverse pressure gradient is steepest. The attendant thickening of the boundary layer favors transition, and it has been shown in the past in numerous high-speed boundary-layer investigations that the transition point coincides rather accurately with the beginning of the steep pressure rise. It is believed that the inboard lines of vorticity are the result of an overlapping effect or rolling up of the shed vortices along the transition line, directly associated with the high sweep of the transition line and leading edge. The outer lines of vorticity are probably due in part to a realization of the Kutta-Joukowski condition, which calls for strong parallel vortices extending downstream from the point of maximum width of the airfoil. With sufficient drying time allowed, the entire area enclosed by the vorticity lines in the liquid-film tests became dry, indicating a completely turbulent region in this area. However, in order to associate the phenomenon better with that shown by the schlieren photographs, the drying time was shortened for the figures presented herein. No separation is apparent from the profile schlieren photographs of figure 17, but this does not preclude the possibility of local separation near the leading edge or ridge line.

The plan-form schlieren photographs of wings 5 and 11 show a somewhat different phenomenon than that exhibited by wing 1. (See figs. 16 (b) and 16 (c).) Similar photographs of wing 5 at a Mach number of 1.92 are shown in figure 18. At zero angle of attack, shocks are seen leaving the trailing edge of each wing well inboard of the tips and are apparently composed of two or more shocks arising from points on the wing. If these shocks are traced forward, the apparent point of origin will be found between the apex of the ridge line and the forward tip of the sting, this point being nearer the former. As the angle of attack of the wing is increased, these shocks separate into two distinct shocks, neither of which occupies the position in relation to the wing

tips that occurred for the $\alpha=0°$ condition. One shock has moved inboard and the other, outboard. The rate of outward travel with angle of attack for the outboard shock is much greater than the rate of inward travel for the inner shock. For wedge-leading-edge wing 5, tracing the shocks forward places the apparent point of origin behind the ridge-line apex and well ahead of the forward tip of the sting. For wedge-leading-edge wing 11, tracing the inboard shock at $\alpha=4°$ produces a point of origin behind the sting tip, while the outer shock continues to maintain a point of origin between the sting tip and the ridge-line apex. Thus the sting may be eliminated as a source of these shocks. Comparison of the photographs of the elliptical-leading-edge wings (fig. 19) and the corresponding photographs of the wedge-leading-edge wings (fig. 16 (b)) shows that the shocks leave the trailing edge of the elliptical-leading-edge wing slightly further inboard than on the wedge-leading-edge wing. The shocks are evidently produced by second-order compressibility effects similar to those observed on unswept wings at transonic speeds. It is possible that thickness distribution, leading-edge shape, and ridge-line angularity are predominant factors in formation and location of the shocks. The easy curvature of the ridge line of the elliptical-leading-edge wings would probably favor a delay in formation of the shocks. As stated previously, a relatively large exposure time was necessary for the schlieren photographs of the elliptical-leading-edge wings. This probably explains the appearance of the shed vortices in these photographs.

The liquid-film patterns for wings 5 and 11 are shown in figures 20(a), 20(b), and 20(d). In contrast to wing 5, wing 11 shows the area of large shear intensity near the leading edge to extend even behind the ridge line for both the wedge- and elliptical-leading-edge configurations. This phenomenon is probably associated with the higher component of free-stream velocity normal to the leading edge of wing 11. The sequence of liquid-film photographs presented in figure 20(d) shows the progressive shifting of the transition line on both upper and lower surfaces with angle of attack for wing 5. The difference in absolute location of the transition lines on upper and lower surfaces at other than zero angle of attack is practically the same as the difference in location of the two shocks observed in the schlieren photographs. In addition, the location and curvature of the transition line shown on each surface at angle of attack, when superimposed on the schlieren photographs, indicate that the inboard shock arises from the upper surface and the outboard shock, from the lower surface. With increase in angle of attack, the Mach number of the flow over the lower wing surface behind the ridge line would decrease while that of the corresponding upper wing surface would increase. The Mach lines from a fixed point of origin would change their inclination with angle of attack in a direction which is in agreement with the observed changes of the shock inclinations. However, it is doubtful that the inclinations, locations, and curvatures of the shocks can be so simply accounted for; rather, a more complex phenomenon involving flow angularity and degree of local separation would appear to be involved.

From the profile schlieren photographs of wings 1, 5, and 11 (fig. 17), the shocks emanating from the rear portion of the model may be traced to the trailing edge only. In some instances a very weak shock may be traced to the sting tip on the wing surface; however, this observation is confined to the profile view and its overall effect is probably negligible.

PRESSURE DISTRIBUTIONS

Pressure distributions were measured in an effort to show that the location of the steep adverse pressure gradient and the line of transition were practically coincident. Pressure-distribution tests of wedge-leading-edge wing 5 were made at a Mach number of 1.62 at the wing center line, 25.5 percent semispan, and 60.3 percent semispan. The results are presented in figure 21. Similar tests were made on wing 11 for both the wedge- and elliptical-leading-edge configurations at 22.5 percent and 64.1 percent semispan. These results are presented in figures 22 and 23. Except for the elliptical-leading-edge wing, for which a smooth pressure-distribution curve void of sharp peaks has been assumed to exist, no attempt has been made to fair the curves ahead of the ridge line because of insufficient test points in this vicinity.

For the wedge-leading-edge wings, the theoretical pressure distribution at the test stations has been computed for zero angle of attack by the method given in reference 13. (See appendix B.) In all cases the theory gives a fair prediction of the actual results, the greatest discrepancies appearing in the curve for wing 11 at 64.1 percent semispan. Most of the discrepancies are undoubtedly a result of the shocks on the wing surfaces that are not accounted for in the theoretical solution.

At the center-line station of wing 5, test results indicate that no effect is transmitted from the sting tip forward through the boundary layer. At the 25.5-percent-semispan station the difference in the abruptness of the pressure rise behind the ridge line between upper and lower surfaces with increase in angle of attack is quite obvious. At an angle of attack of 4.20°, for example, the initially steep adverse pressure gradient on the lower surface favors transition immediately behind the ridge line while the lower and more uniform adverse pressure gradient on the upper surface would, by comparison, indicate a delay in transition. The liquid-film tests have shown this to be the actual result. At the 60.3-percent-semispan station, similar trends in the pressure distributions occur. However, the positions of the steep adverse pressure gradients on upper and lower surfaces indicate that the point of transition on the lower surface would be nearer the ridge line than was the case at the inboard station and, conversely, the point of transition on the upper surface would be farther removed from the ridge line. As before, the liquid-film tests exhibit such a pattern. Thus, the characteristics of the chordwise pressure distribution with varying angle of attack concur with the liquid-film observations in regard to the curvature of the shocks arising on the wing surfaces and their position.

The pressure distributions for wedge-leading-edge wing 11 indicate that the adverse pressure gradient originates immediately behind the Mach lines from the ridge-line apex, except at the outboard station where the test results show the pressure rise to begin behind the ridge line. The pressure distributions indicate the same effects as shown for wing 5, an appreciable forward movement of the shocks arising on

the lower surface and little rearward shift of the shocks on the upper surface. At the 22.5-percent-semispan station, it is interesting to note the change in shape of the curve ahead of the ridge line for the upper surface at an angle of attack of 10.75°. Although the initial wedge angle of the wing still produces a positive angle with respect to stream direction, the initial negative pressure followed by a positive pressure, both points ahead of the ridge line, may possibly be due to the detached shock and the resulting subsonic nature of the flow accompanied by the tendency of the high pressure on the lower surface to relieve itself by flow around the leading edge and over the upper surface.

The pressure distributions for elliptical-leading-edge wing 11 show trends similar to those of the wedge-leading-edge wing though not quite so marked. A delay in the transition point as shown by the liquid-film tests would be expected from the very gradual rise of the adverse pressure gradient. The difference in location of the shocks on the wing surface with change in angle of attack is still evident from the curves.

GENERAL REMARKS

It appears that the peaks and breaks in the curves of this report that were calculated by the linear theory will not in most instances be realized experimentally. The theoretical pressure-distribution curves for the wings of angular or abrupt ridge line are possibly an exception. Much of the discrepancy between test and theoretical values may be attributed to two factors omitted in the linear theory: viscosity and shocks resulting from second-order compressibility effects. Certainly the presence of the shocks observed on the wing surfaces and their movement with angle of attack influence the lift and drag results. The transition line in the boundary layer is obviously determined by the position of these shocks and the associated adverse pressure gradient. It follows that a greater or lesser turbulent area will affect the drag accordingly. Thus the lower minimum drag of the elliptical-leading-edge wings for values of $\tan \epsilon/\tan \mu$ less than 1.6 may be attributed to their lesser areas of turbulent boundary layer. Furthermore, it appears that, regardless of whether the leading edge is supersonic, until complete attachment of the shock is realized along the wing leading edge, the flow at or near the leading edge is physically similar to the flow over two-dimensional wings at high subsonic Mach numbers; under such conditions, the aerodynamic characteristics of the wing may be expected to deviate from the theoretical. At the lower values of $\tan \epsilon/\tan \mu$ it is possible that an increased lift may be experienced at the leading edge of sufficient magnitude to raise the total lift above the predicted theoretical value. Of course, at extremely low values of $\tan \epsilon/\tan \mu$ such an effect would diminish. At the larger values of $\tan \epsilon/\tan \mu$ the effect of boundary layer and shock interaction may be blamed for the reduced lift with respect to theory; but as $\tan \epsilon/\tan \mu$ approached the value for complete attachment of the shock to the leading edge, the transonic nature of the flow in the vicinity of the ridge line would give way to entirely supersonic flow and the actual lift would be expected to attain a value somewhat near the theoretical. It is possible that a wing having a sharp leading edge and a ridge line of easy curvature might retain the smaller region of turbulent boundary layer associated with the elliptical-leading-edge series. This configuration would also favor early attachment of the leading-edge shock, with the consequent higher lift and lower drag exhibited by the wedge-leading-edge series at values of $\tan \epsilon/\tan \mu$ much greater than 1.

CONCLUSIONS

Supersonic tests were made at Mach numbers of 1.62, 1.92, and 2.40 of 22 triangular wings having a thickness ratio of 8 percent and location of maximum-thickness point at 18 percent chord. Two leading-edge configurations, wedge and elliptical, were represented for each apex angle. The following results were obtained:

1. For a given wing series and any given ratio of the tangent of the vertex half-angle to the tangent of the Mach angle ($\tan \epsilon/\tan \mu$), the ratio of the actual lift-curve slope to the theoretical two-dimensional value was relatively independent of Mach number.
2. The experimental lift-curve slopes for the elliptical- and wedge-leading-edge configurations were essentially the same but were slightly higher than theory for wings with leading edges well behind the Mach cone. With the Mach cone in the vicinity of the leading edge, the lift-curve slopes were considerably lower than theory. With the leading edge well ahead of the Mach cone, the lift-curve slope for the wedge-leading-edge configuration approached the theoretical two-dimensional lift-curve slope.
3. Except for cases with the Mach cone well behind the leading edge, the elliptical-leading-edge configuration gave lower minimum drag. This advantage was attributed to the lesser area of turbulent boundary layer on these wings.
4. The linear theory applied to the wedge-leading-edge series was quite inadequate for prediction of the drag.
5. The maximum lift-drag ratios for the elliptical-leading-edge configuration were higher up to a value of $\tan \epsilon/\tan \mu$ of approximately 1.3, from which point the wedge-leading-edge configuration exhibited the greater values.
6. The location of the center of pressure was relatively independent of Mach number for a given wing series and approached the center of area. An essentially linear variation of the center of pressure with $\tan \epsilon/\tan \mu$ occurred, the overall travel being approximately 10 percent. For the elliptical-leading-edge wings, the center of pressure lay 3 to 4 percent ahead of its location for the wedge-leading-edge wings.
7. Any leading-edge suction achieved by the elliptical-leading-edge wings was evidently of such magnitude as to be overshadowed by other effects.
8. The position of shocks arising on the wing surfaces, the line of boundary-layer transition, and the steep adverse pressure gradient were found to be practically coincident.
9. The agreement of the theoretical and experimental pressure distributions was much better for the wing with subsonic leading edge than for the wing with supersonic leading edge.

Langley Aeronautical Laboratory,
National Advisory Committee for Aeronautics,
Langley Air Force Base, Va., *March 30, 1949.*

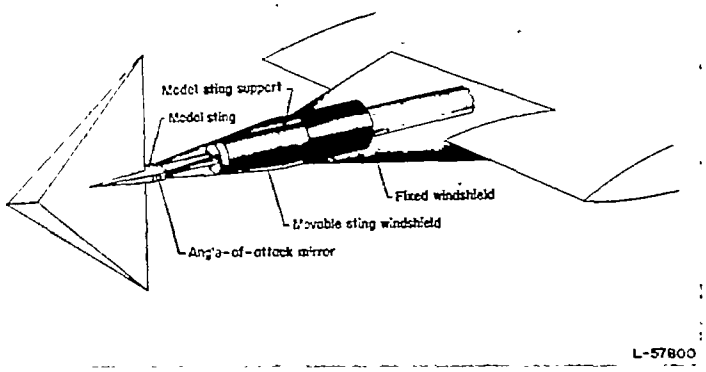

FIGURE 1.—Drawing of model and support installation.

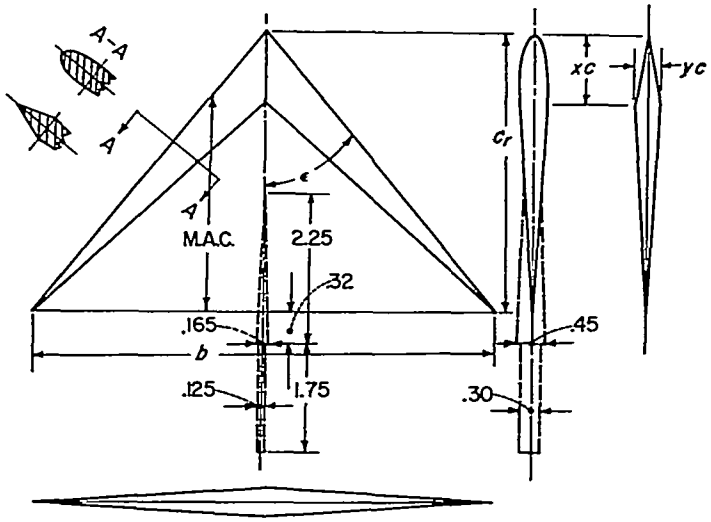

FIGURE 2.—Dimensions of 8-percent-thick triangular-wing models. (Sting dimensions identical for all wings.)

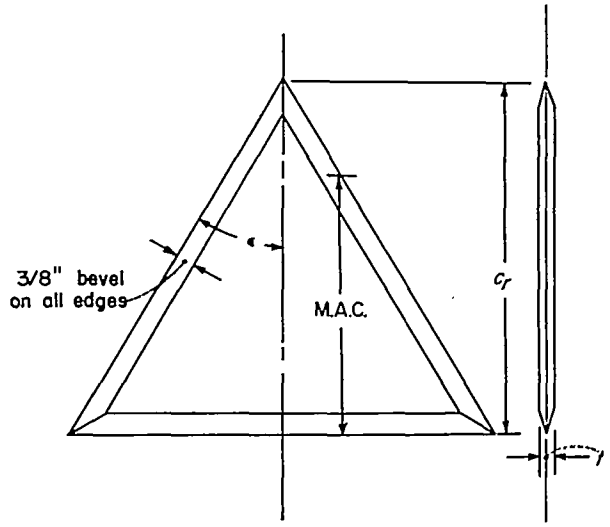

FIGURE 3.—Dimensions of flat-plate triangular-wing models. (Sting supports are identical with those of thick-wing installation.)

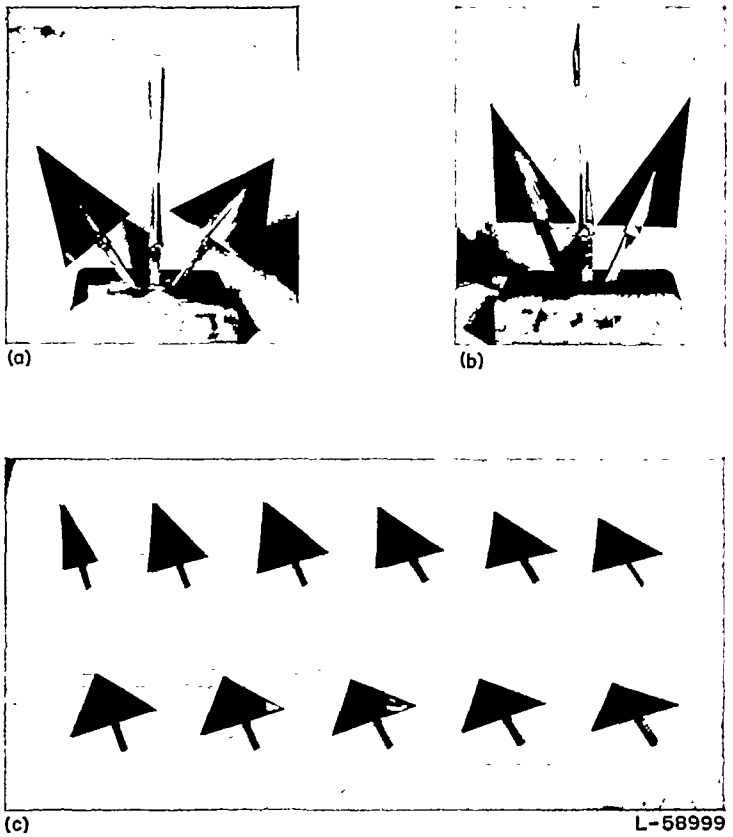

(a) Elliptical-leading-edge wings. (b) Wedge-leading-edge wings. (c) Wing series.

FIGURE 4.—Triangular-wing models.

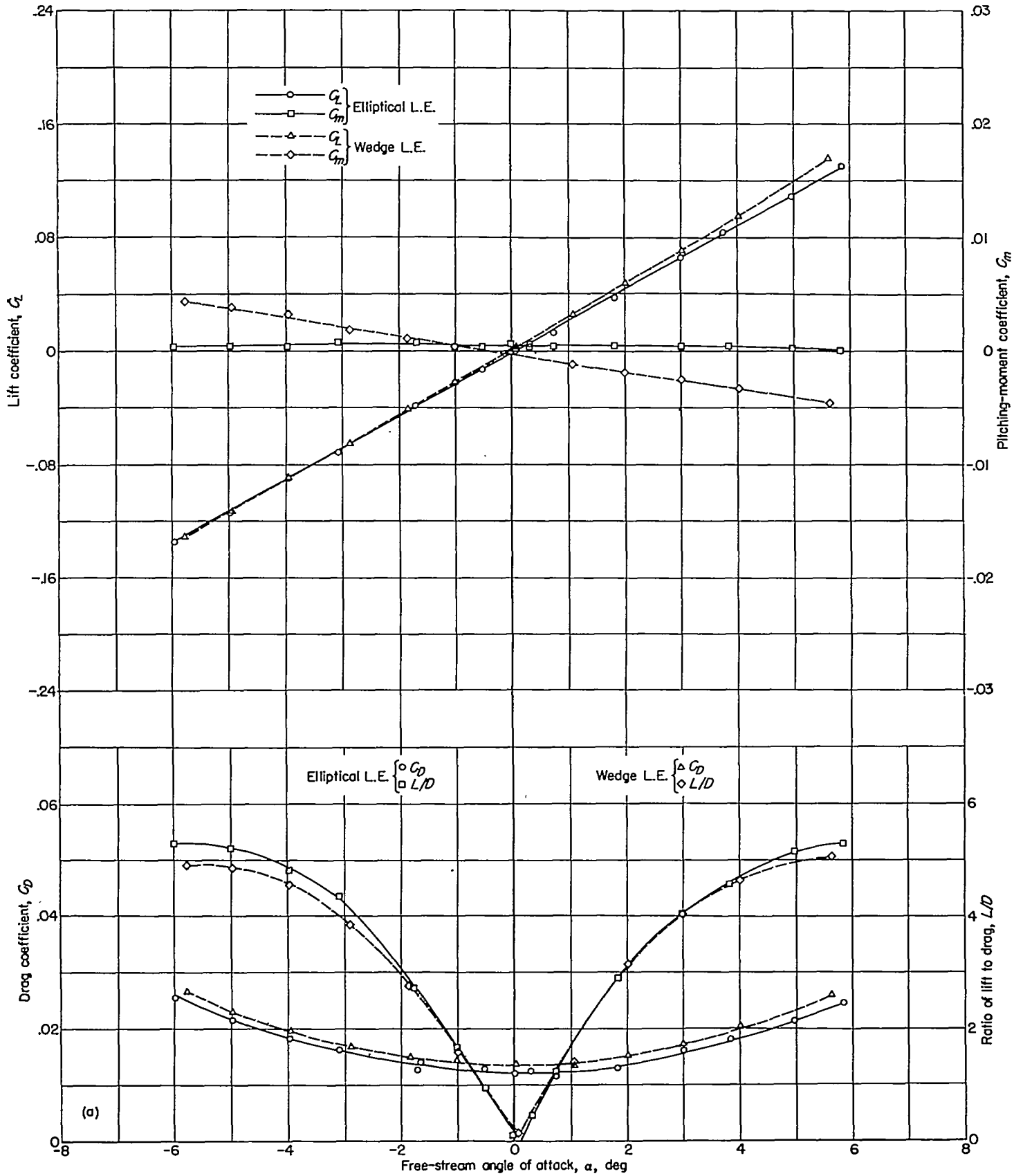

(a) Wing 1. $w=0.223$; $R=1.39\times10^6$.

FIGURE 5.—Aerodynamic characteristics of 8-percent-thick triangular wings at $M=1.62$.

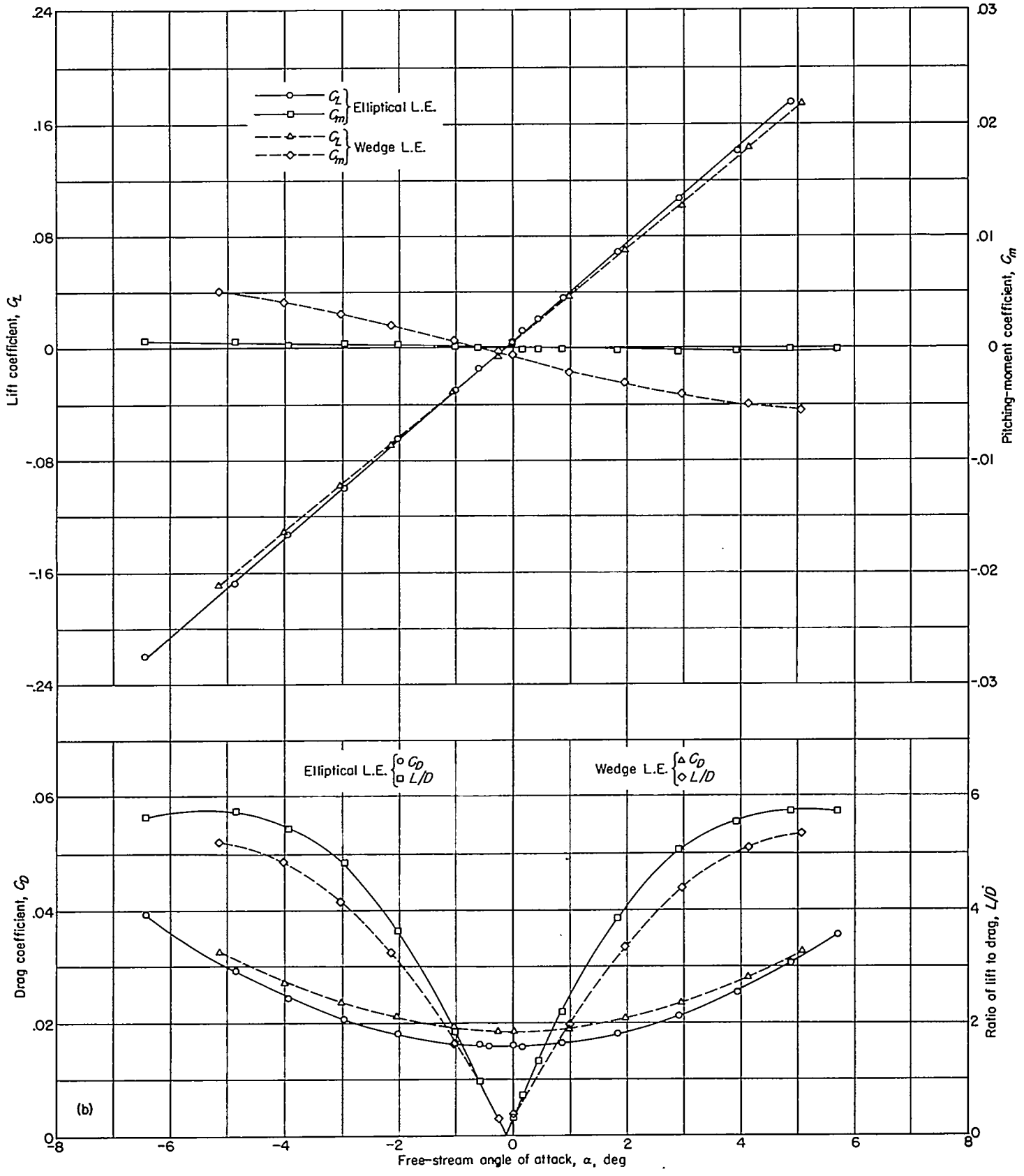

(b) Wing 2. $w=0.412$; $R=1.39\times10^6$.

FIGURE 5.—Continued.

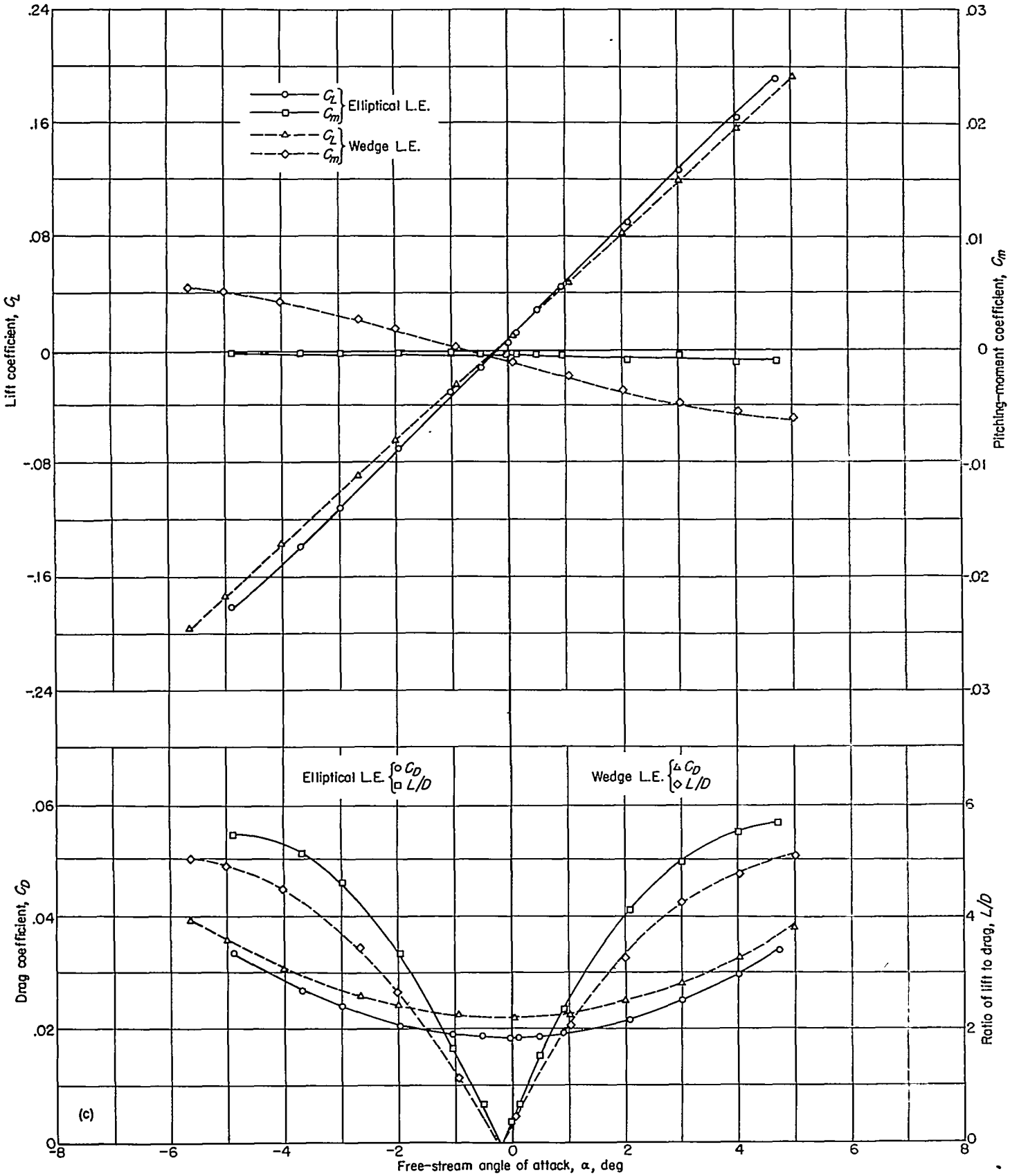

(c) Wing 3. $w=0.514$; $R=1.38\times10^6$.

FIGURE 5.—Continued.

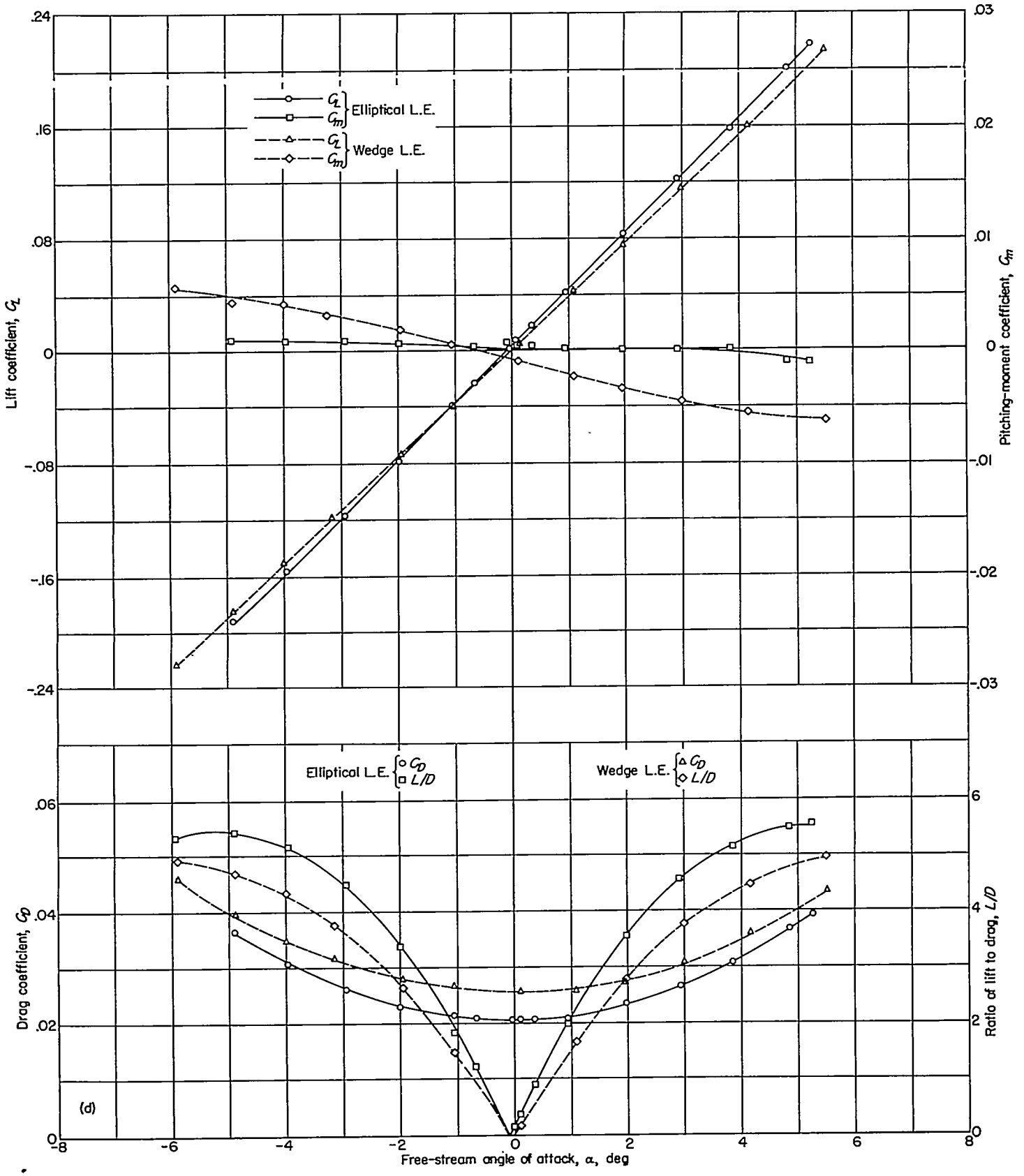

(d) Wing 4. $w=0.594$; $R=1.20\times10^6$.

FIGURE 5.—Continued.

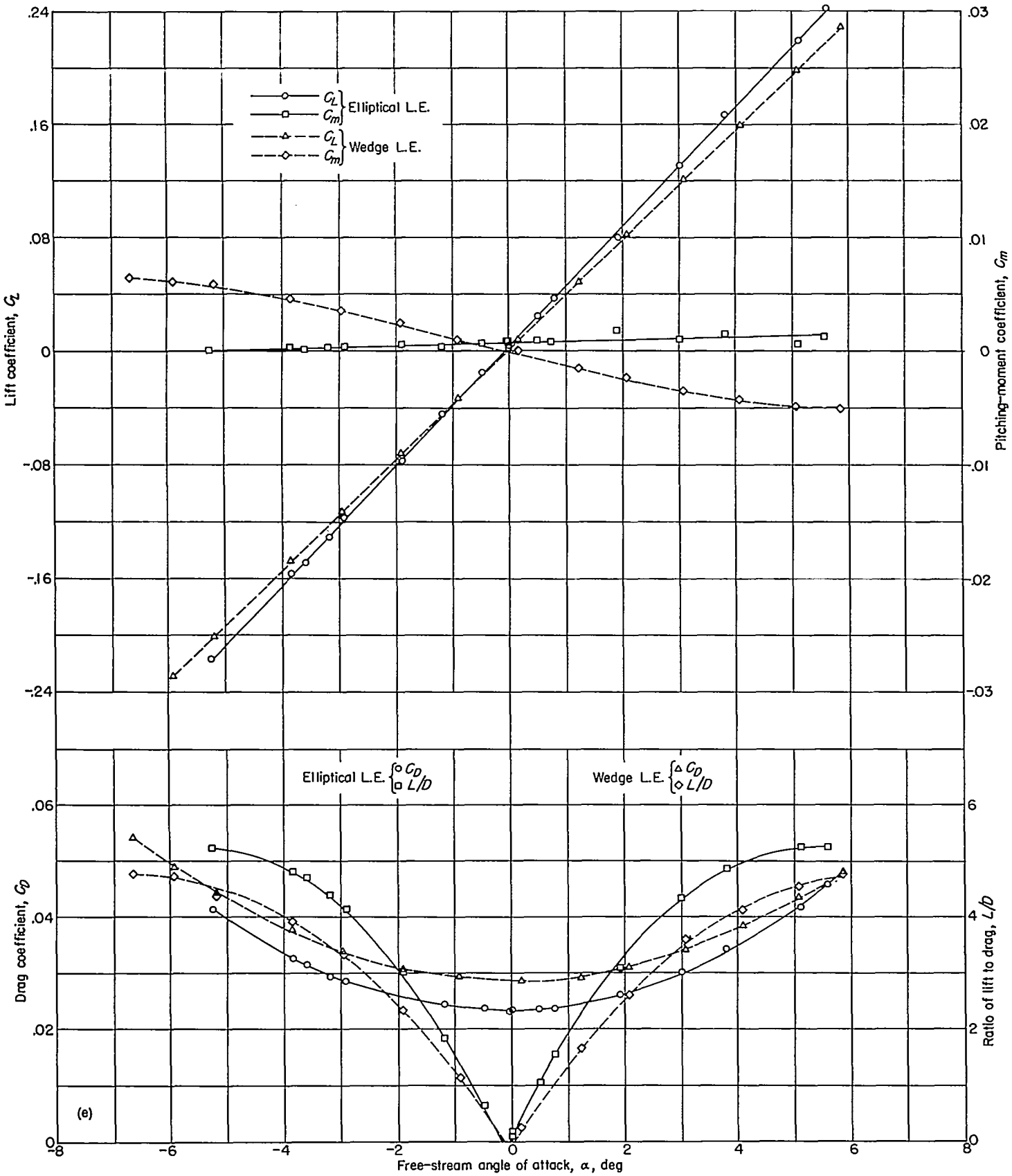

(e) Wing 5. $w=0.675$; $R=1.08\times10^6$.

FIGURE 5.—Continued.

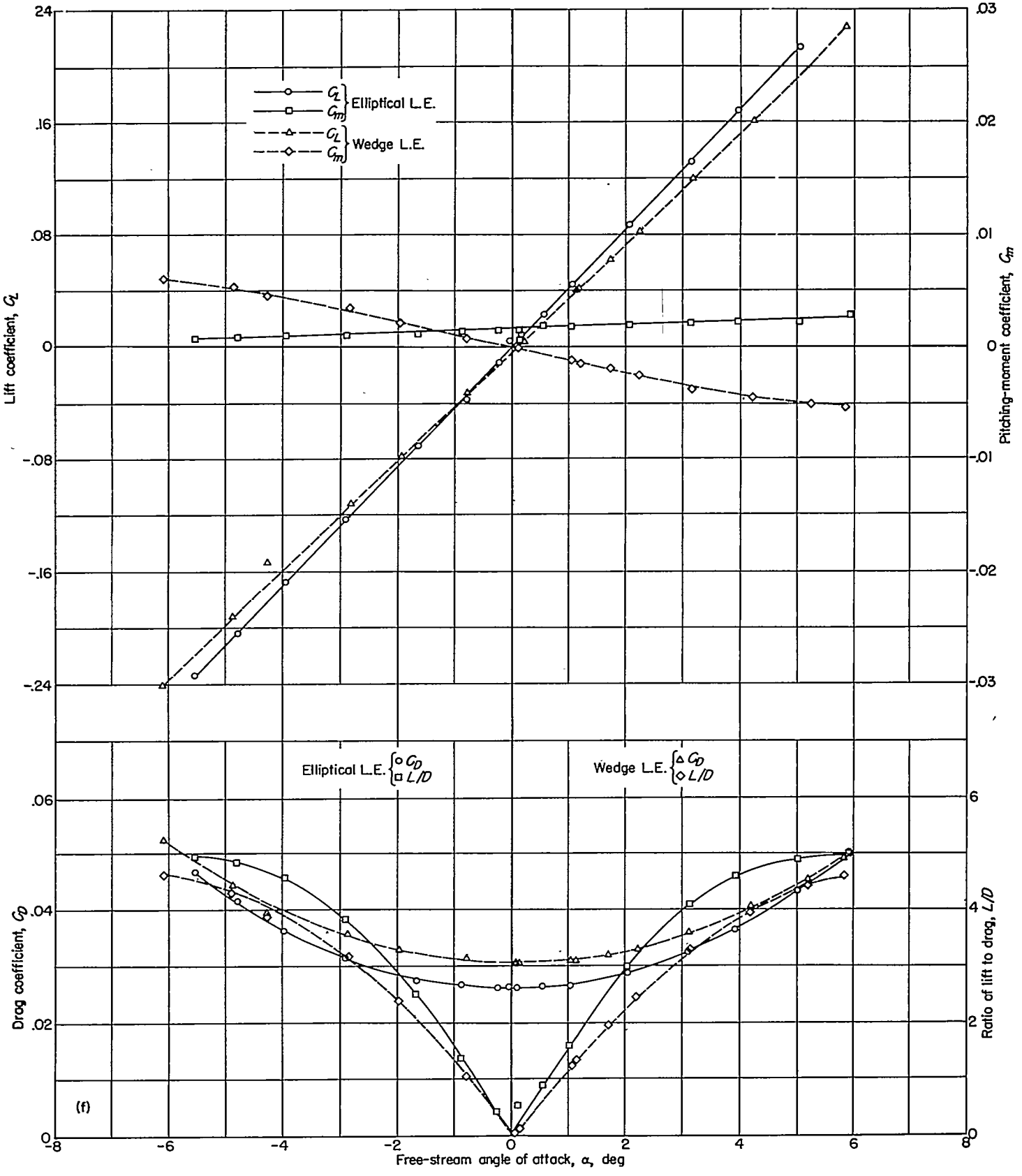

(f) Wing 6. $w=0.731$; $R=1.0\times10^6$.

FIGURE 5.—Continued.

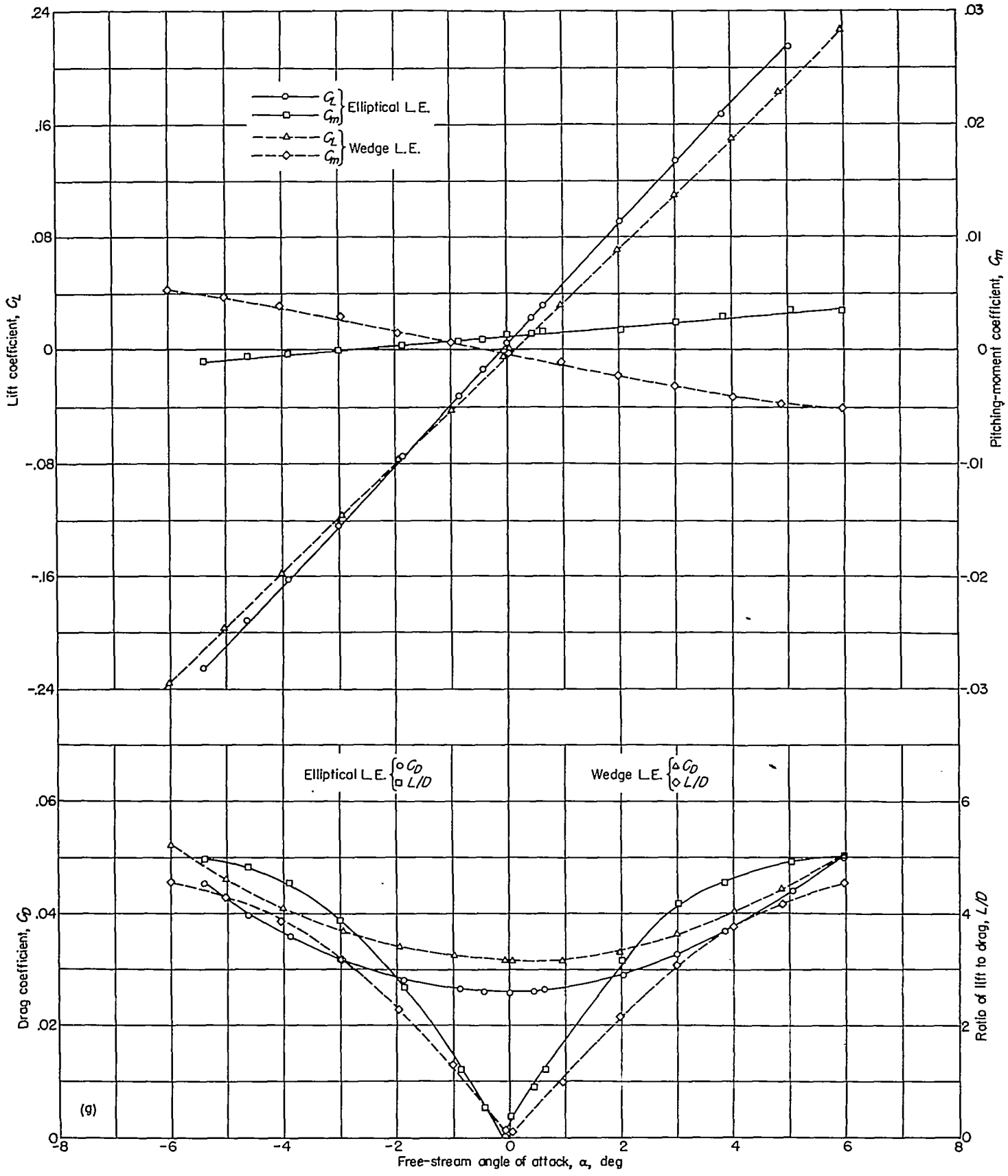

(g) Wing 7. $w=0.801$; $R=0.94\times10^6$

FIGURE 5.—Continued

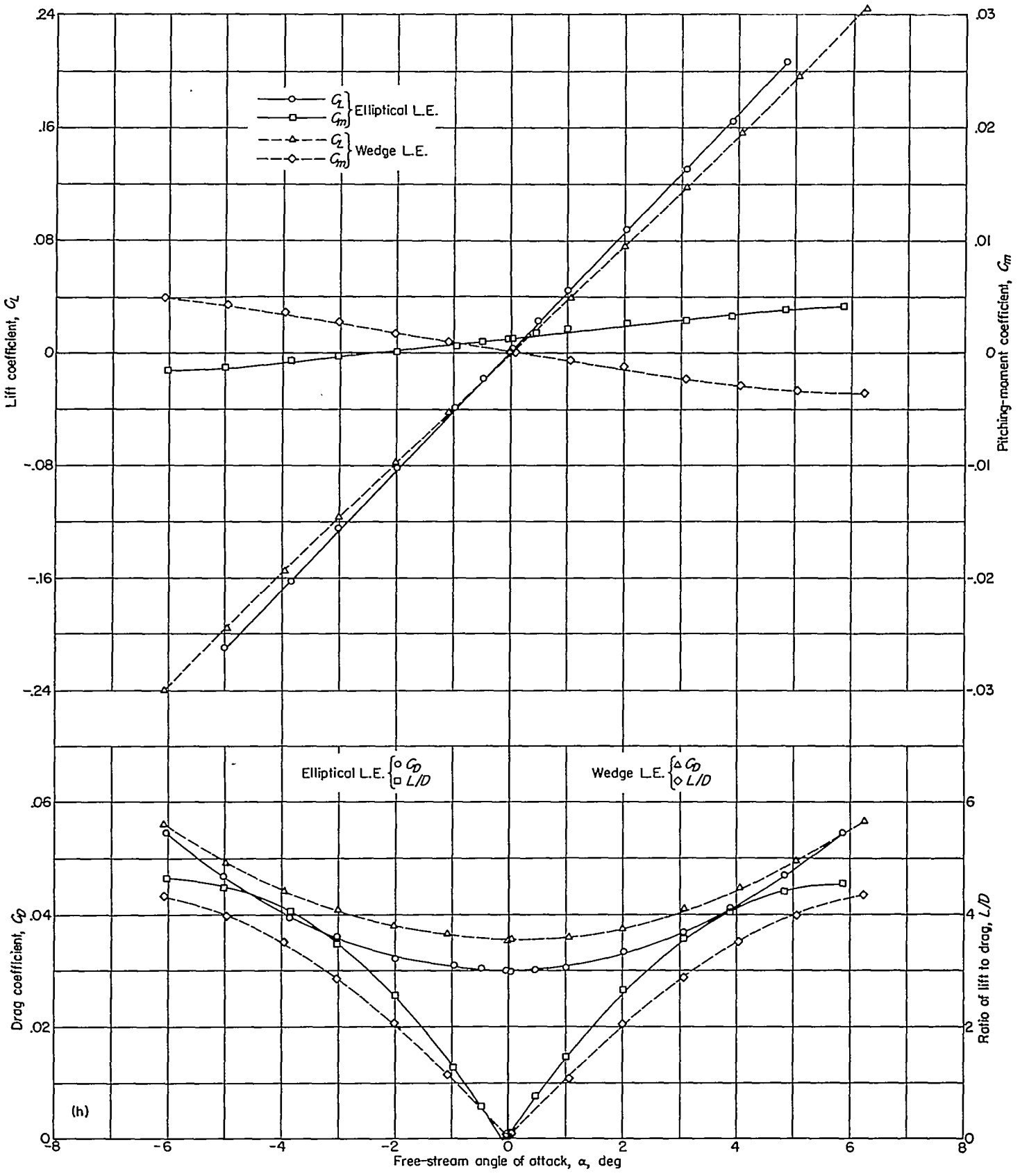

(h) Wing 8. $w=0.899$; $R=0.86\times10^6$.

FIGURE 5.—Continued.

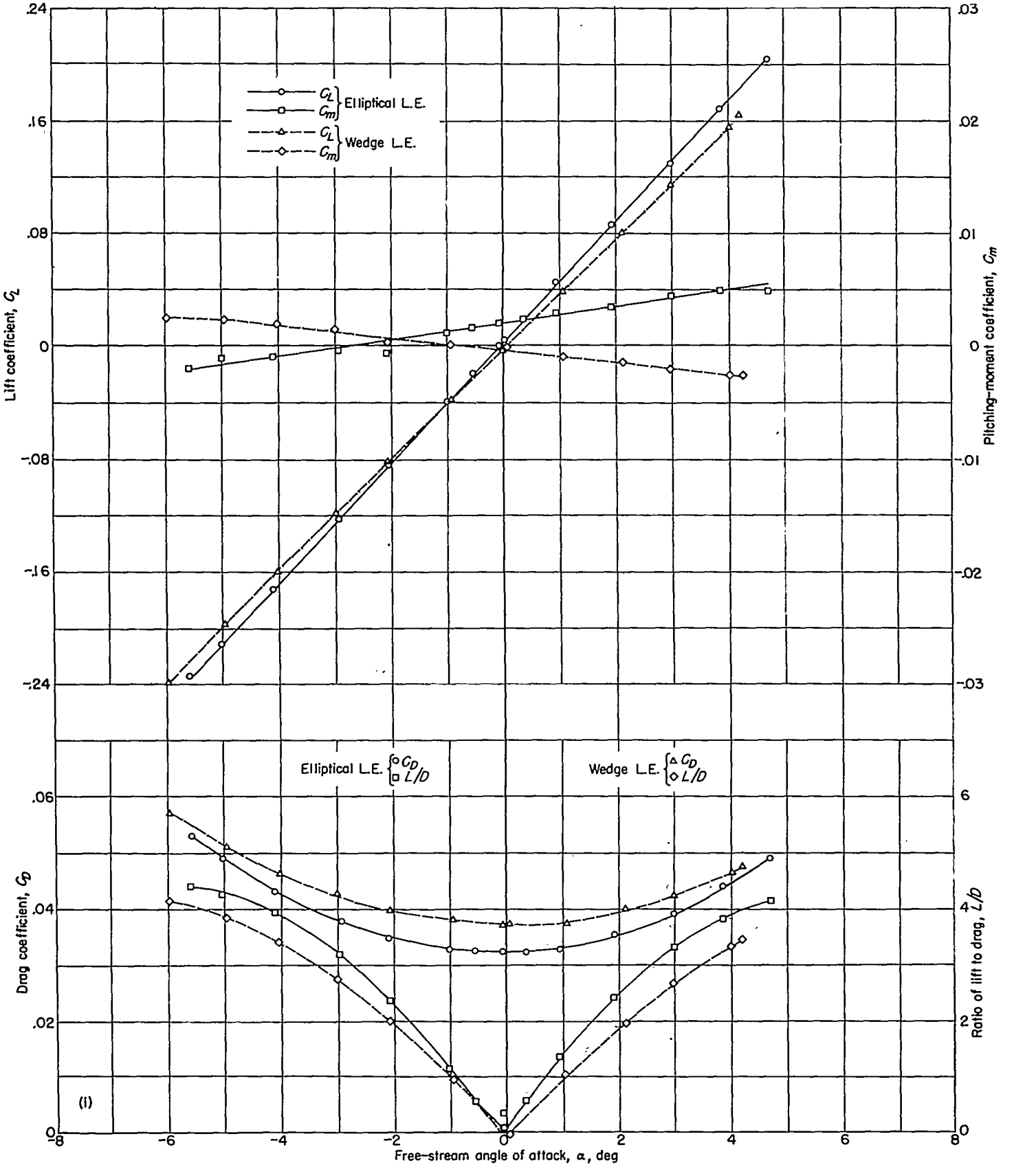

(i) Wing 9. $w=0.996$; $R=0.78\times10^6$.

FIGURE 5.—Continued.

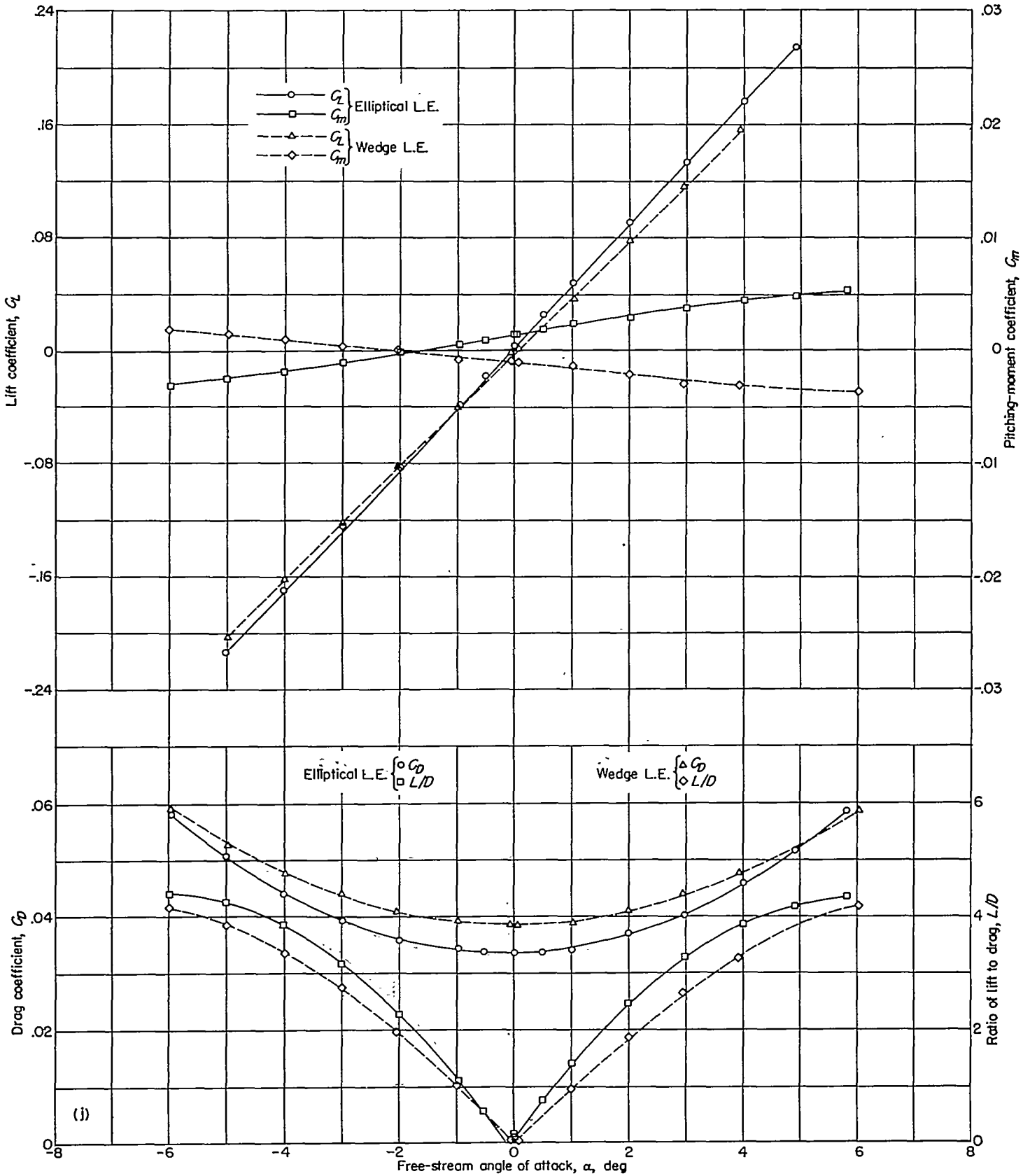

(j) Wing 10. $w=1.066$; $R=0.74\times10^6$.

FIGURE 5.—Continued.

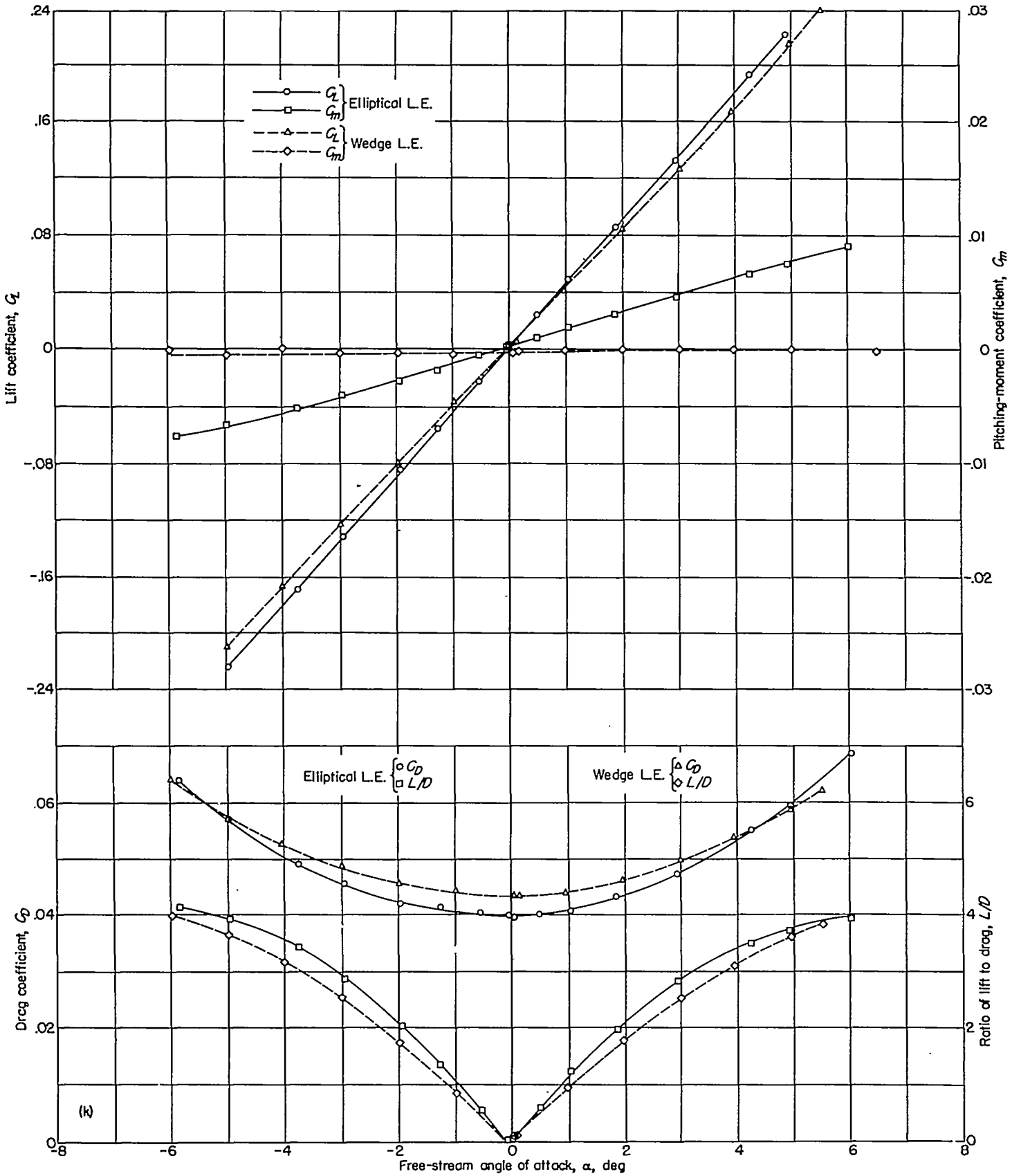

(k) Wing 11. $w=1.280$; $R=0.64\times10^6$.

FIGURE 5.—Concluded.

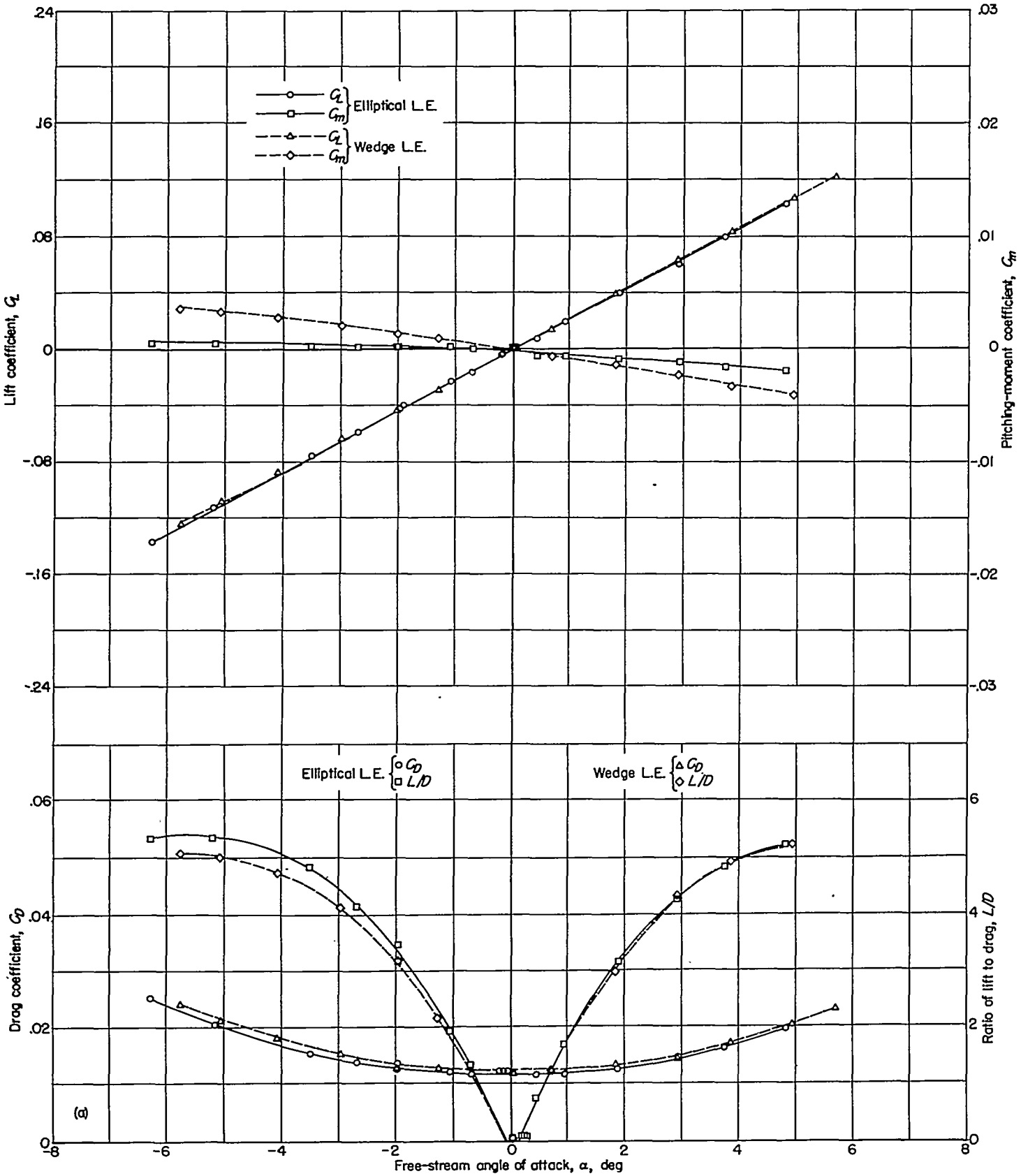

(a) Wing 1. $w=0.287$; $R=1.25\times10^6$.

FIGURE 6.—Aerodynamic characteristics of 8-percent-thick triangular wings at $M=1.92$.

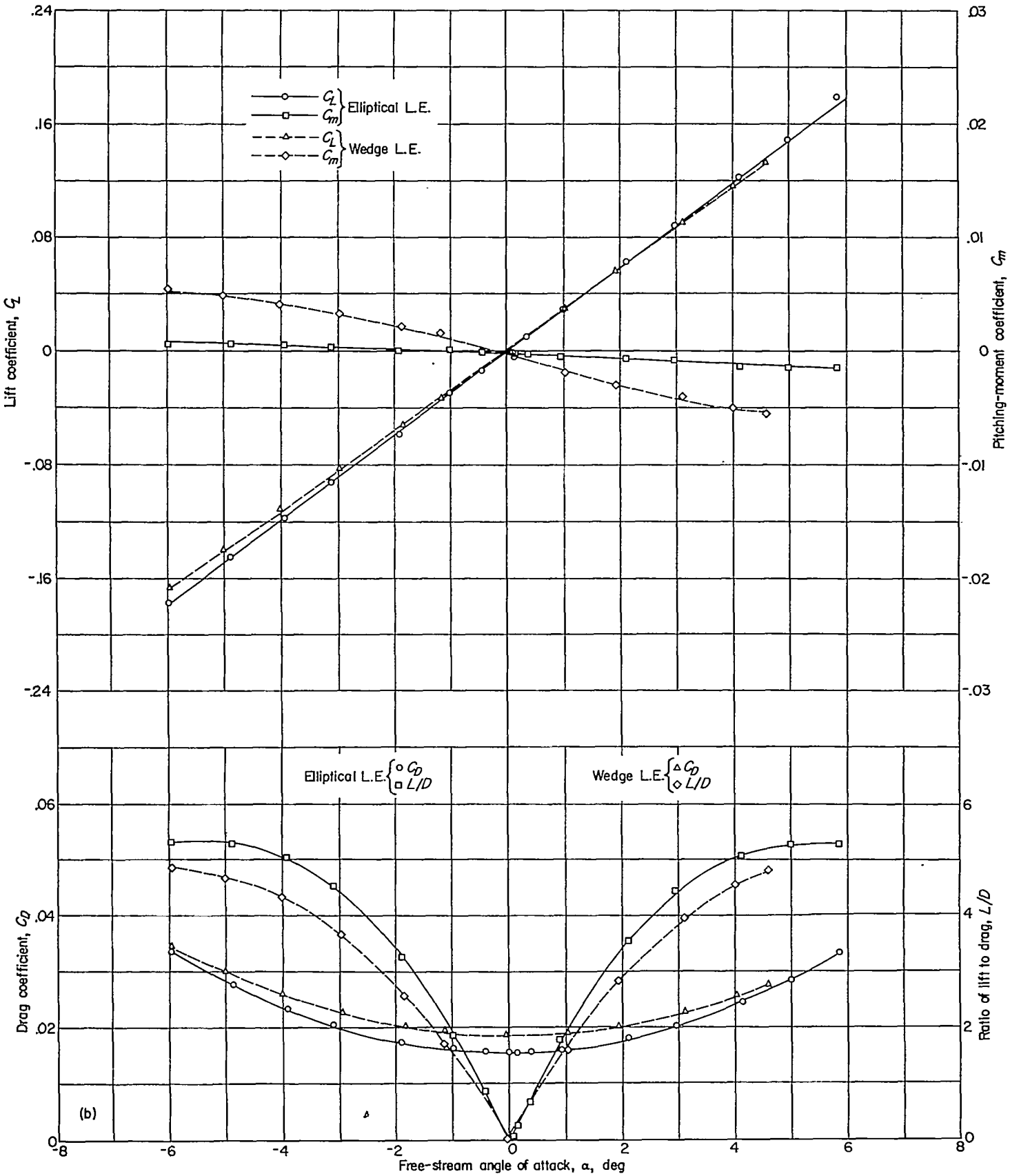

(b) Wing 2. $w=0.530$; $R=1.25\times10^6$.

FIGURE 6.—Continued.

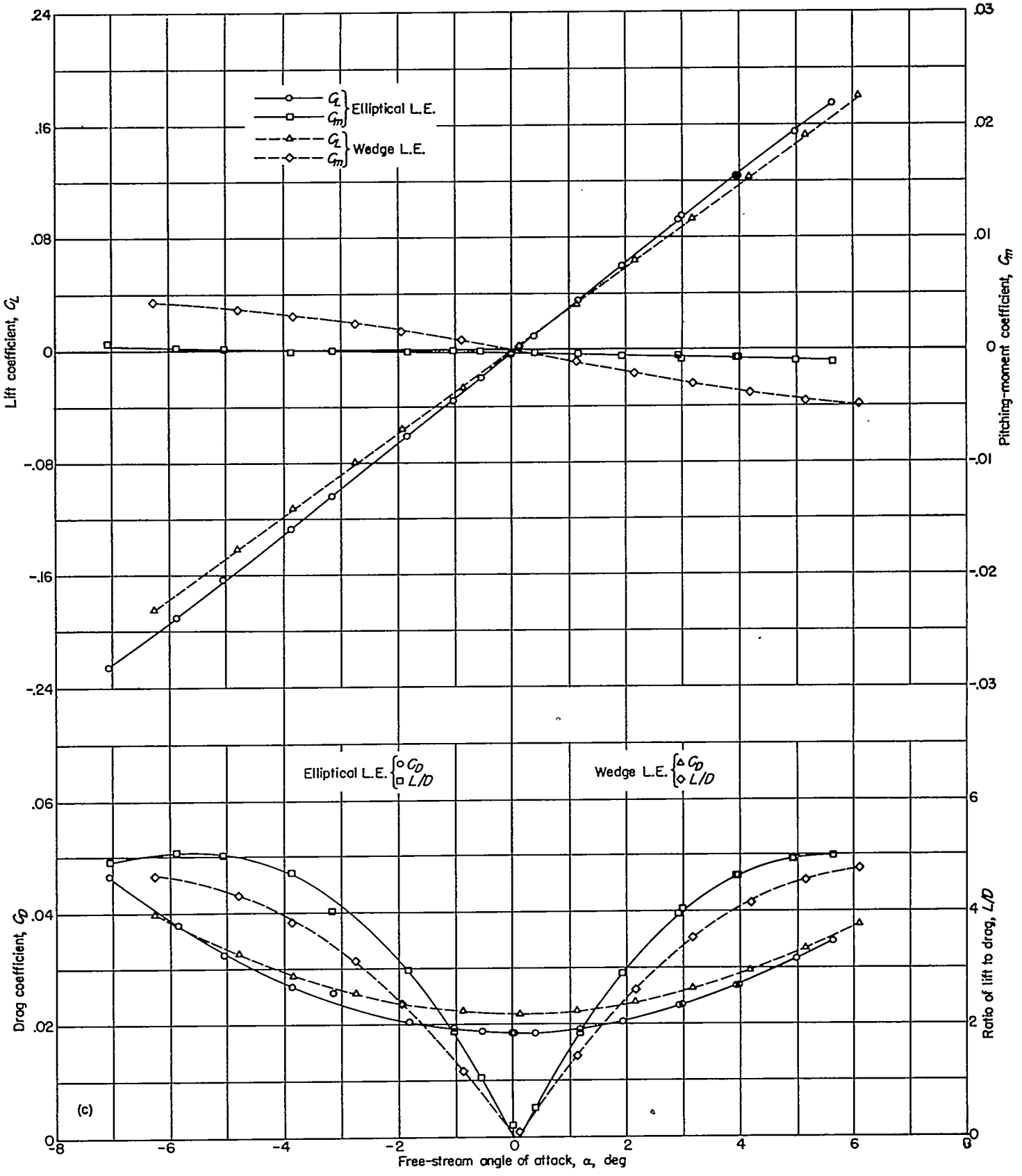

(c) Wing 3. $w=0.661$; $R=1.23\times10^6$.

FIGURE 6.—Continued.

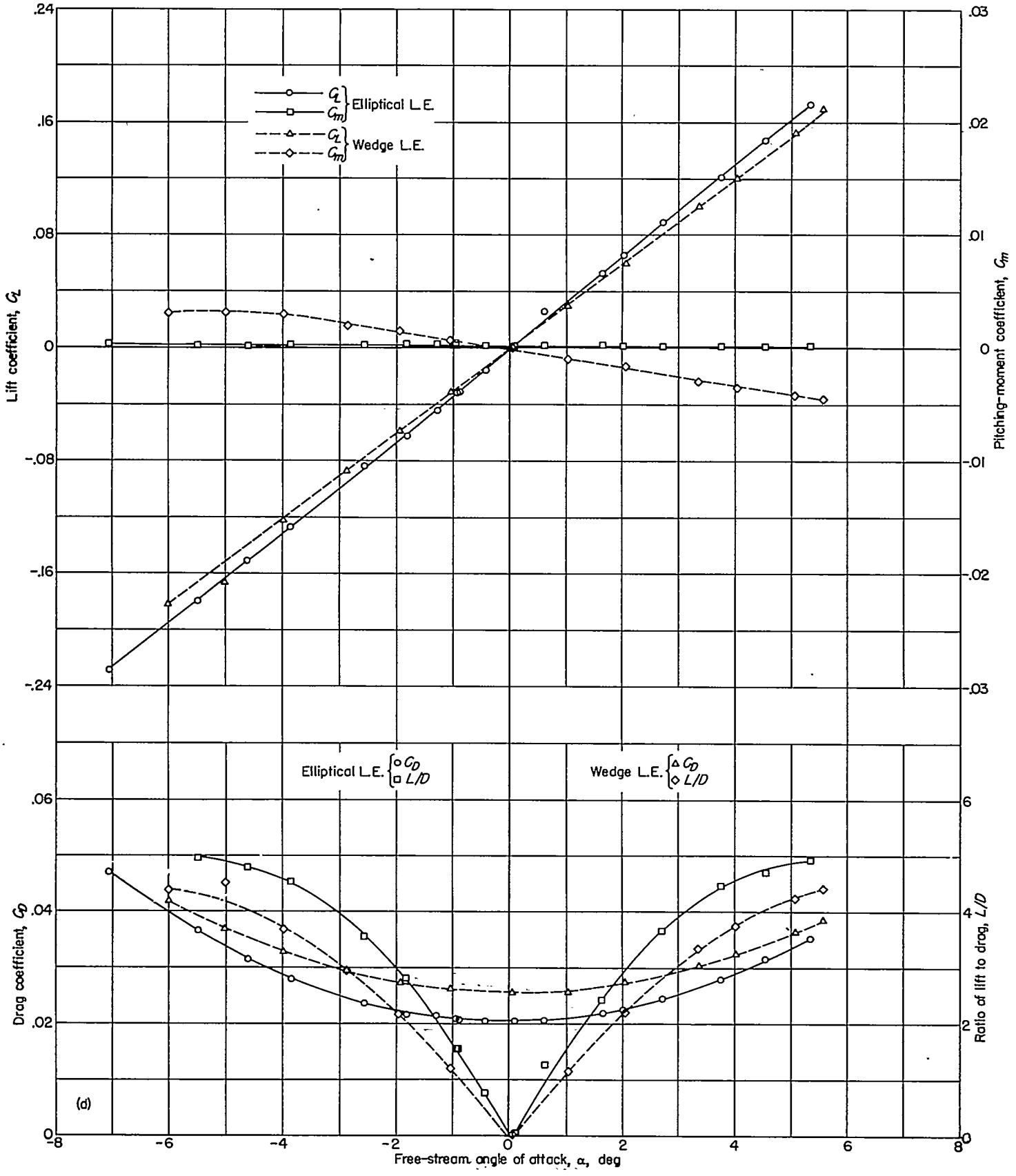

(d) Wing 4. $w=0.765$; $R=1.08\times10^6$.

FIGURE 6.—Continued.

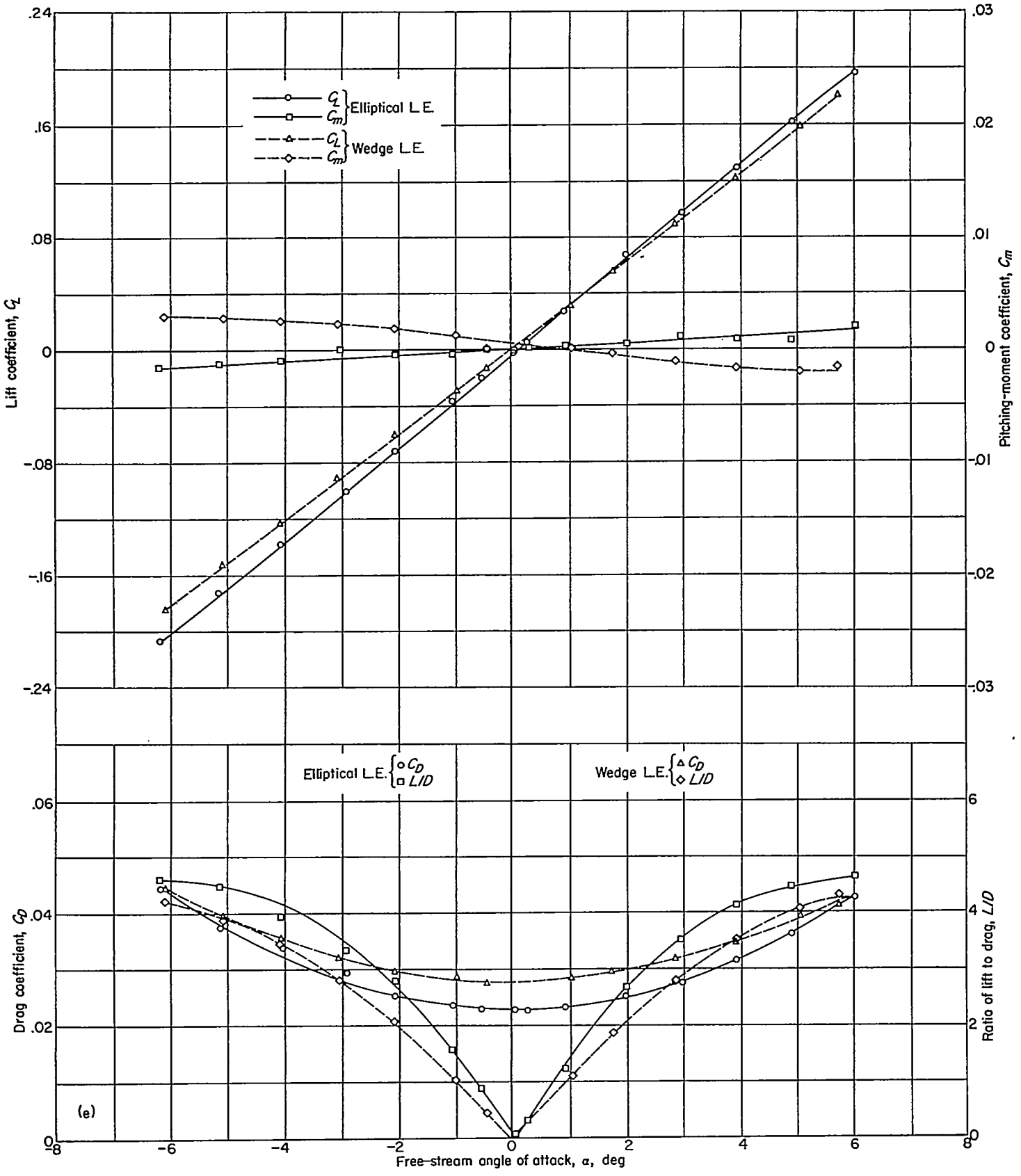

(e) Wing 5. $w=0.869$; $R=0.96\times10^6$.

FIGURE 6.—Continued.

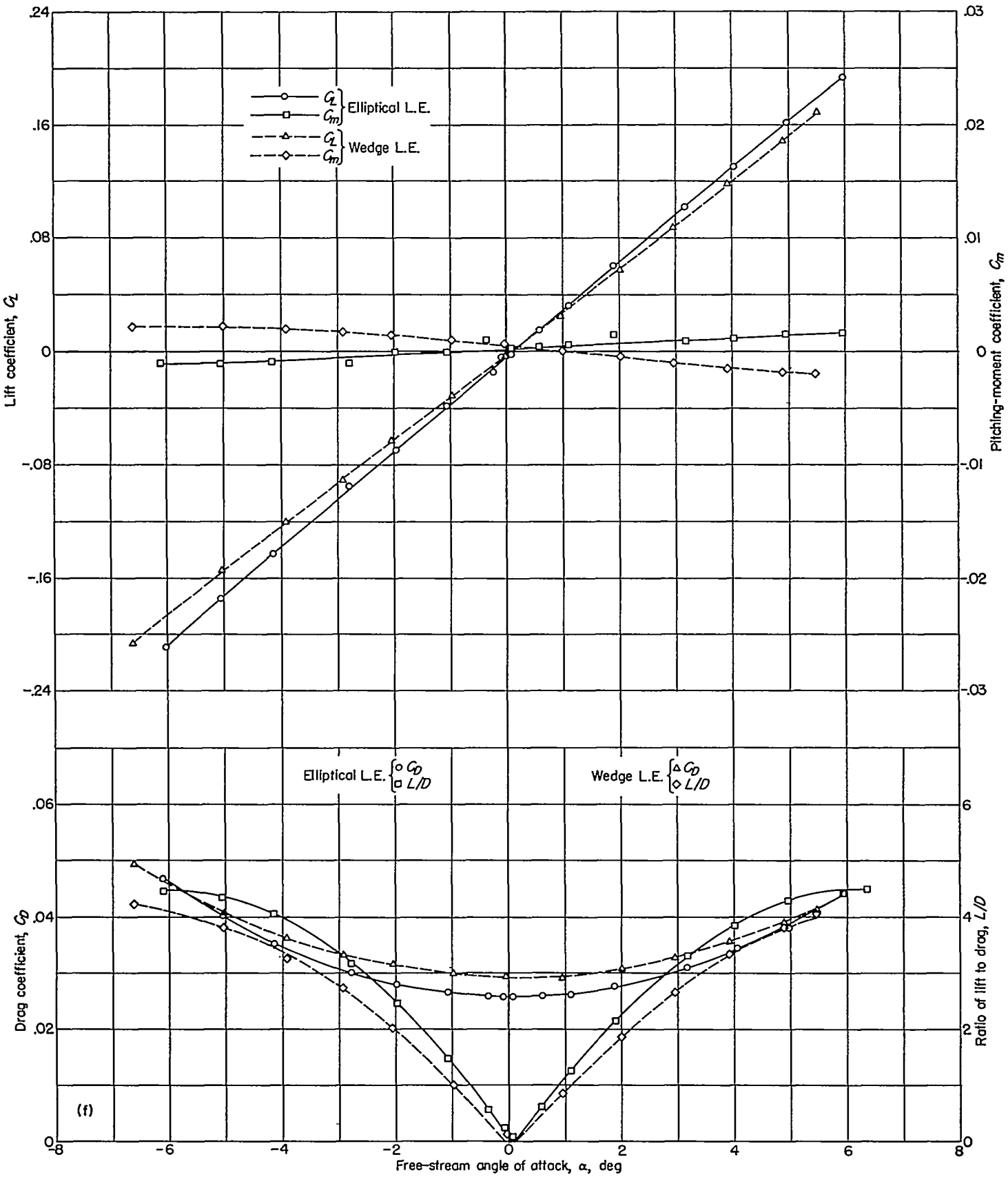

(f) Wing 6. $w=0.940$; $R=0.90\times10^6$.

FIGURE 6.—Continued.

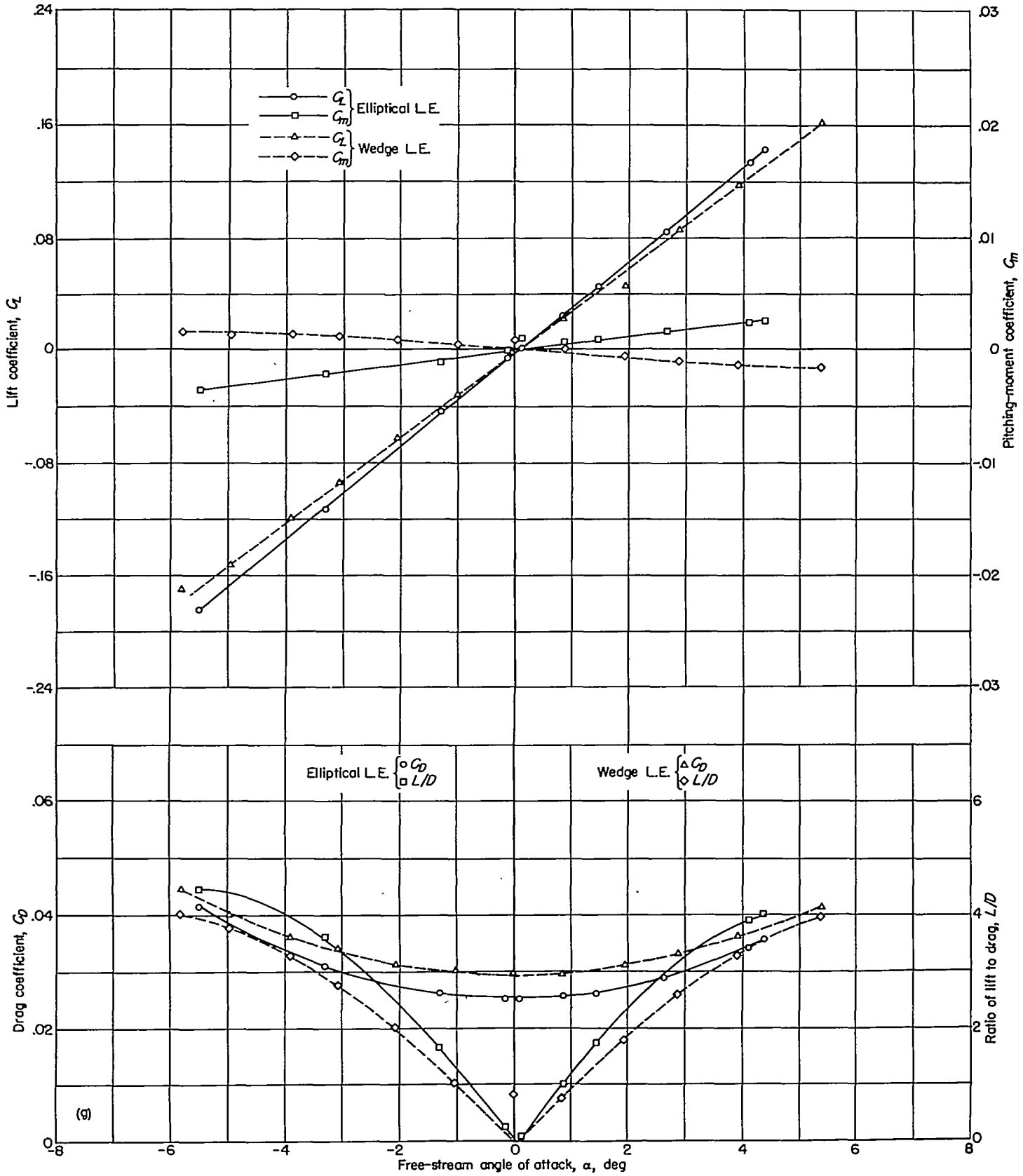

(g) Wing 7. $w=1.030$; $R=0.84\times10^6$.

FIGURE 6.—Continued.

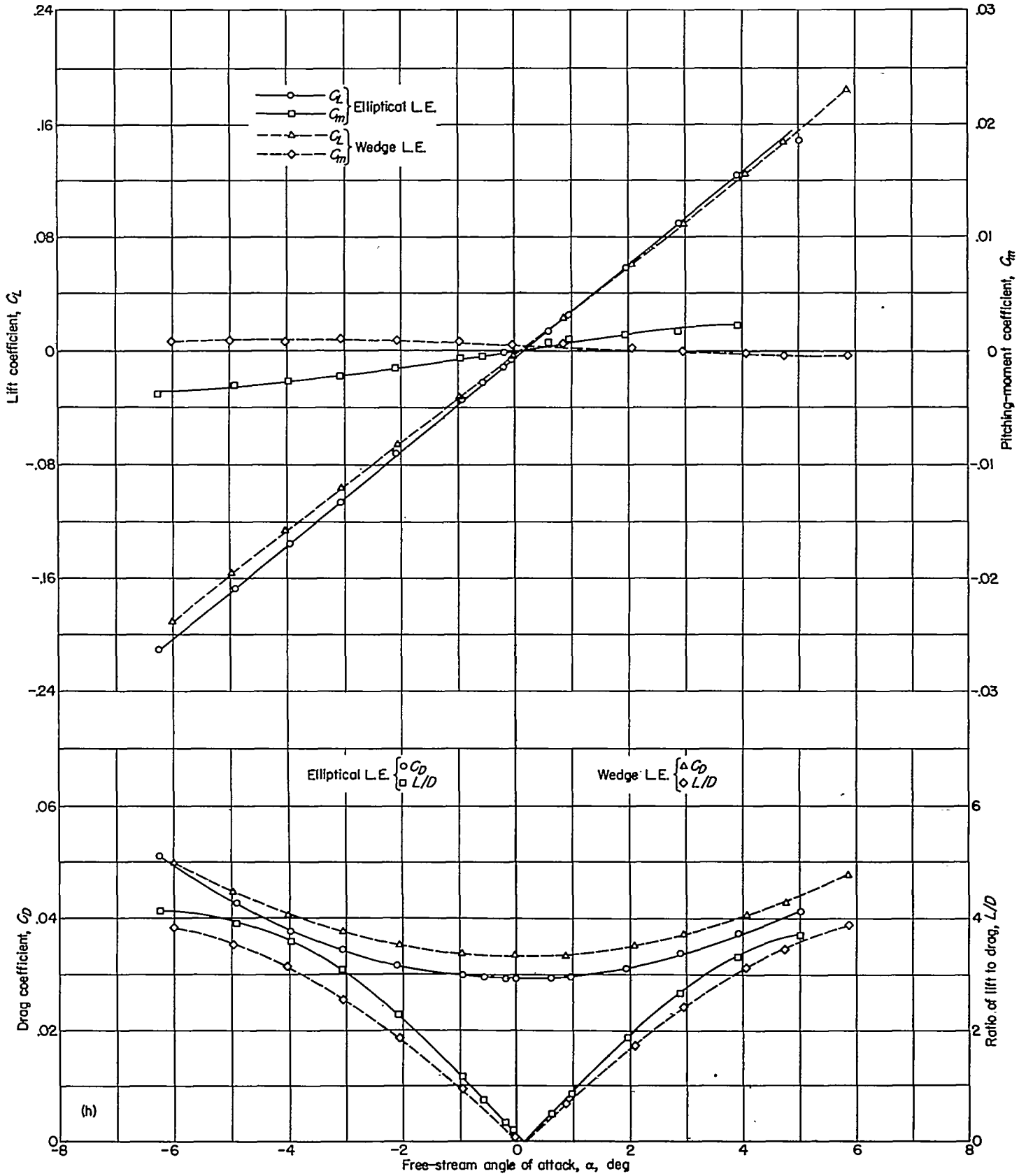

(h) Wing 8. $w=1.156$; $R=0.77\times10^6$.

FIGURE 6.—Continued.

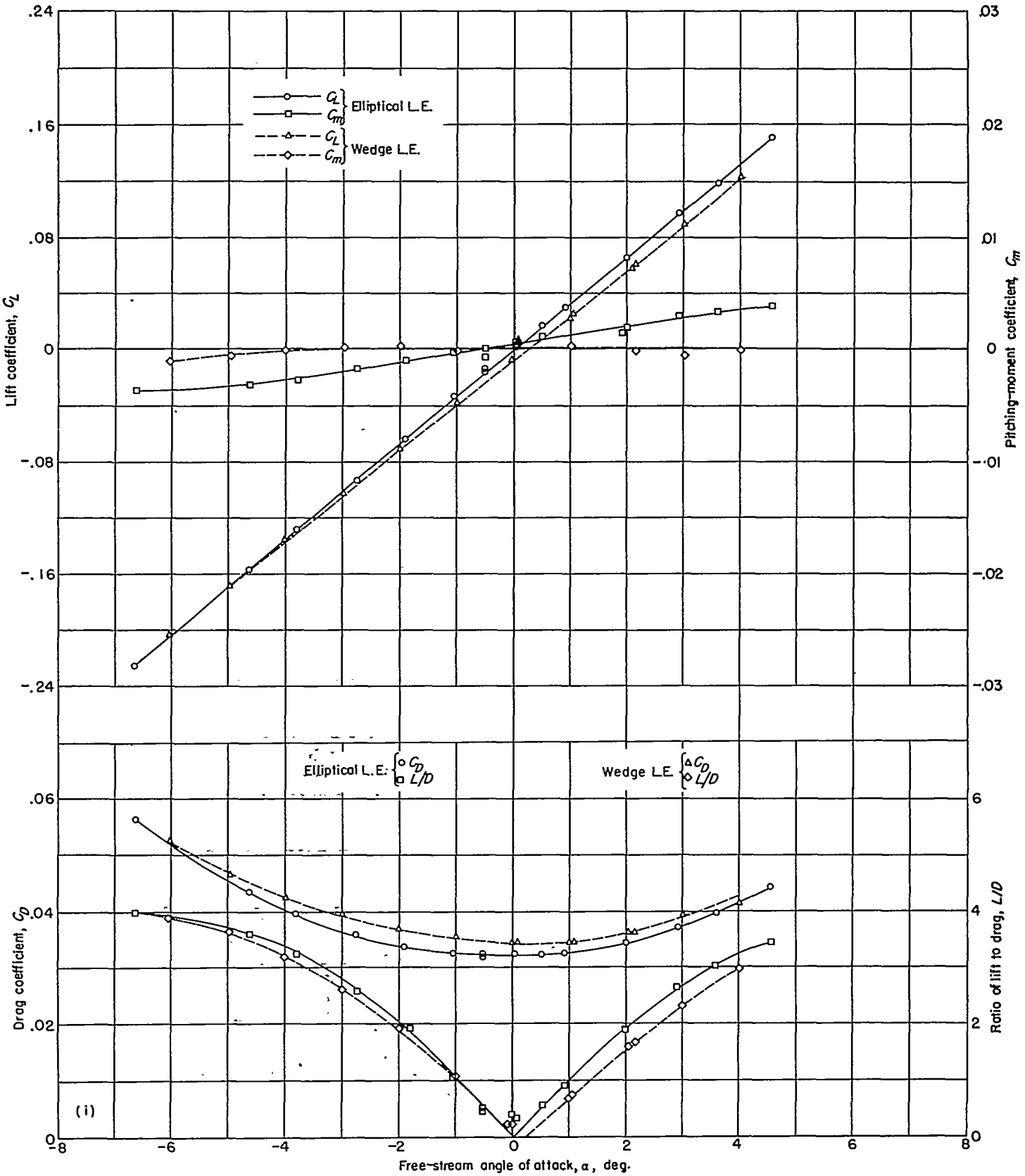

(i) Wing 9. $w=1.280$; $R=0.7\times10^6$.

FIGURE 6.—Continued.

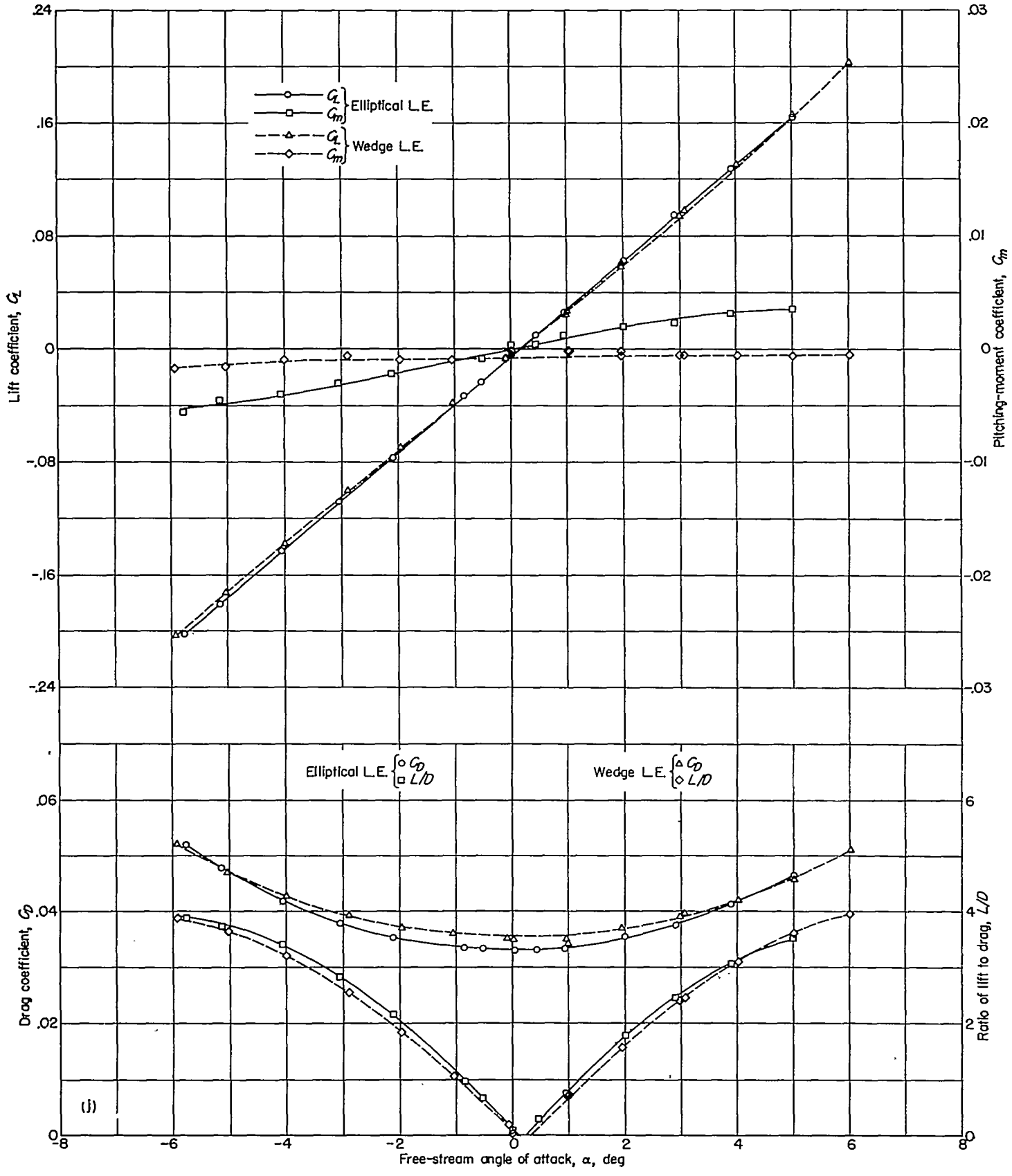

(j) Wing 10. $w=1.371$; $R=0.66\times10^6$.

FIGURE 6.—Continued.

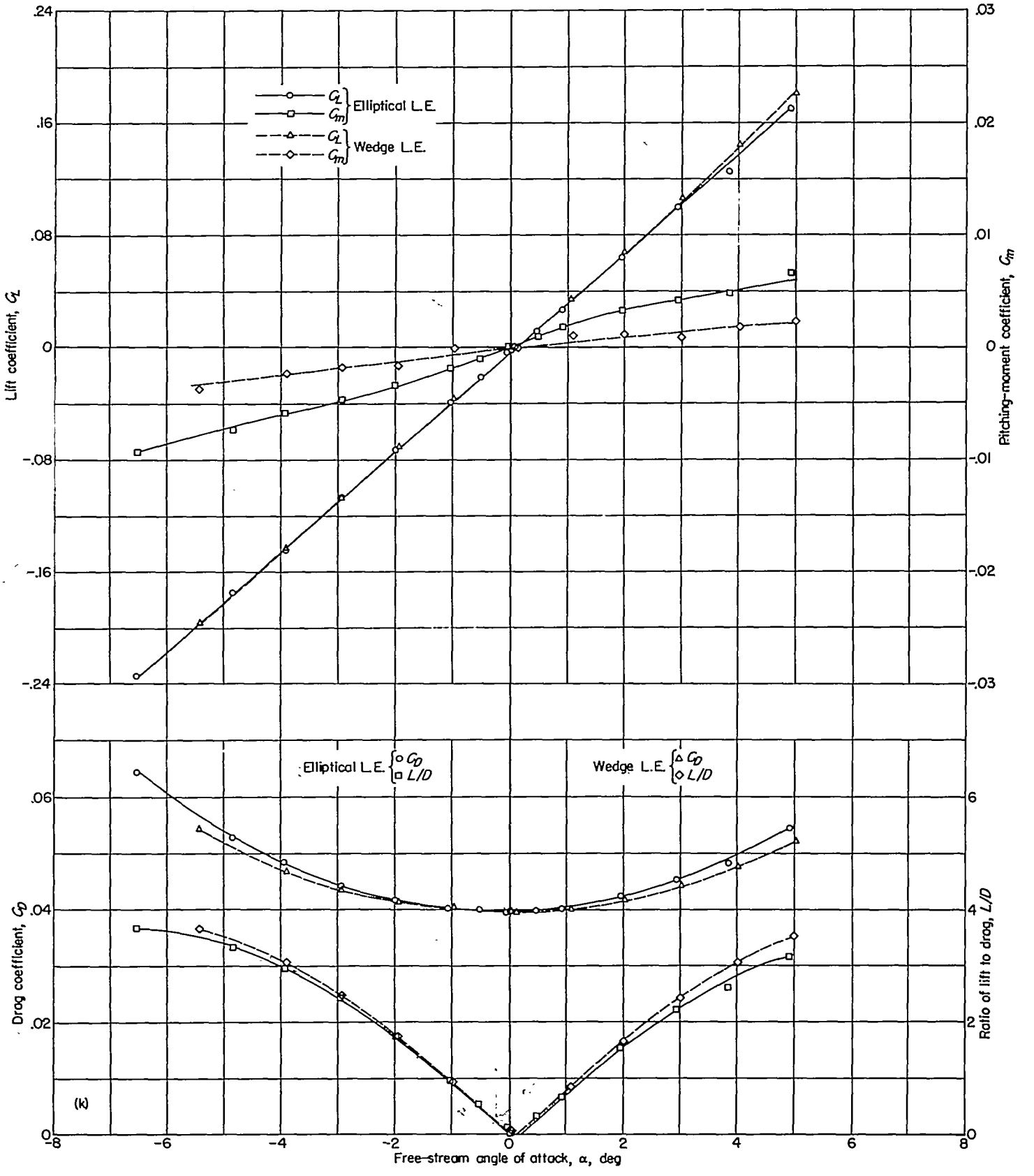

(k) Wing 11. $w=1.647$; $R=0.57\times10^6$.

FIGURE 6.—Concluded

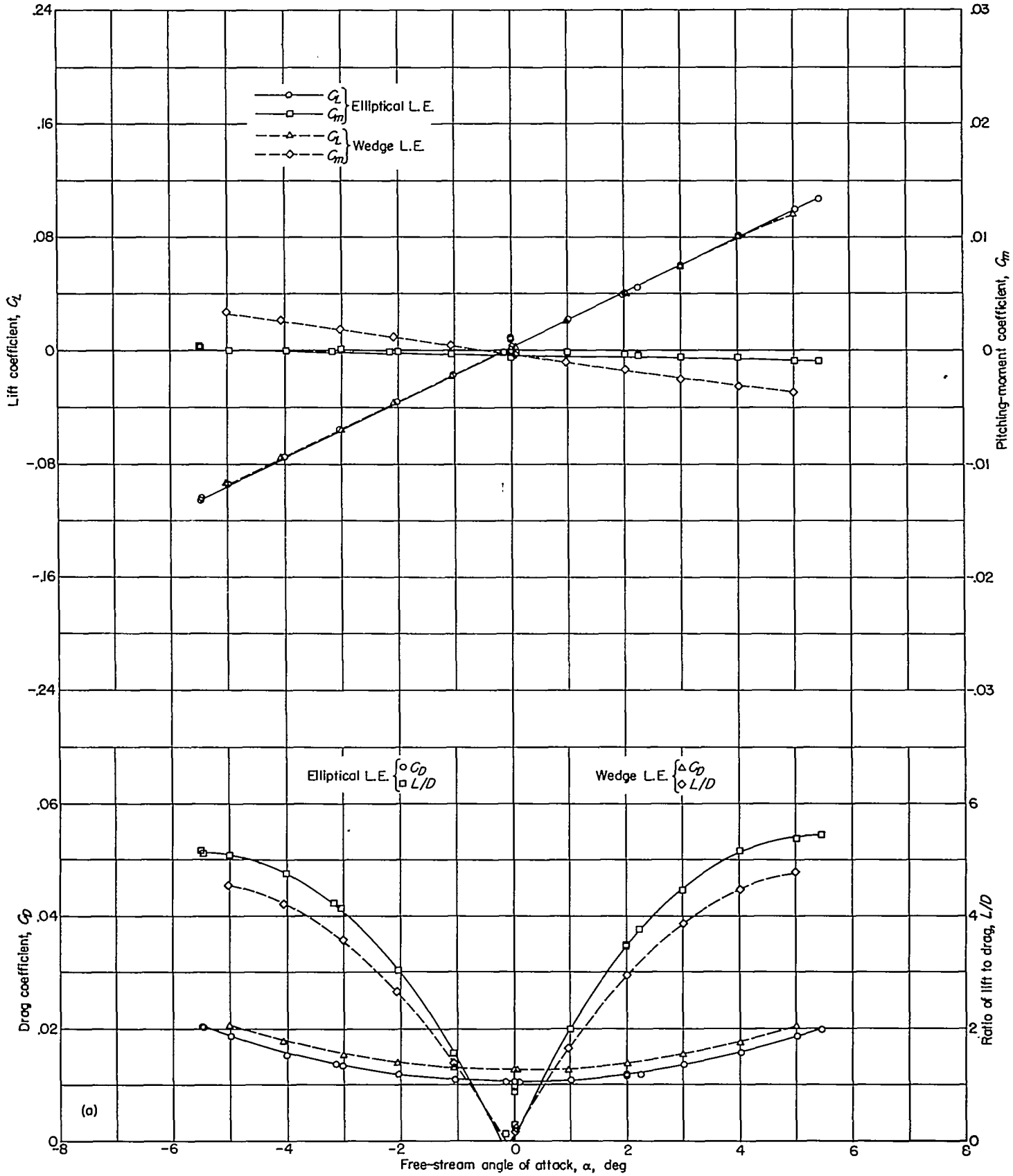

(a) Wing 1. $w=0.382$; $R=1.00\times10^6$.

FIGURE 7.—Aerodynamic characteristics of 8-percent-thick triangular wings at $M=2.40$.

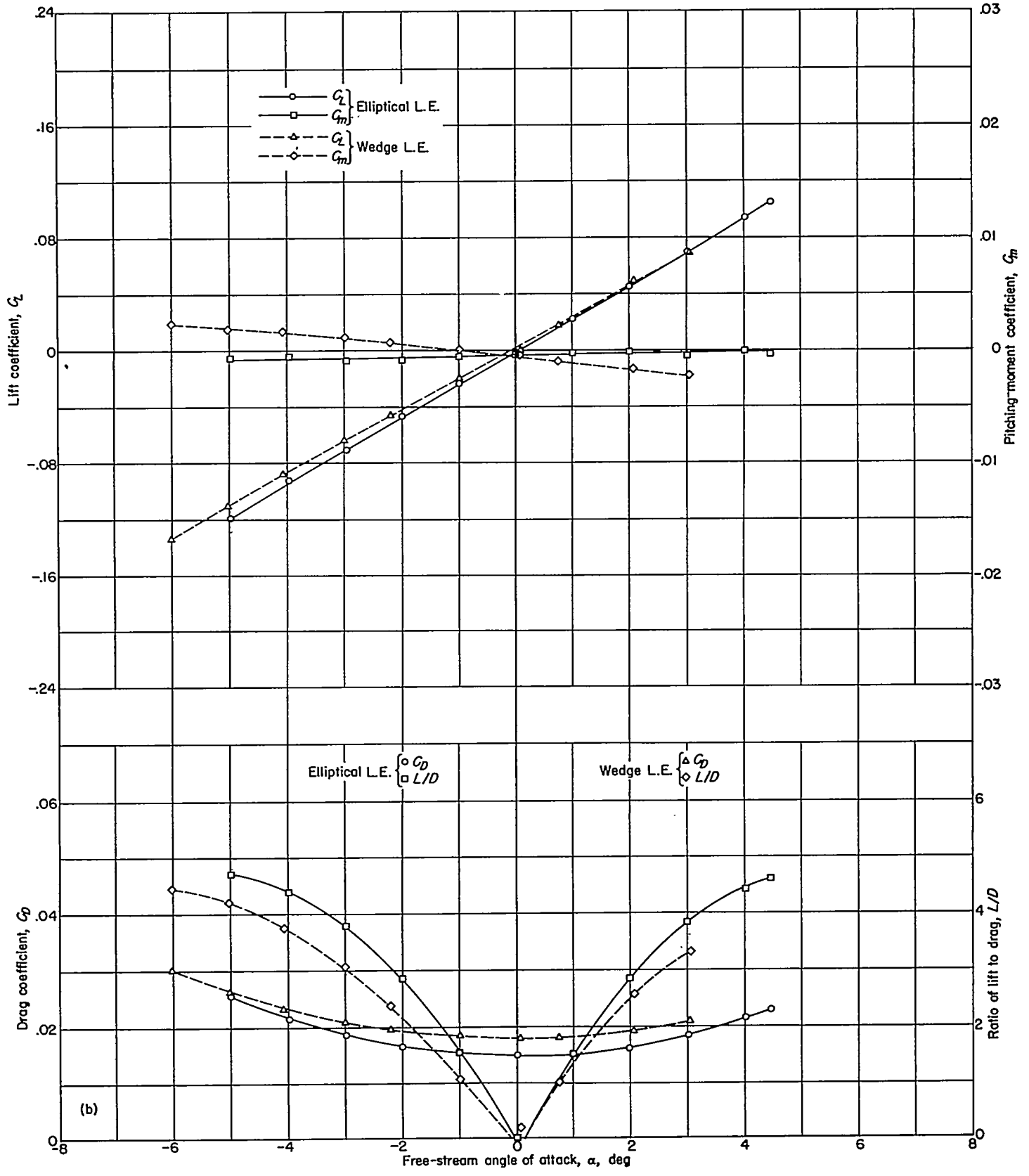

(b) Wing 2. $w=0.705$; $R=1.00\times10^6$.

FIGURE 7.—Continued.

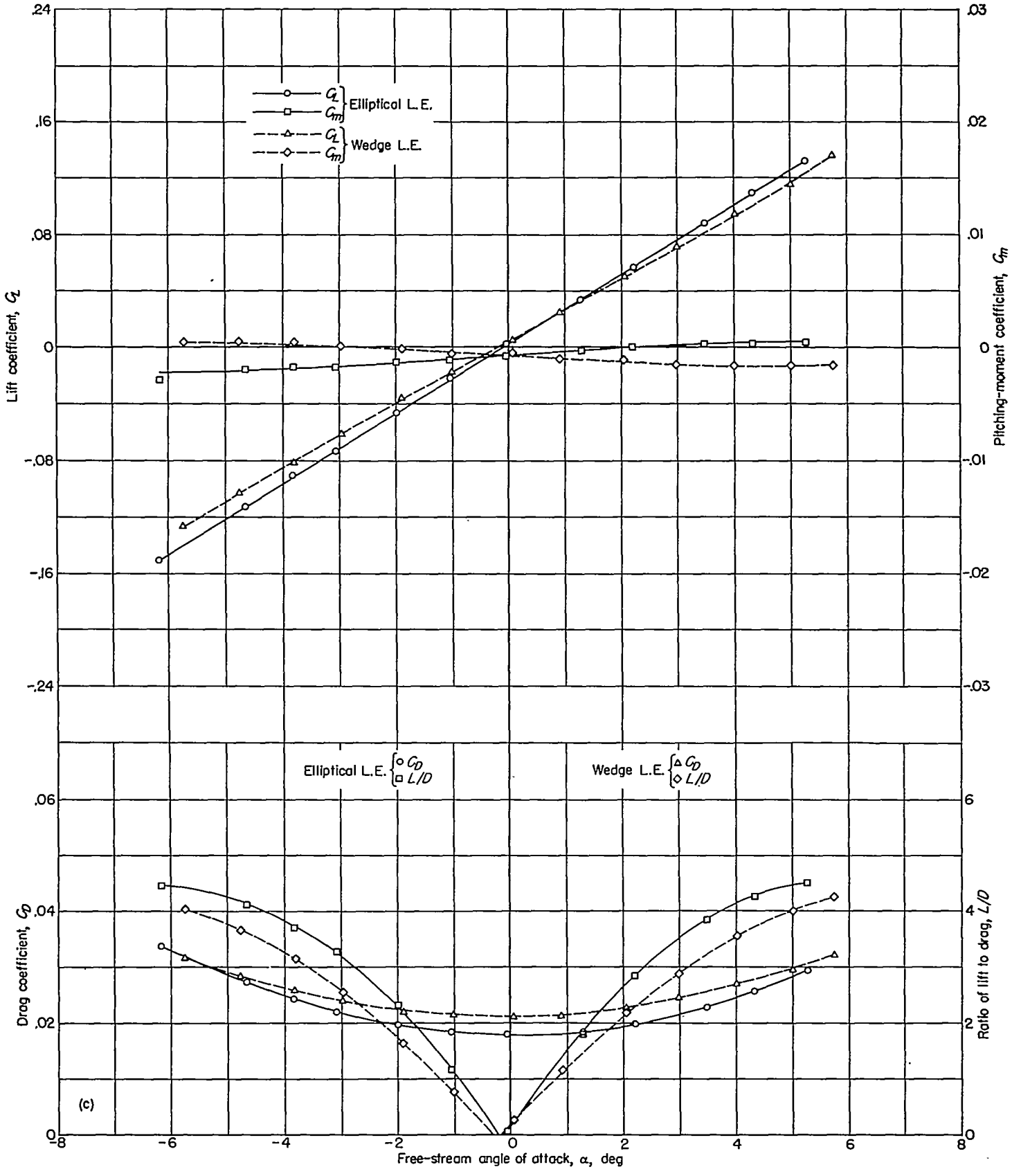

(c) Wing 3. $w=0.880$; $R=0.99\times10^6$.

FIGURE 7.—Continued.

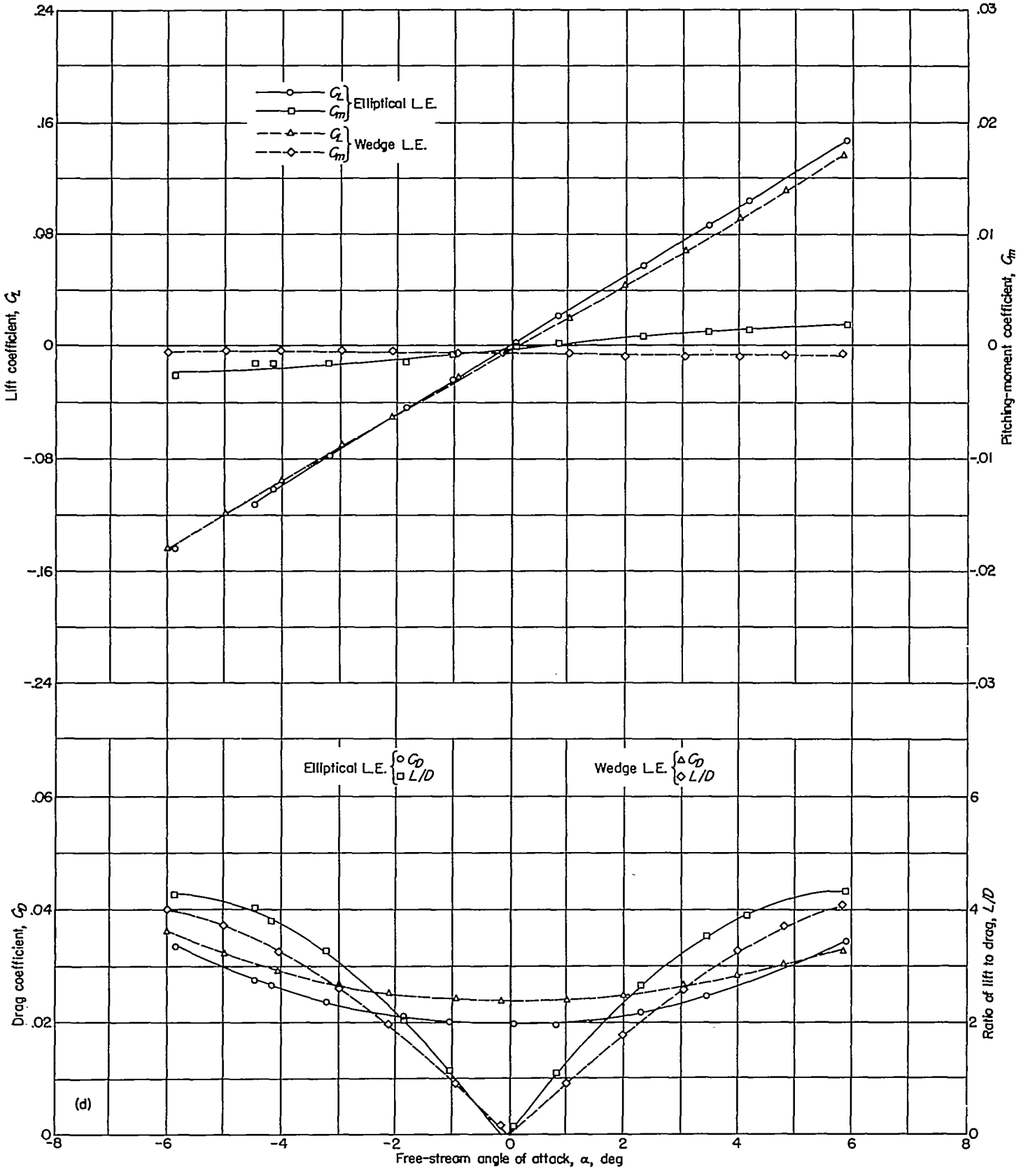

(d) Wing 4. $w=1.017$; $R=0.86\times10^6$.

FIGURE 7.—Continued.

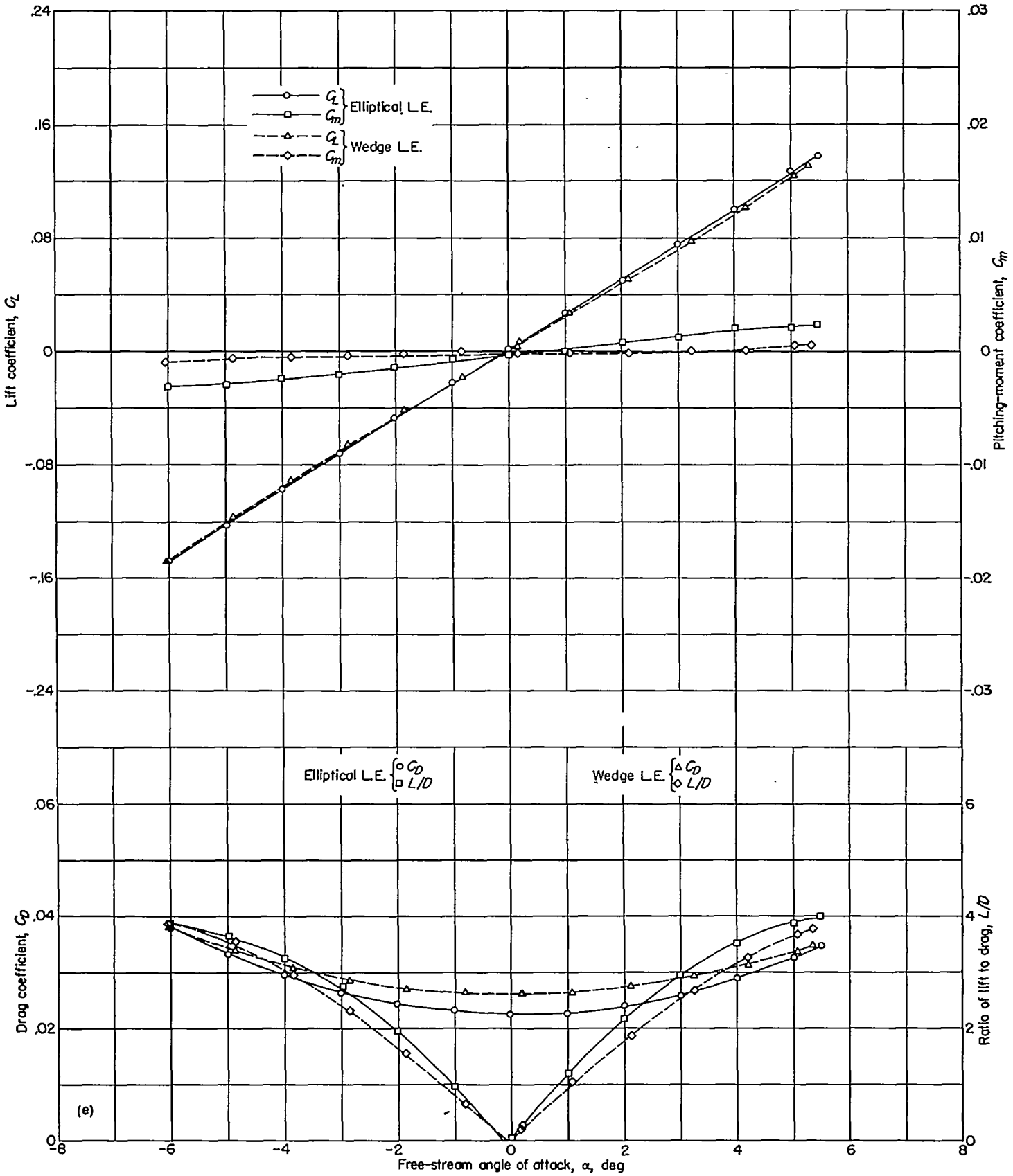

(e) Wing 5. $w=1.156$; $R=0.77\times10^6$.

FIGURE 7.—Continued.

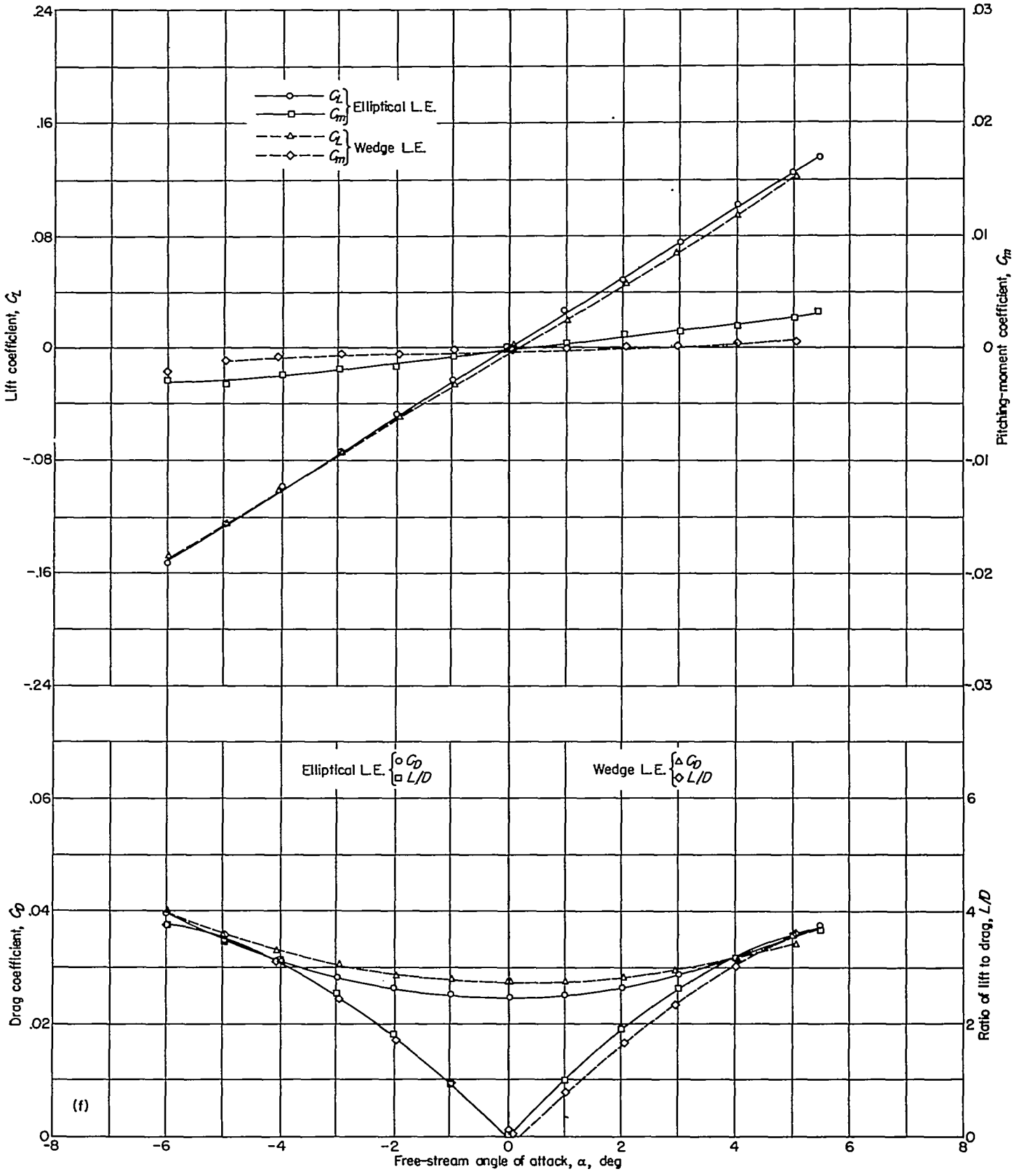

(f) Wing 6. $w=1.252$; $R=0.72\times10^6$.

FIGURE 7.—Continued.

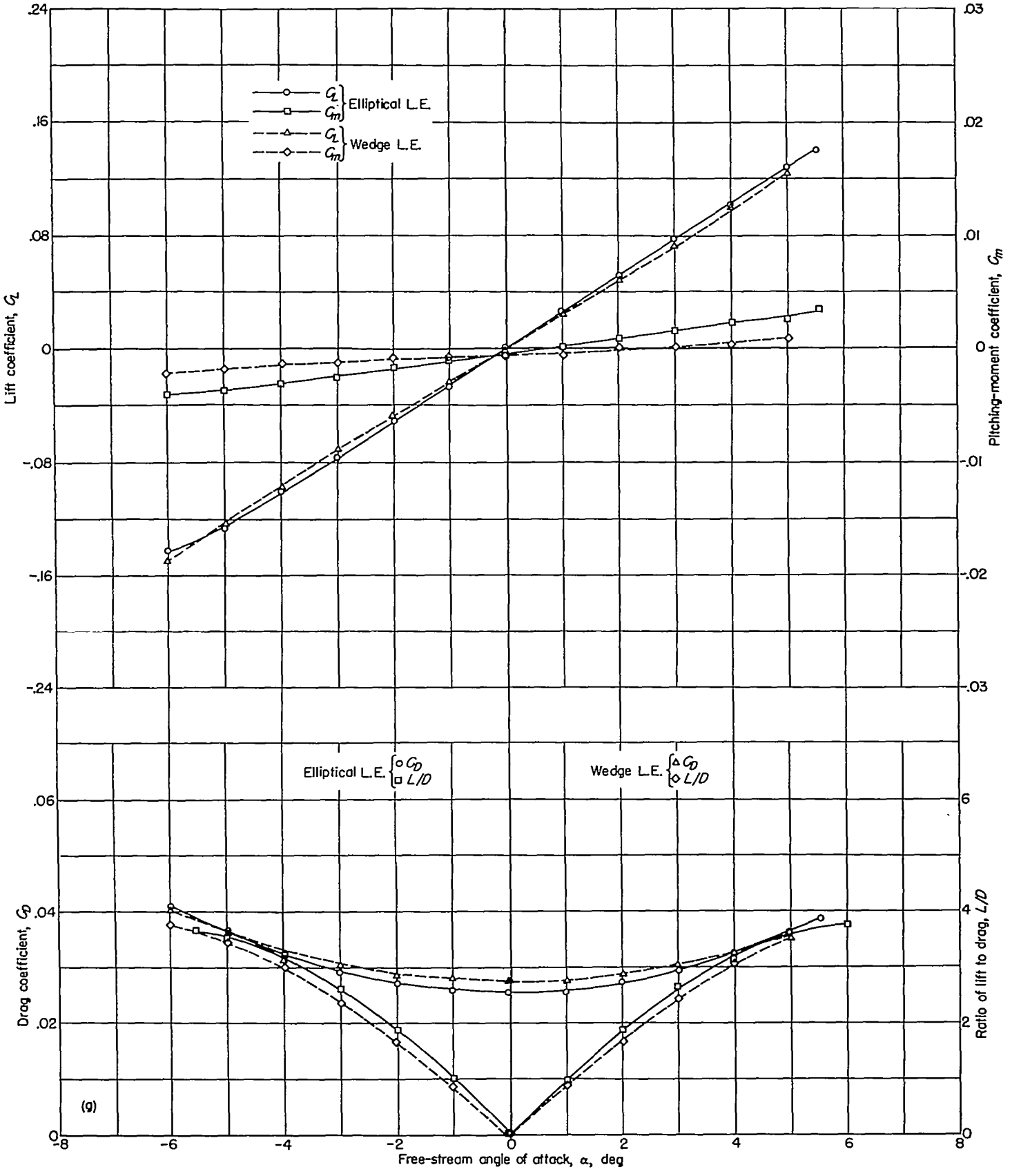

(g) Wing 7. $w=1.371$; $R=0.67\times10^6$.

FIGURE 7.—Continued.

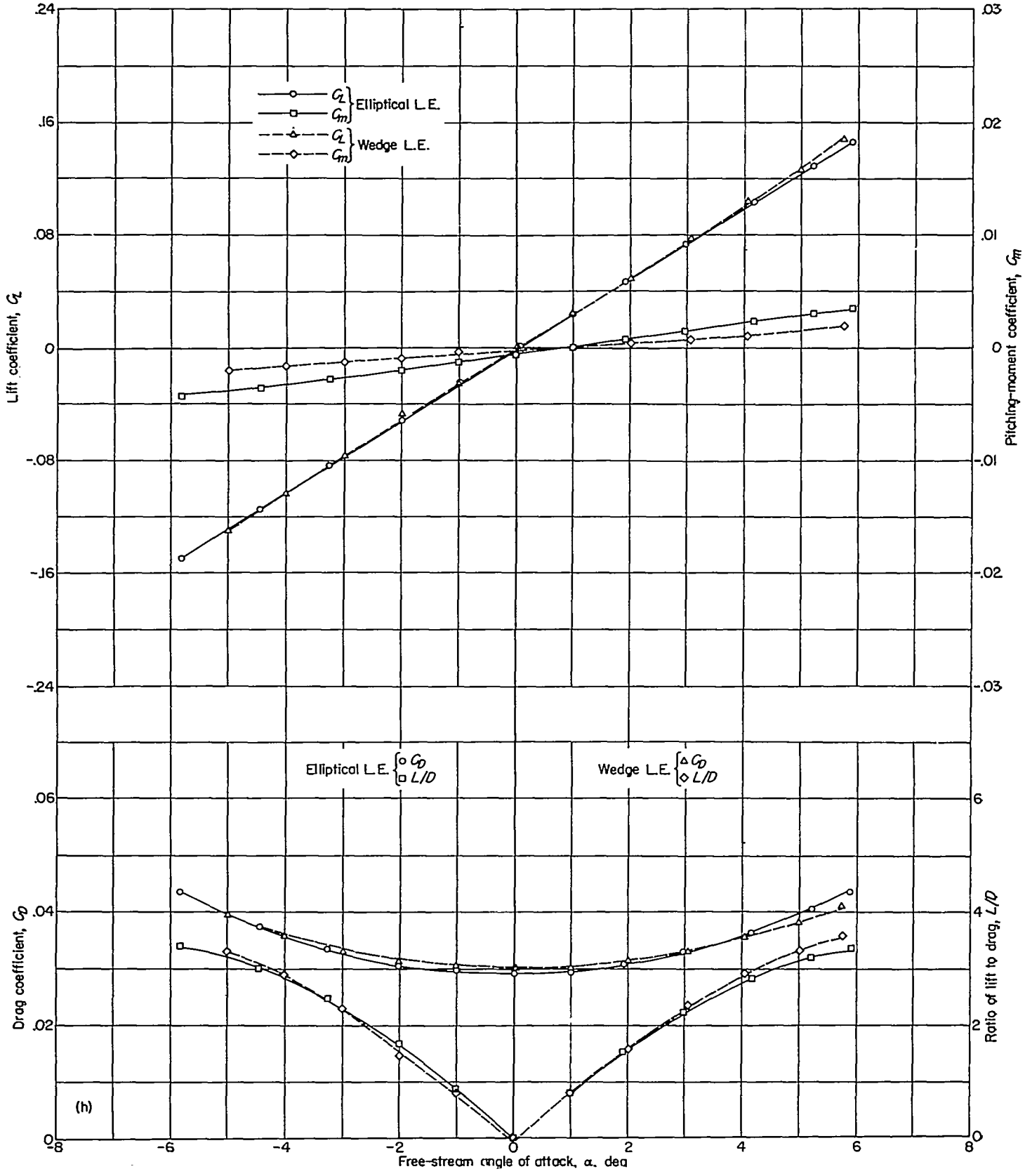

(h) Wing 8, $w=1.540$; $R=0.62\times10^6$

FIGURE 7.—Continued

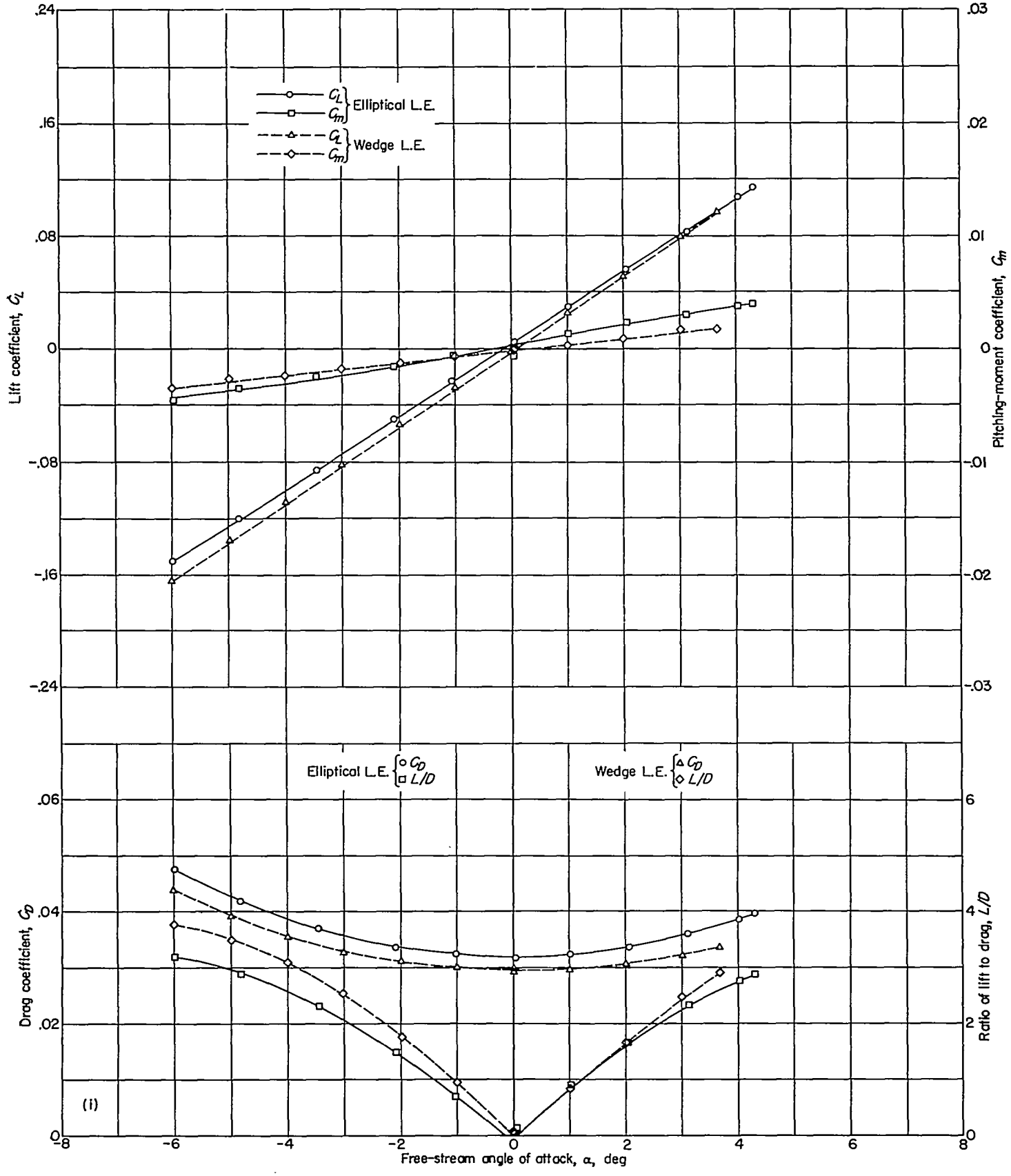

(i) Wing 9. $w=1.705$; $R=0.56\times10^6$.

FIGURE 7.—Continued.

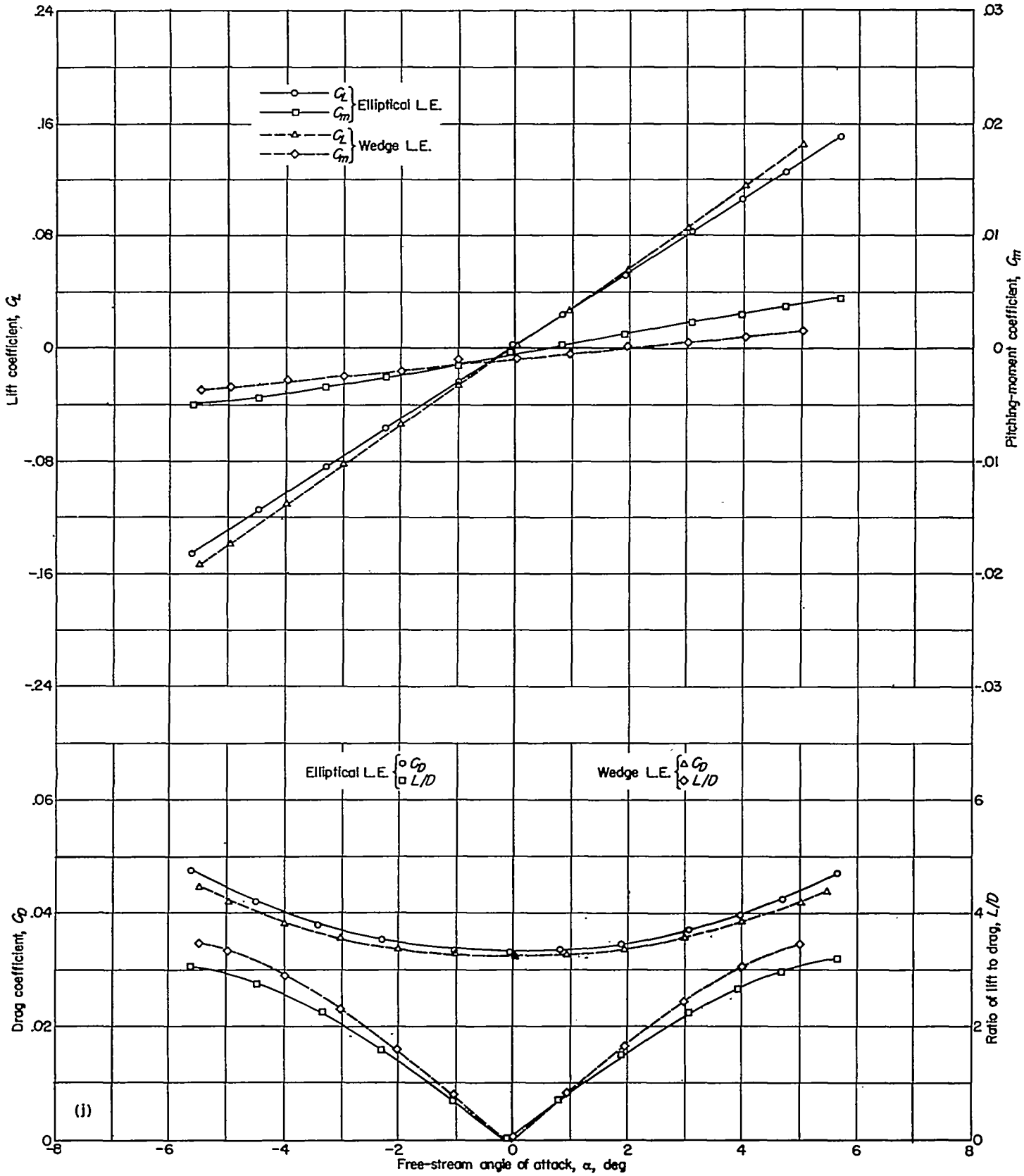

(j) Wing 10. $w=1.826$; $R=0.53\times10^6$.

FIGURE 7.—Continued.

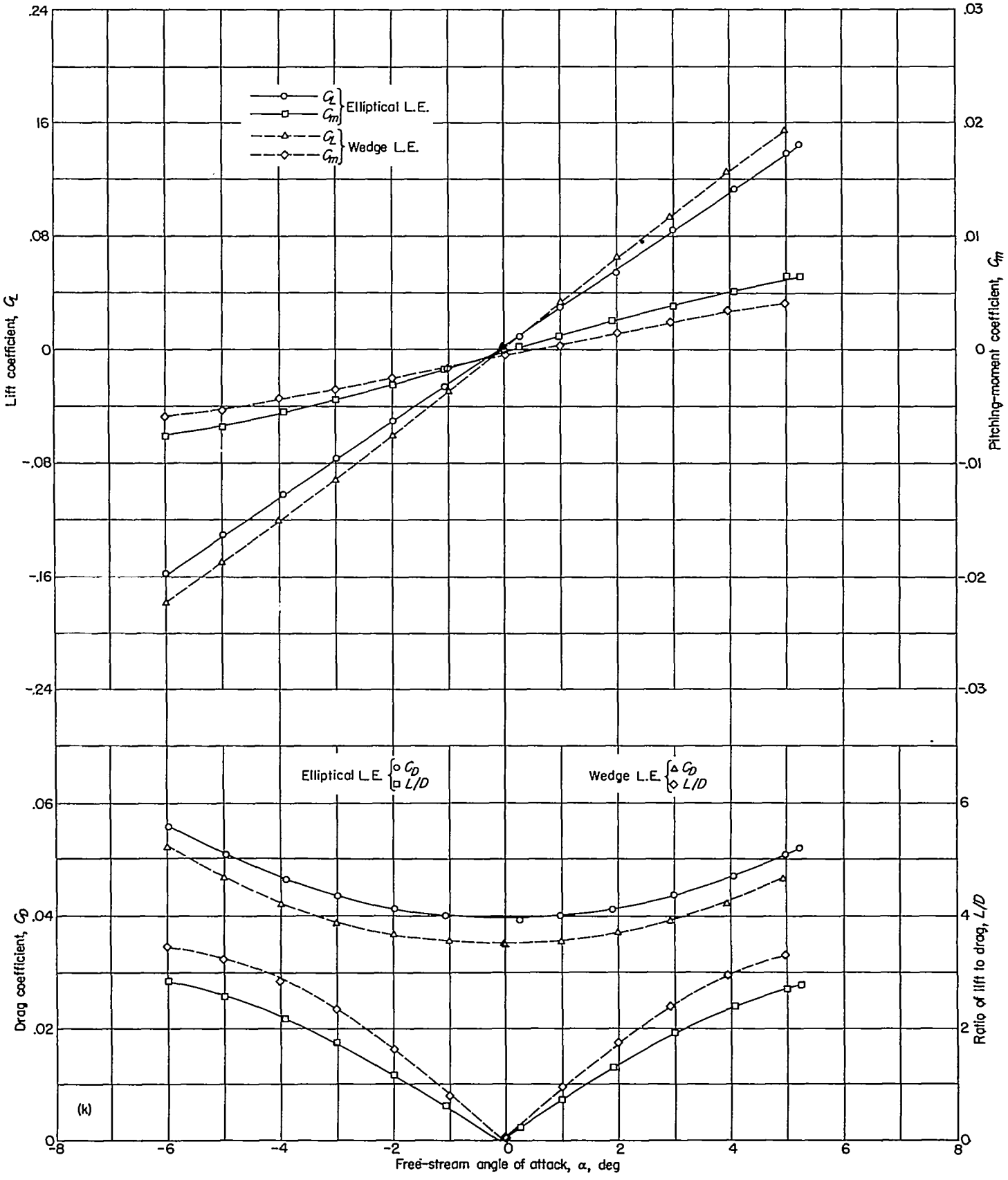

(k) Wing 11. $w=2.193$; $R=0.46\times10^6$.

FIGURE 7.—Concluded.

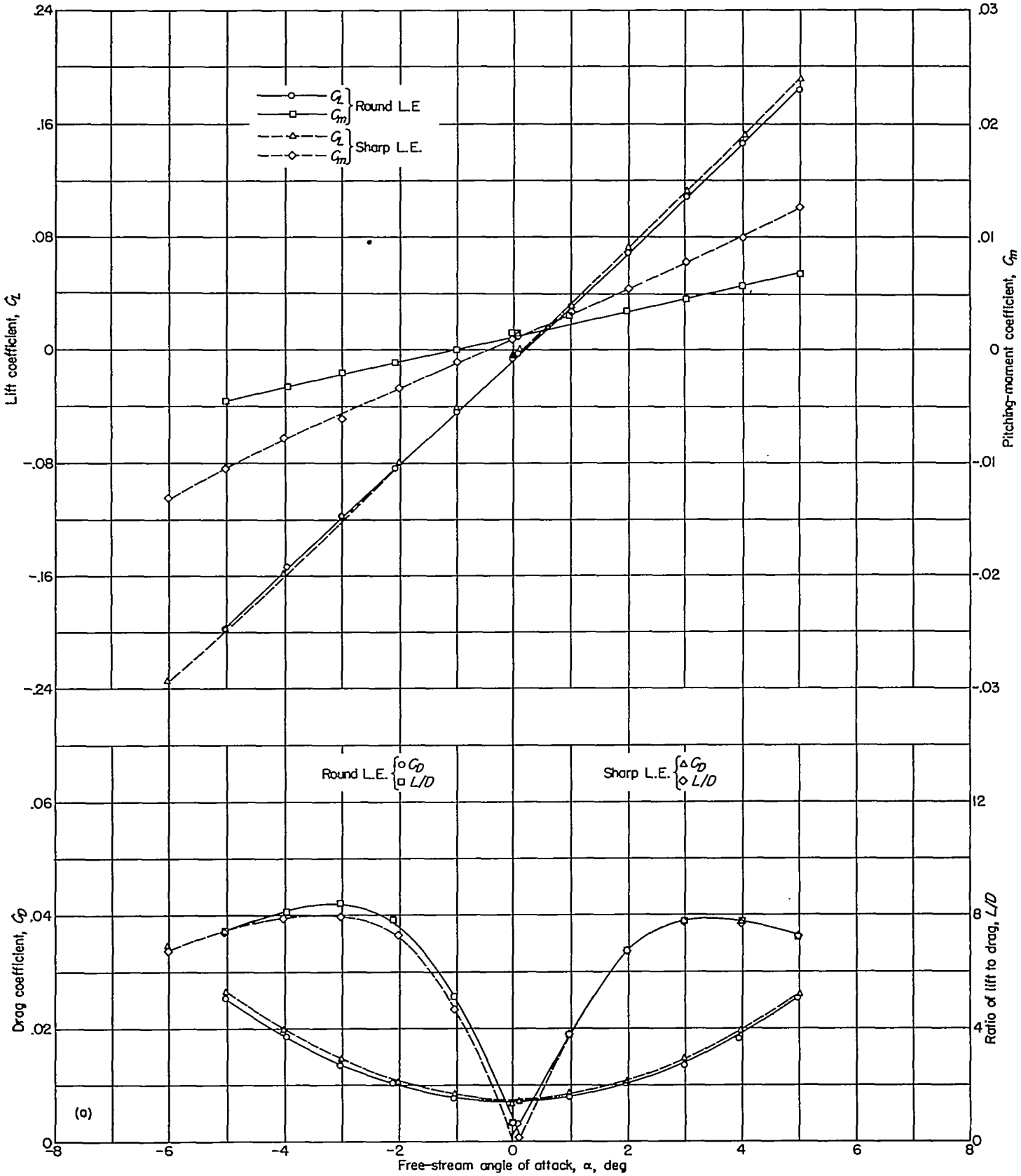

(a) Wing 1. $R=1.06\times10^6$ for round-leading-edge wing.

FIGURE 8.—Aerodynamic characteristics of flat-plate triangular wings at $M=1.92$.

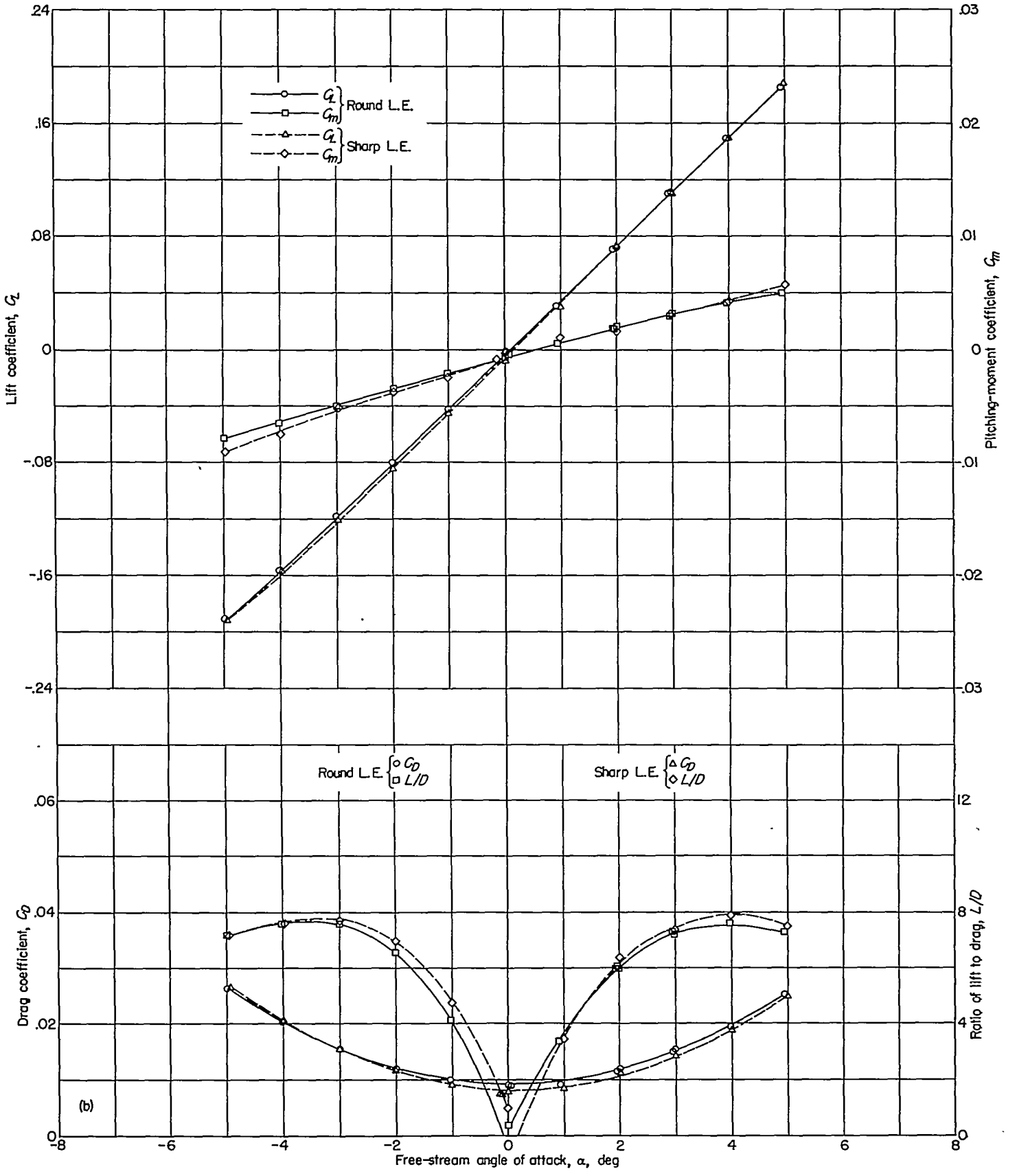

(b) Wing 2. $R=0.85\times10^6$ for round-leading-edge wing.

FIGURE 8.—Continued.

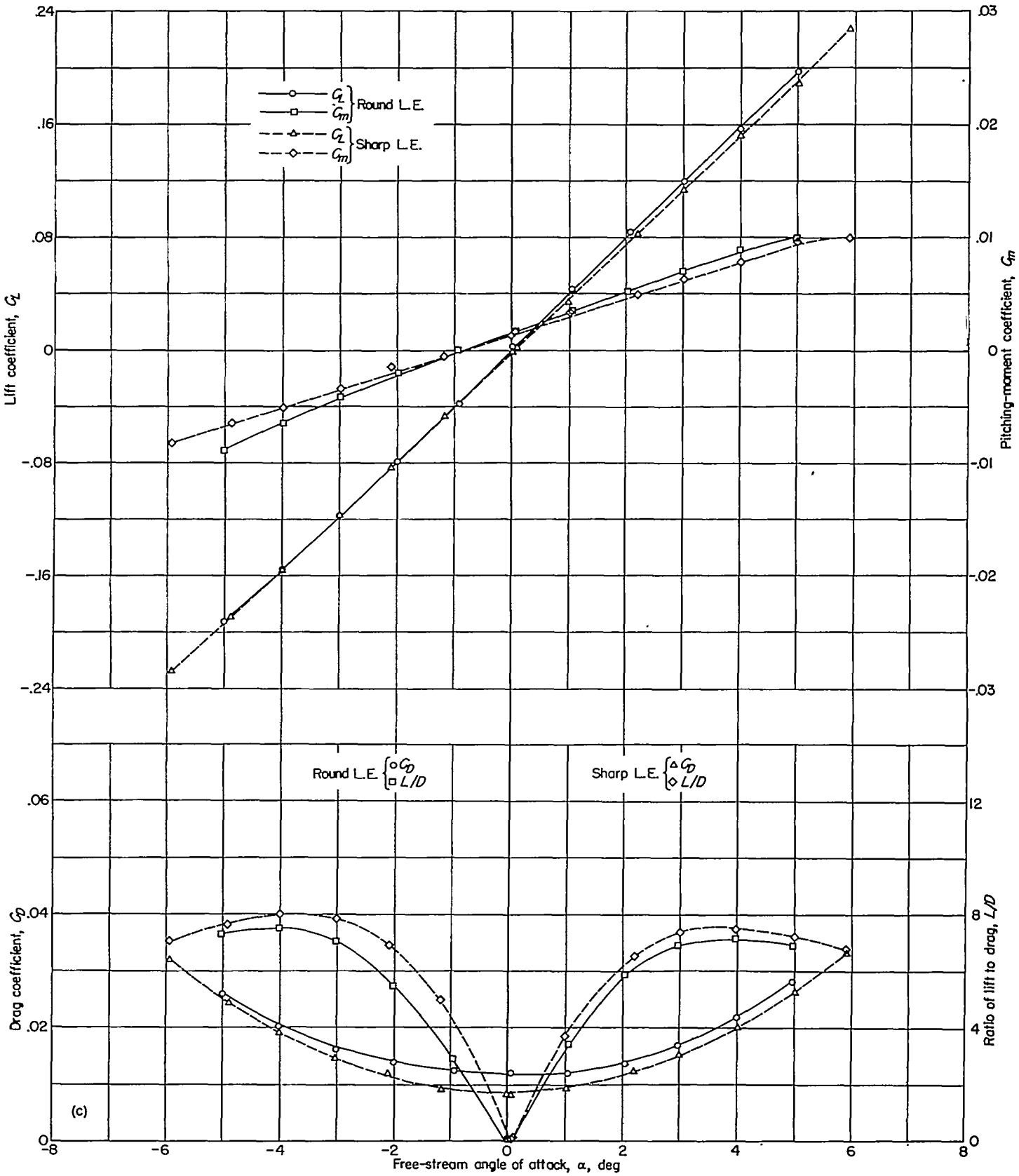

(c) Wing 3. $R=0.77\times10^6$ for round-leading-edge wing.

FIGURE 8.—Continued.

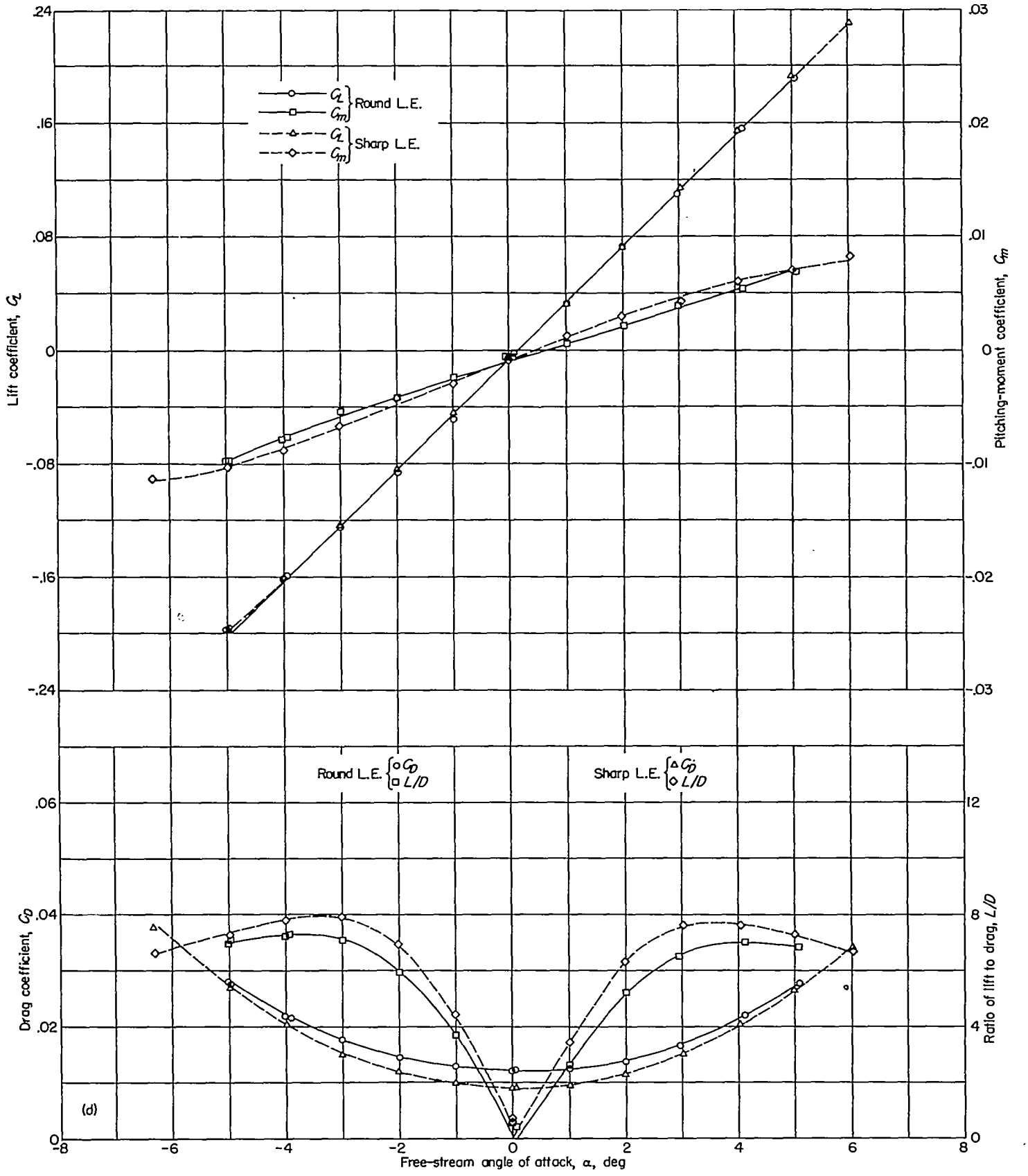

(d) Wing 4. $R=0.75\times10^6$ for round-leading-edge wing.

FIGURE 8.—Concluded.

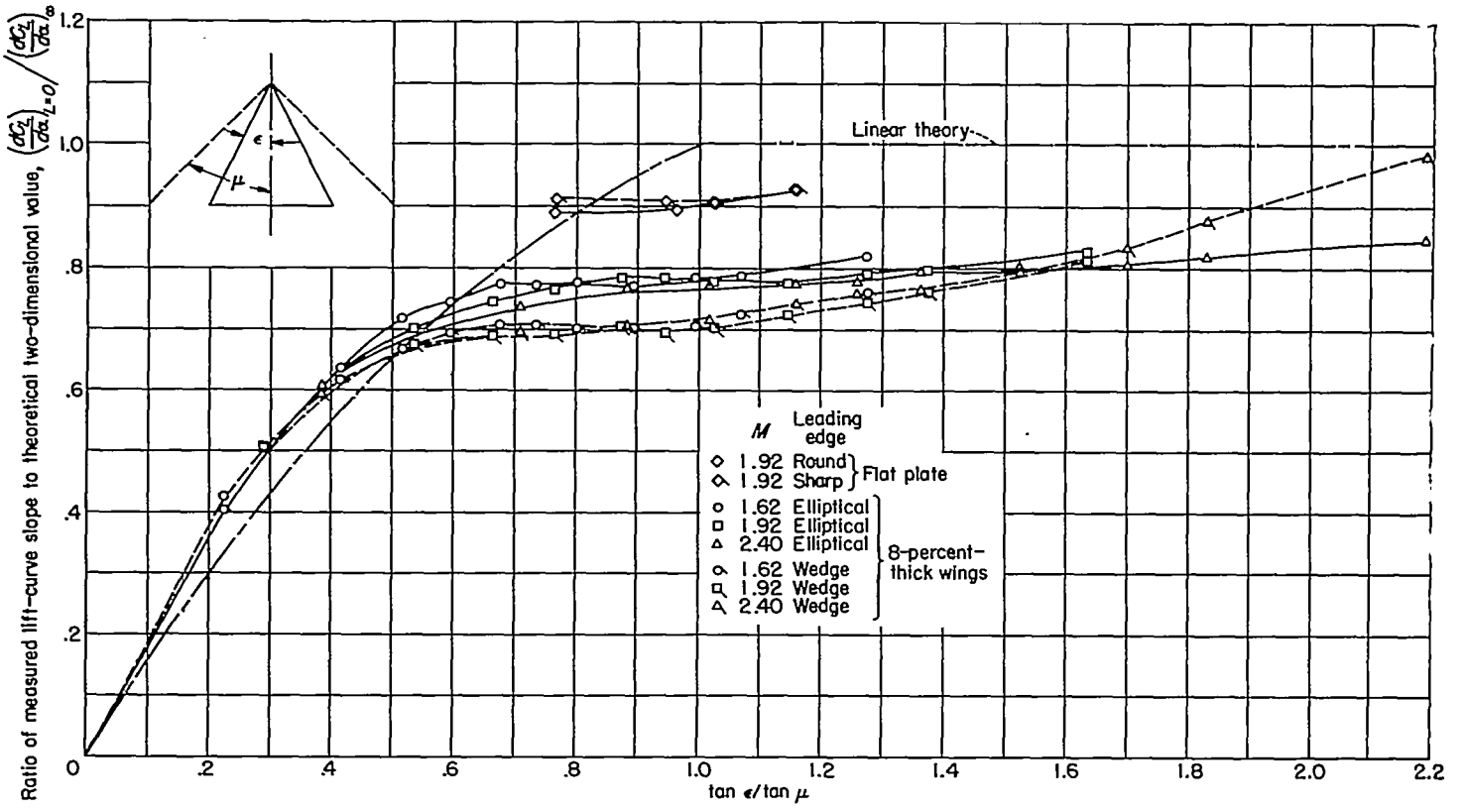

FIGURE 9.—Lift-curve slopes for 8-percent-thick triangular-wing series and flat-plate triangular wings, and comparison with theory.

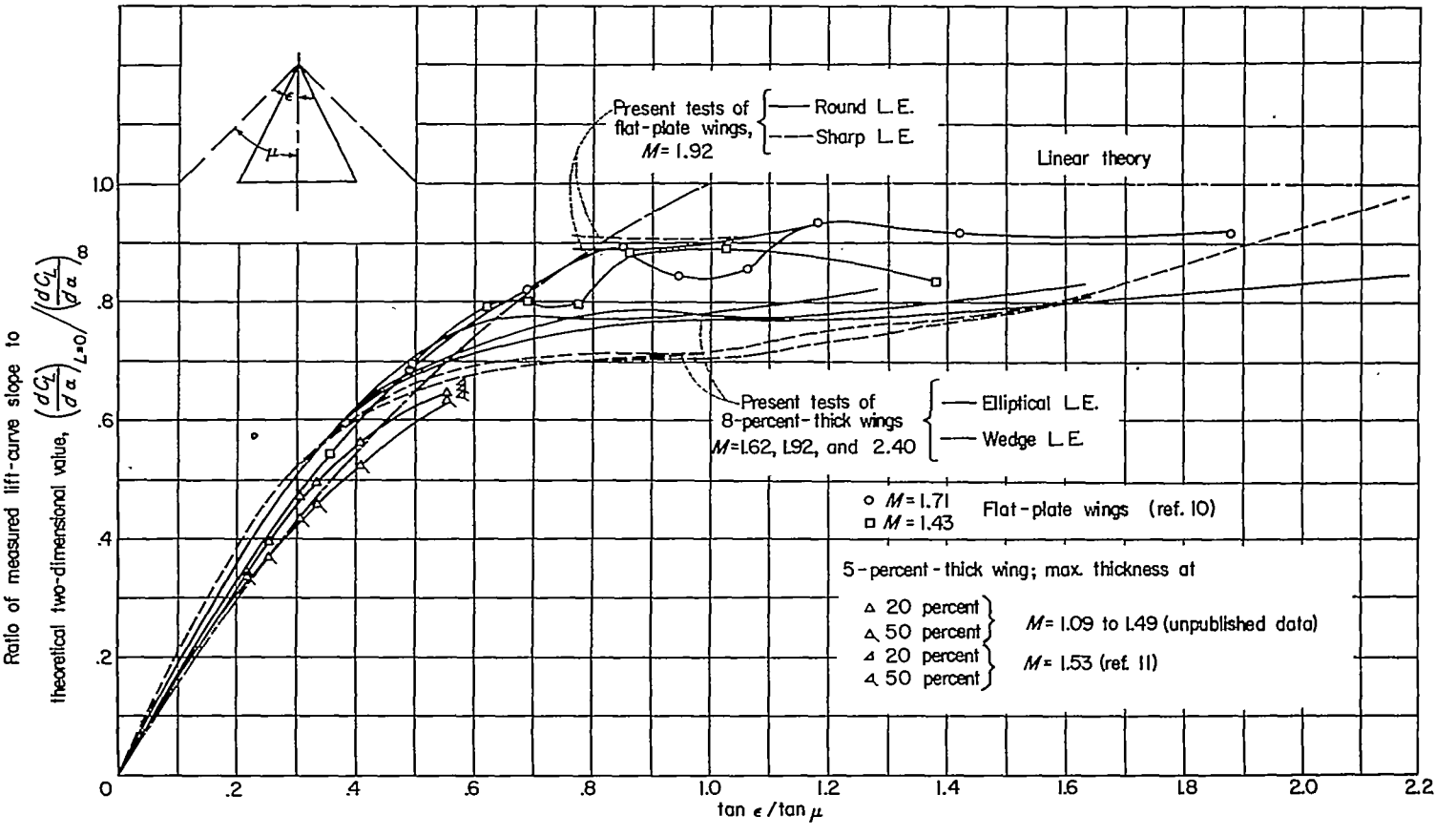

FIGURE 10.—Lift-curve slopes for triangular wings, and comparison with theory.

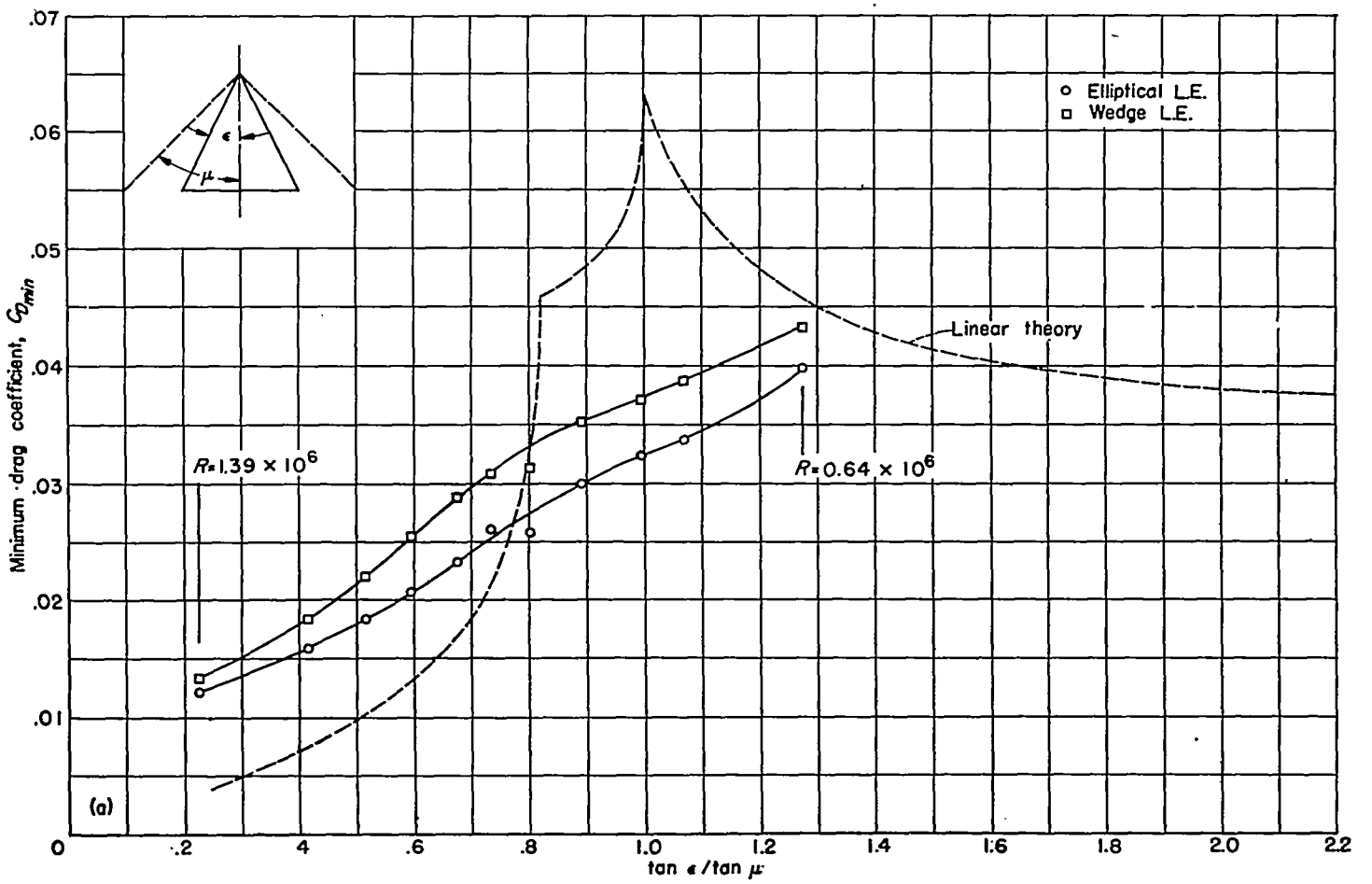

(a) $M=1.62$.

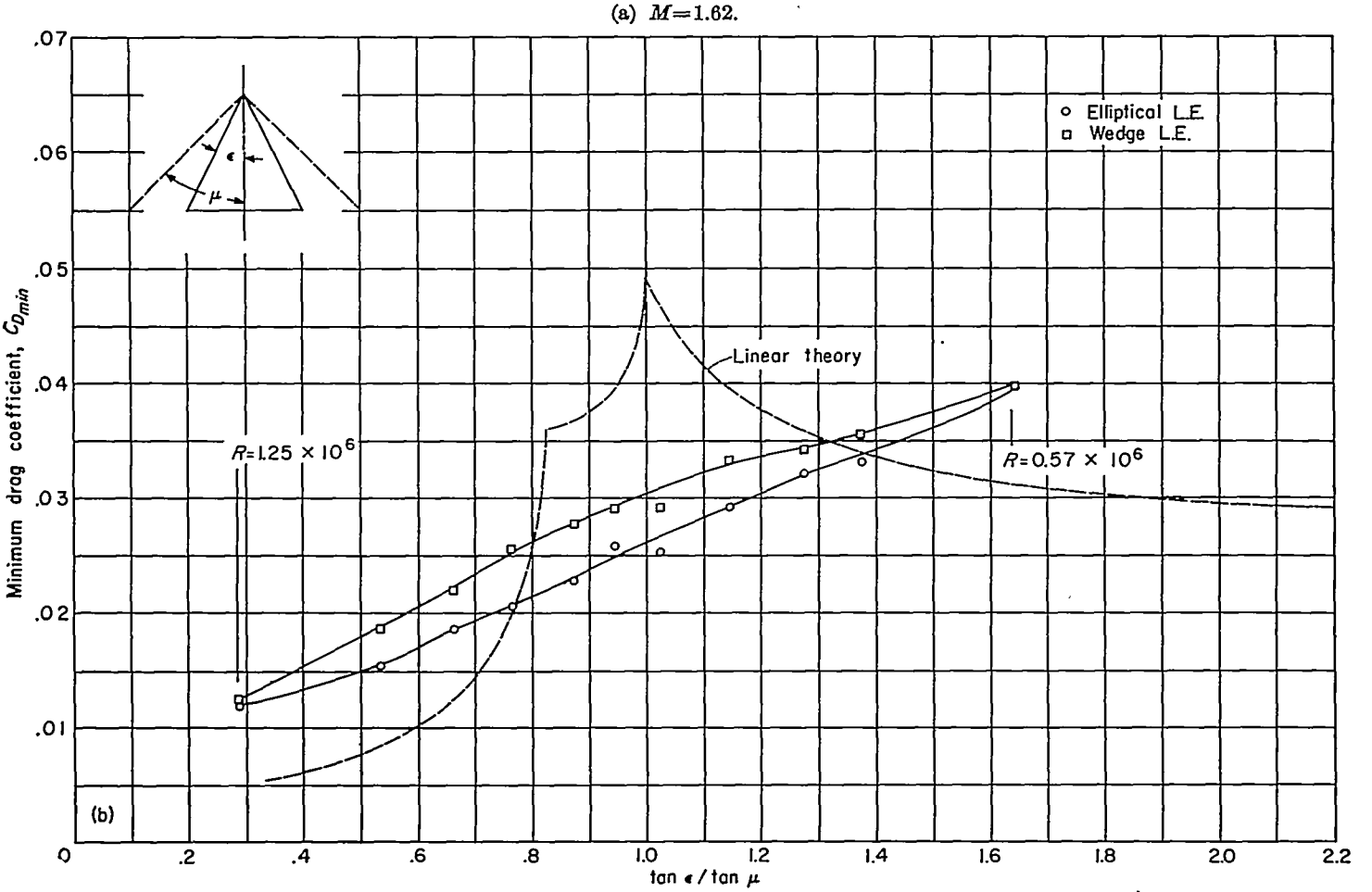

(b) $M=1.92$.

FIGURE 11.—Minimum drag coefficients for 8-percent-thick triangular-wing series, and comparison with theory.

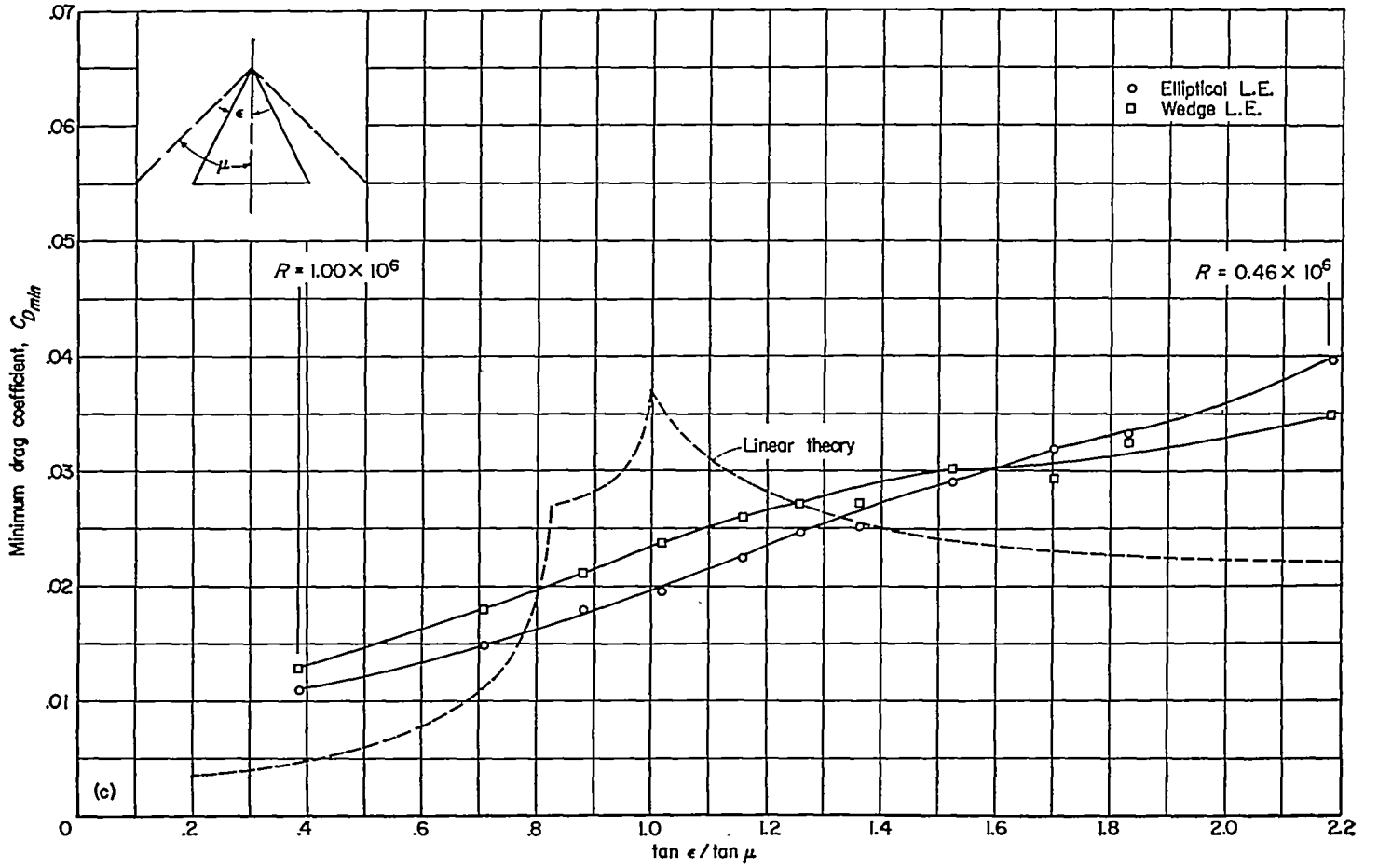

(c) $M=2.40$.

FIGURE 11.—Concluded.

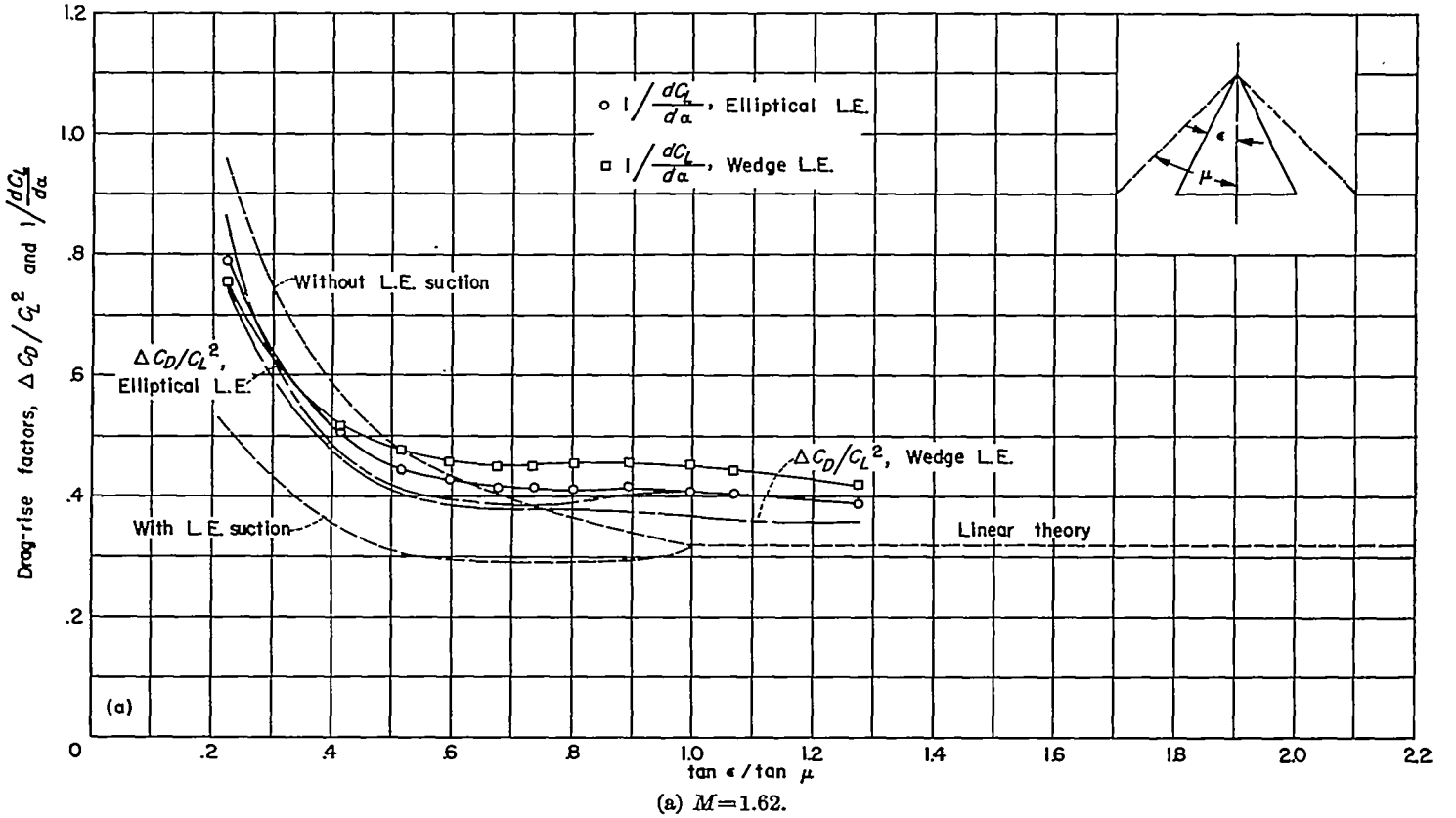

(a) $M=1.62$.

FIGURE 12.—Drag-rise factors for 8-percent-thick triangular-wing series, and comparison with theory.

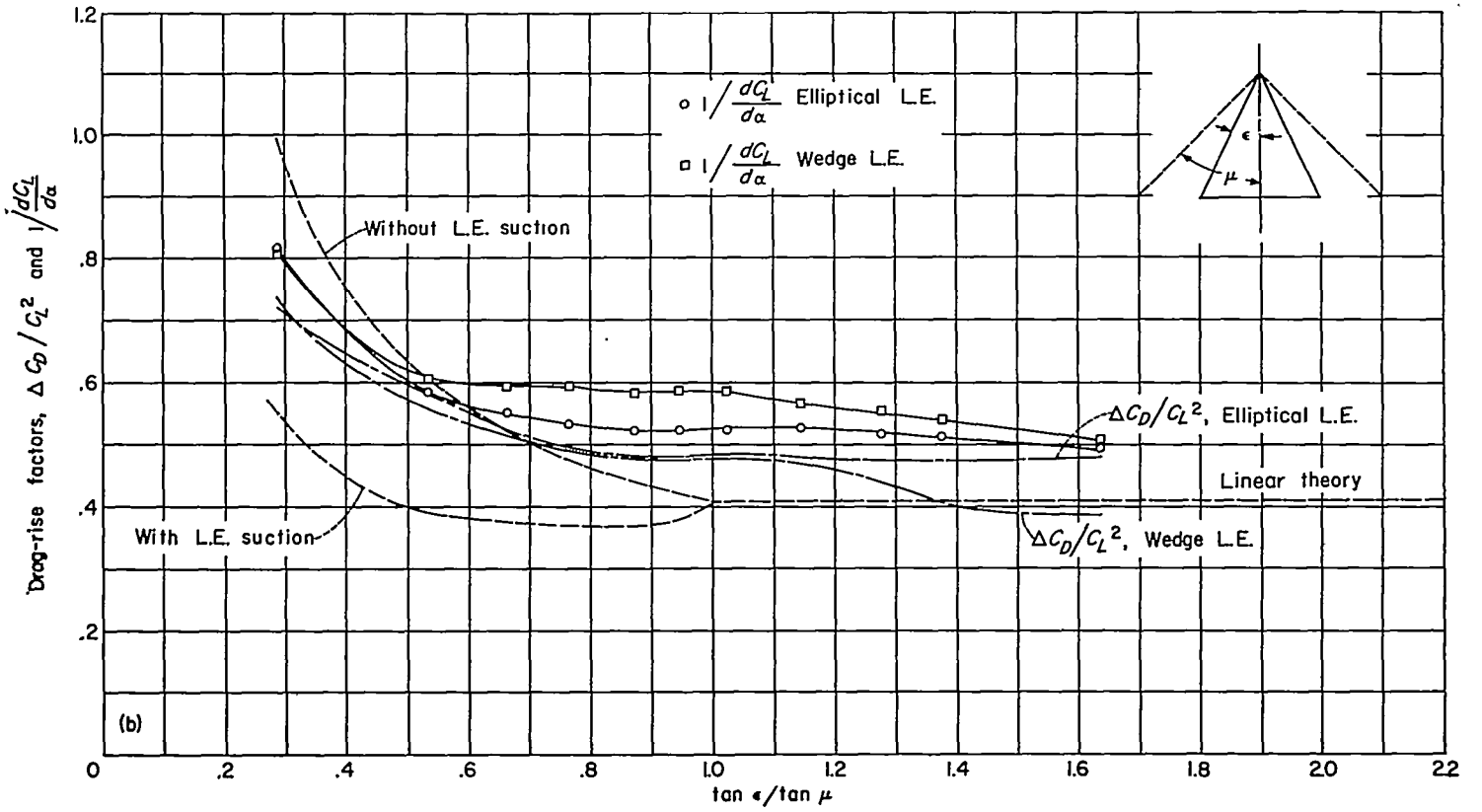

(b) $M=1.92$.

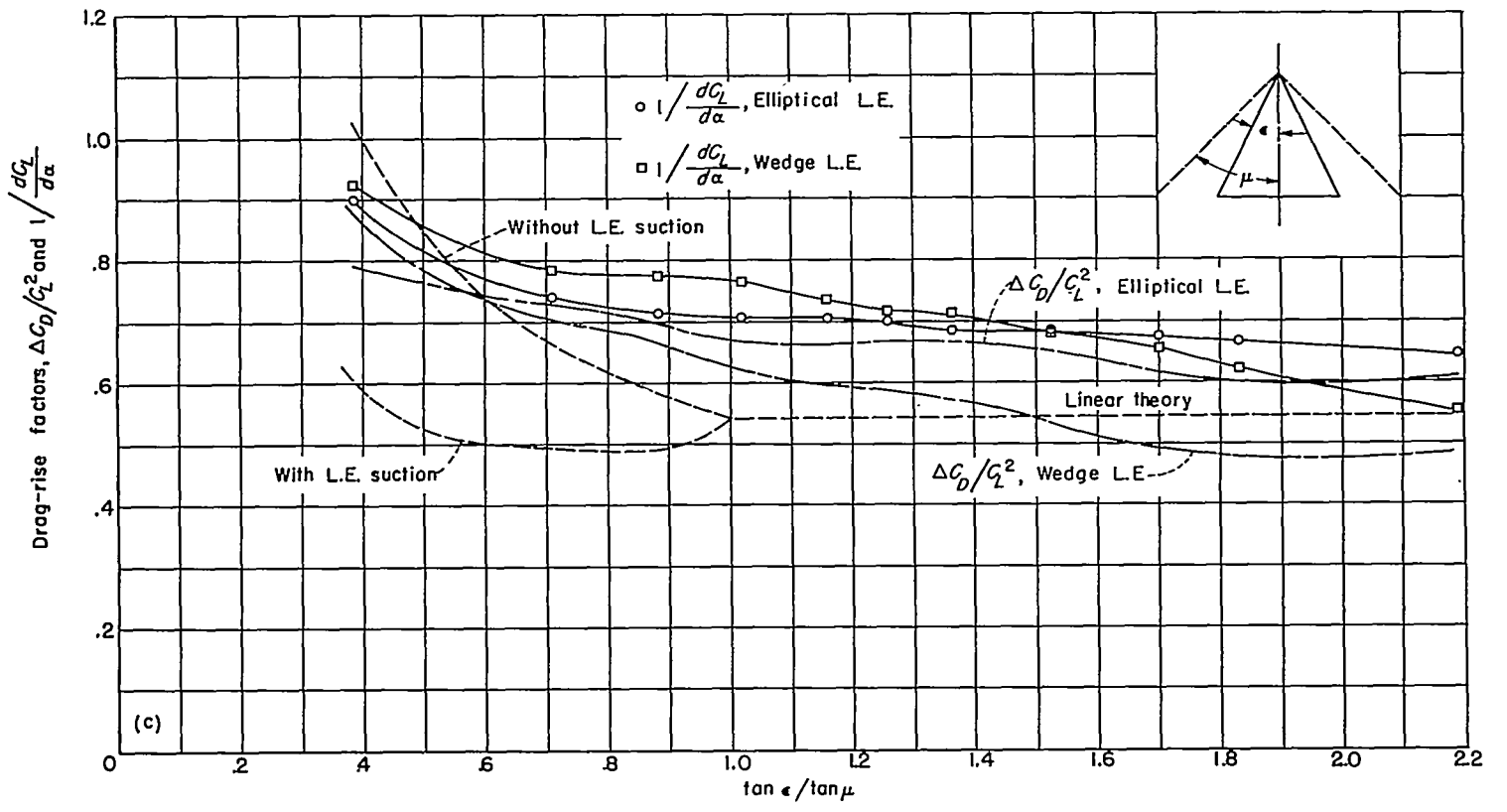

(c) $M=2.40$.

FIGURE 12.—Concluded.

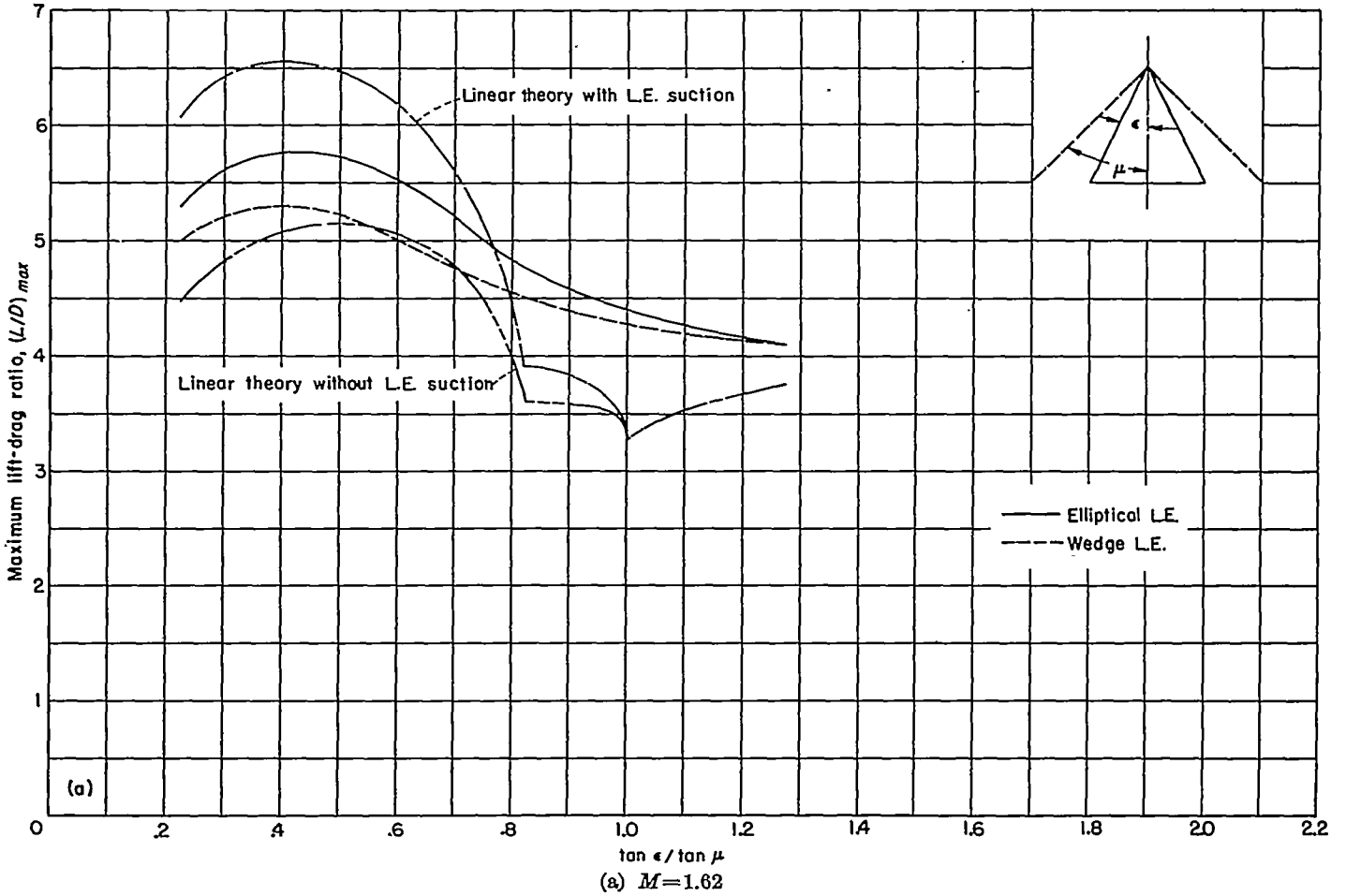

(a) $M=1.62$

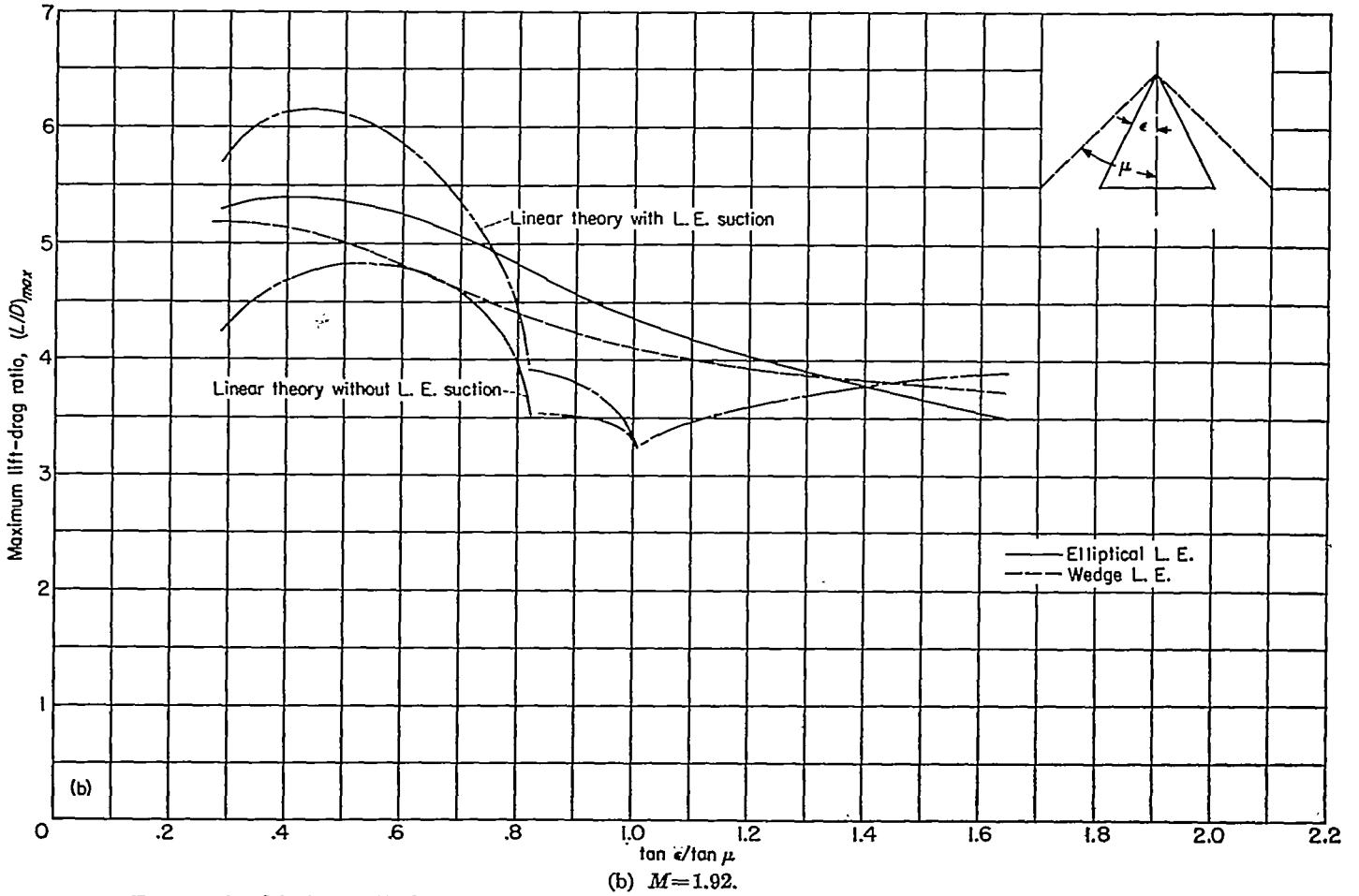

(b) $M=1.92$.

FIGURE 13.—Maximum lift-drag ratios for 8-percent-thick triangular-wing series, and comparison with theory.

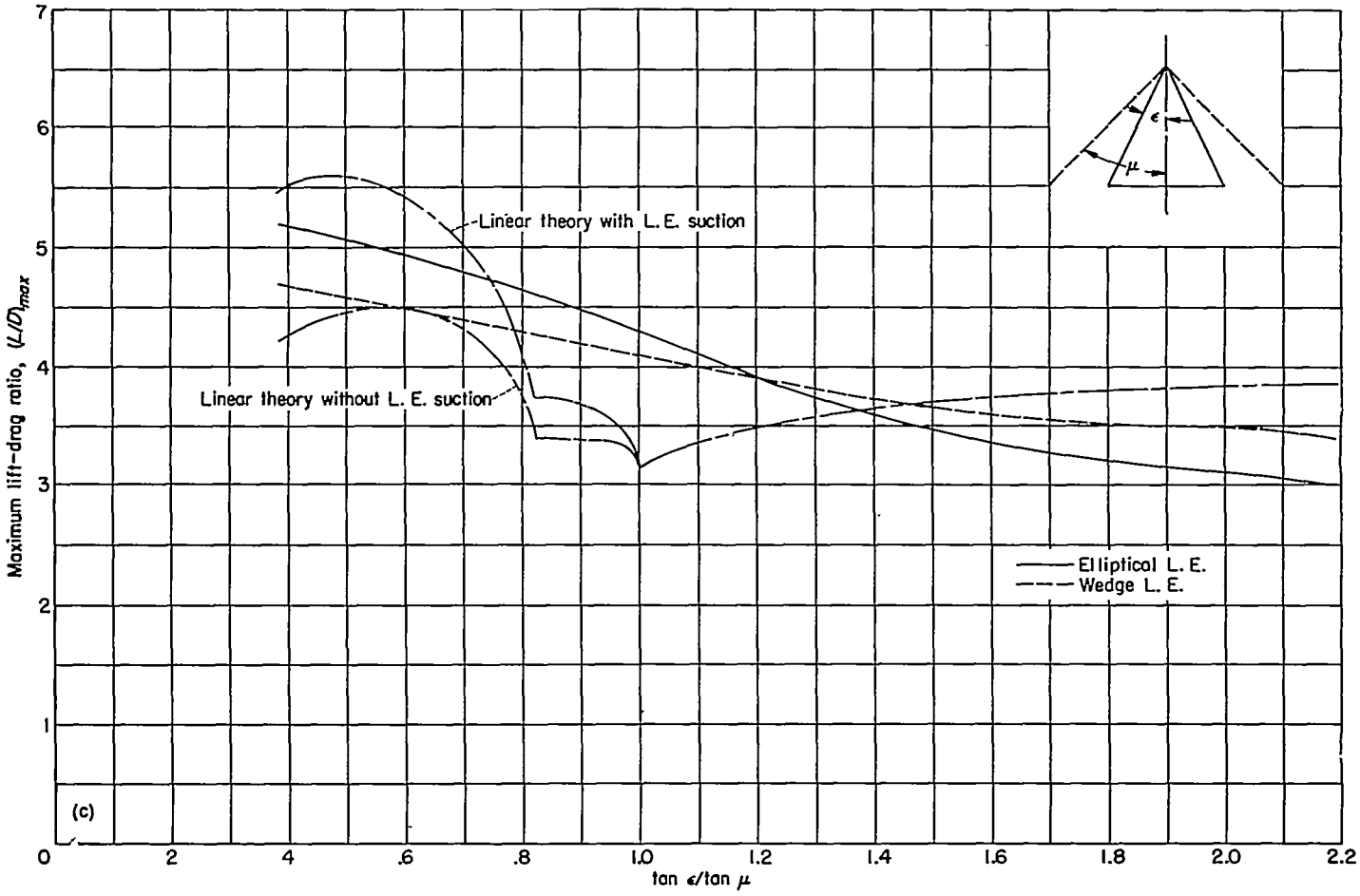

(c) $M=2.40$.
FIGURE 13.—Concluded.

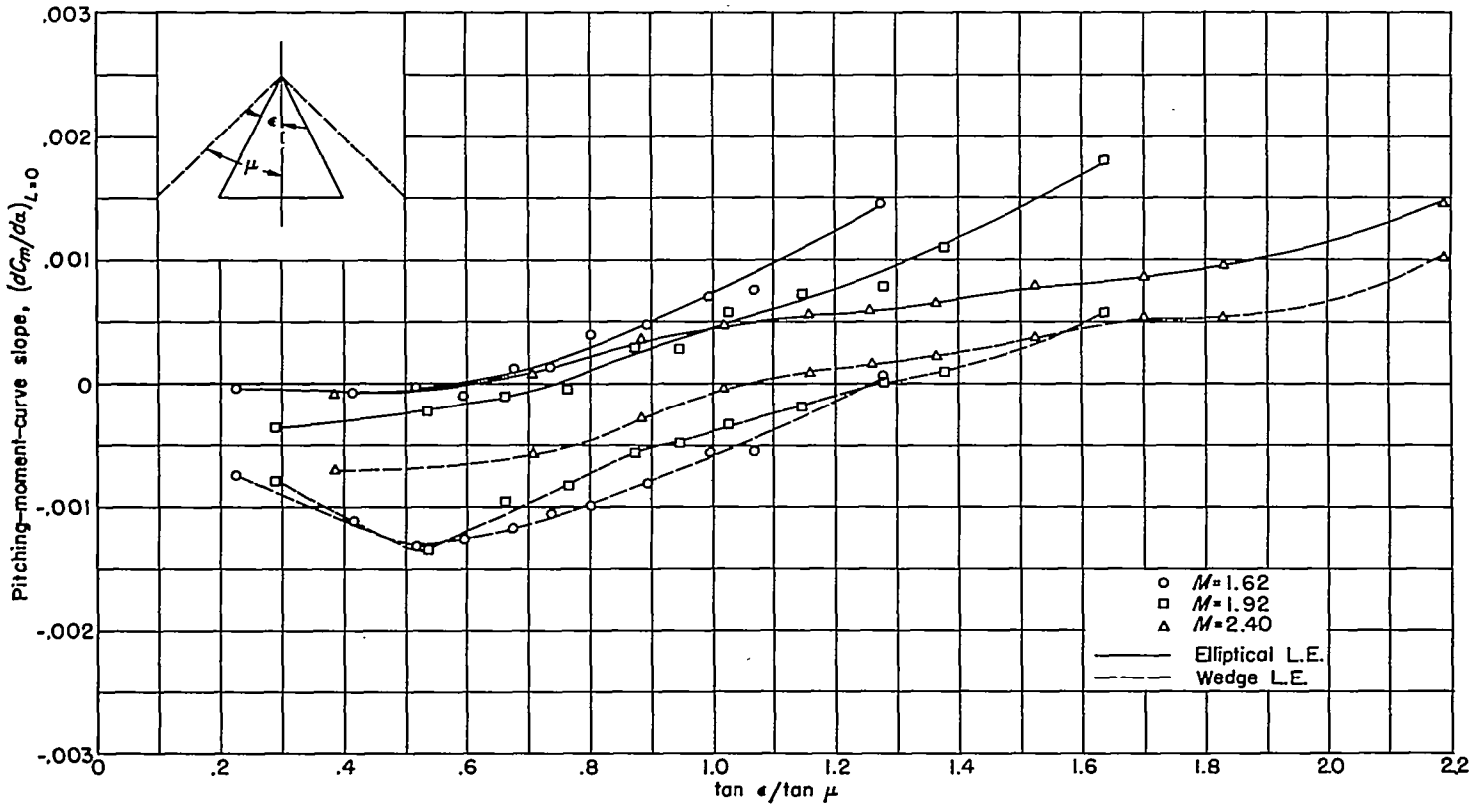

FIGURE 14.—Pitching-moment-curve slopes for 8-percent-thick triangular-wing series.

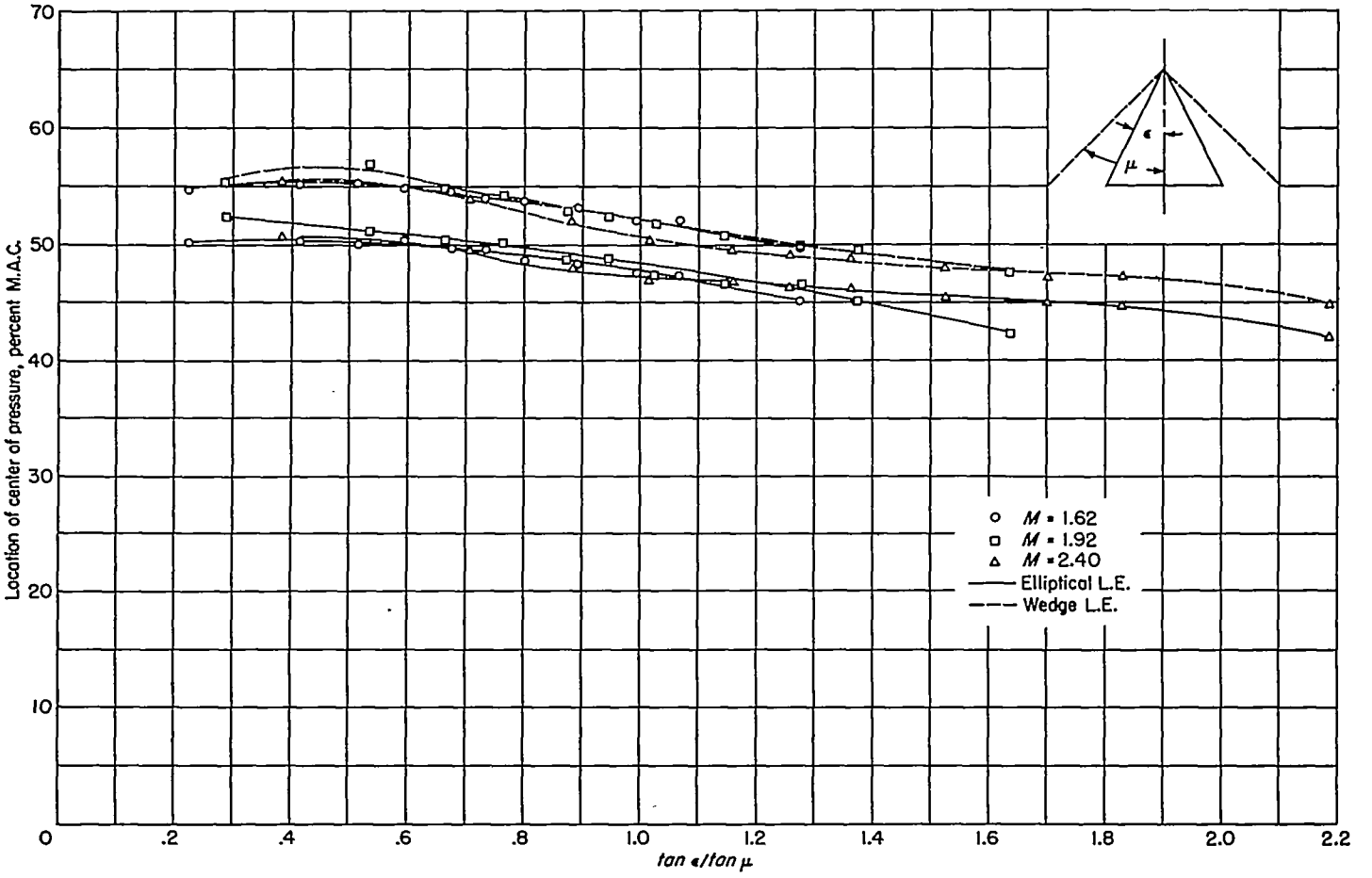

FIGURE 15.—Center-of-pressure location for 8-percent-thick triangular-wing series.

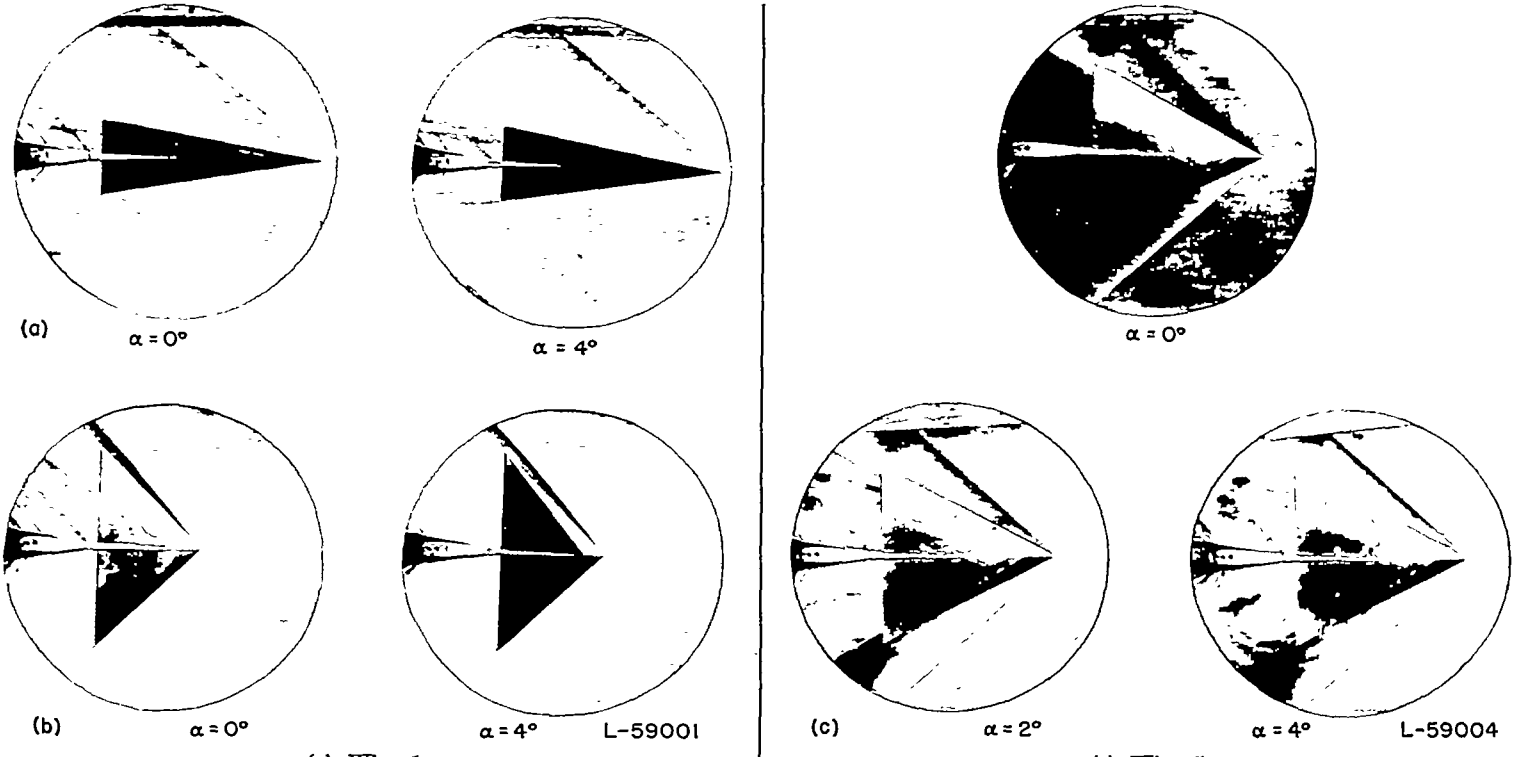

(a) Wing 1.
(b) Wing 11.

(c) Wing 5.

FIGURE 16.—Plan-form schlieren photographs of wedge-leading-edge wings at $M=1.62$.

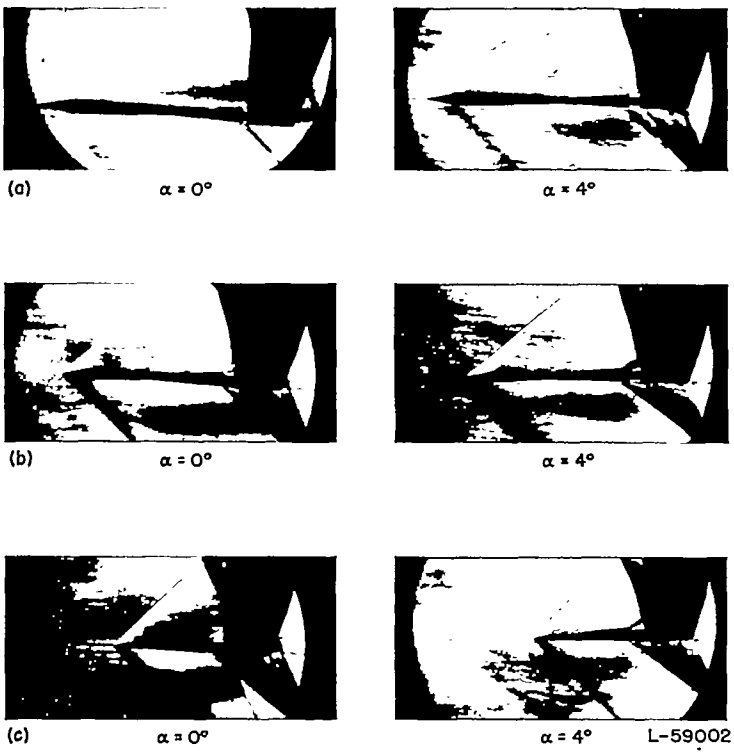

(a) Wing 1.
(b) Wing 5.
(c) Wing 11.

FIGURE 17.—Profile schlieren photographs of wedge-leading-edge wings at $M=1.62$.

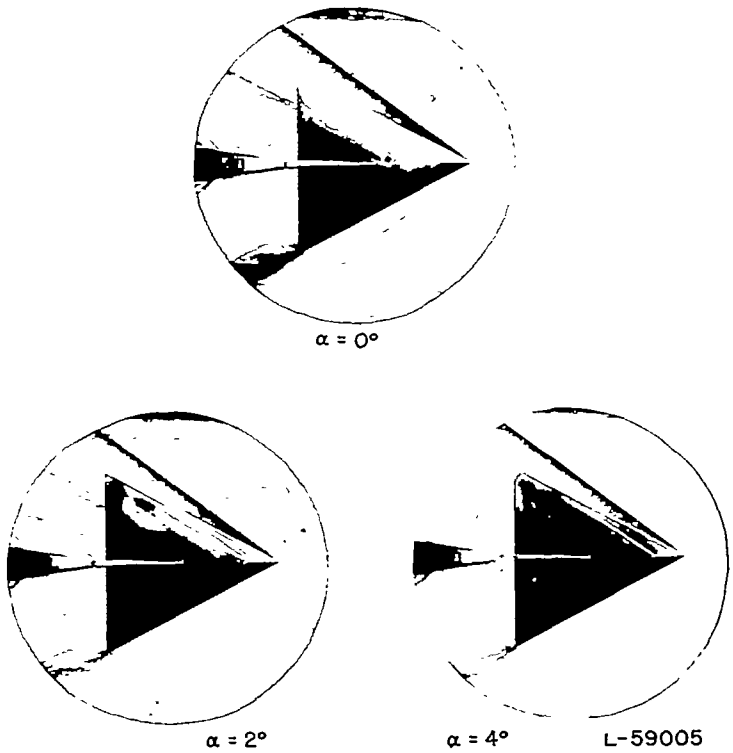

FIGURE 18.—Plan-form schlieren photographs of wedge-leading-edge wing 5 at $M=1.92$.

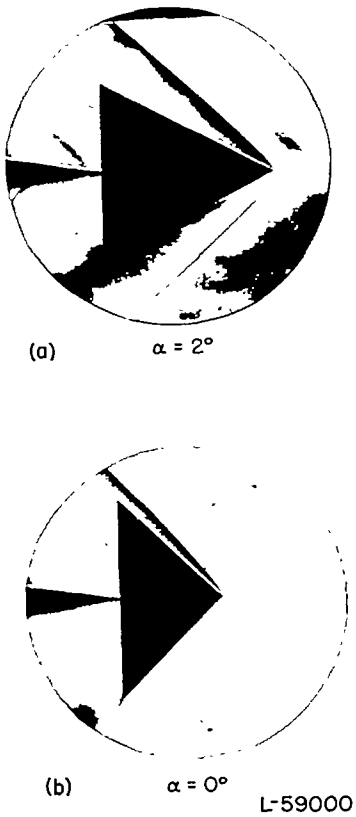

(a) Wing 5.
(b) Wing 11.

FIGURE 19.—Plan-form schlierens of elliptical-leading-edge-wings at $M=1.62$.

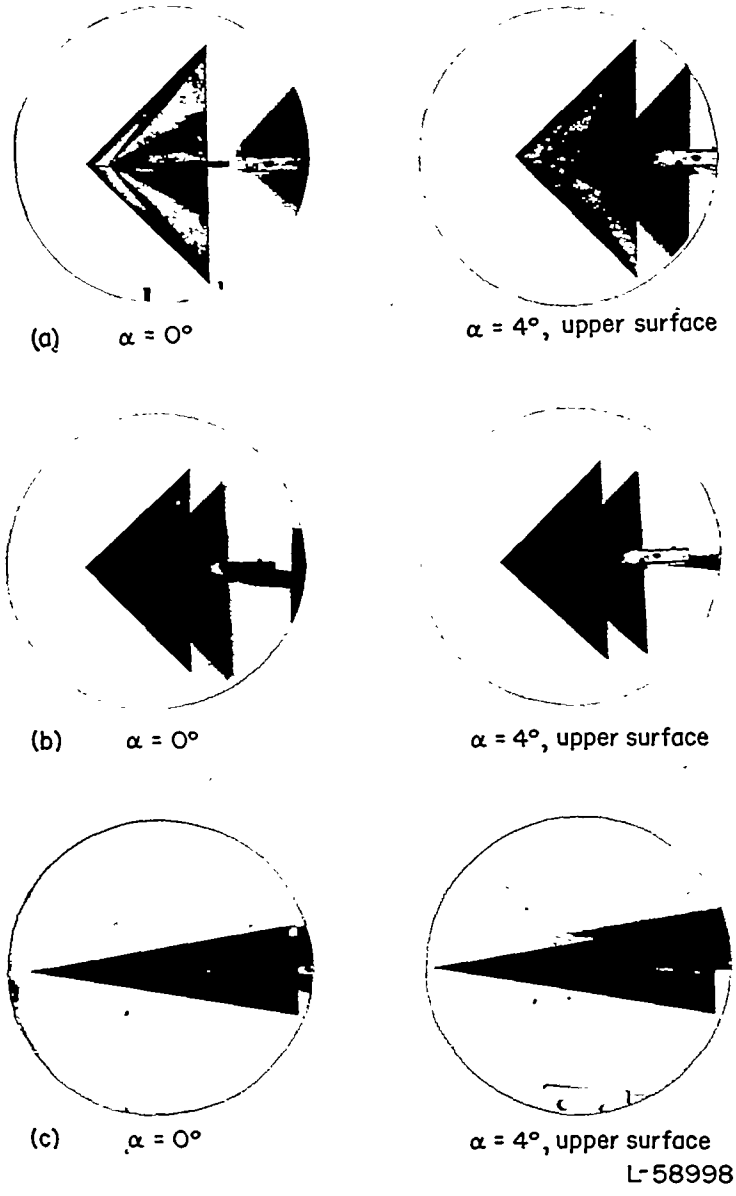

(a) Wedge-leading-edge wing 11.
(b) Elliptical-leading-edge wing 11.
(c) Wedge-leading-edge wing 1.

FIGURE 20.—Liquid-film patterns at $M=1.62$.

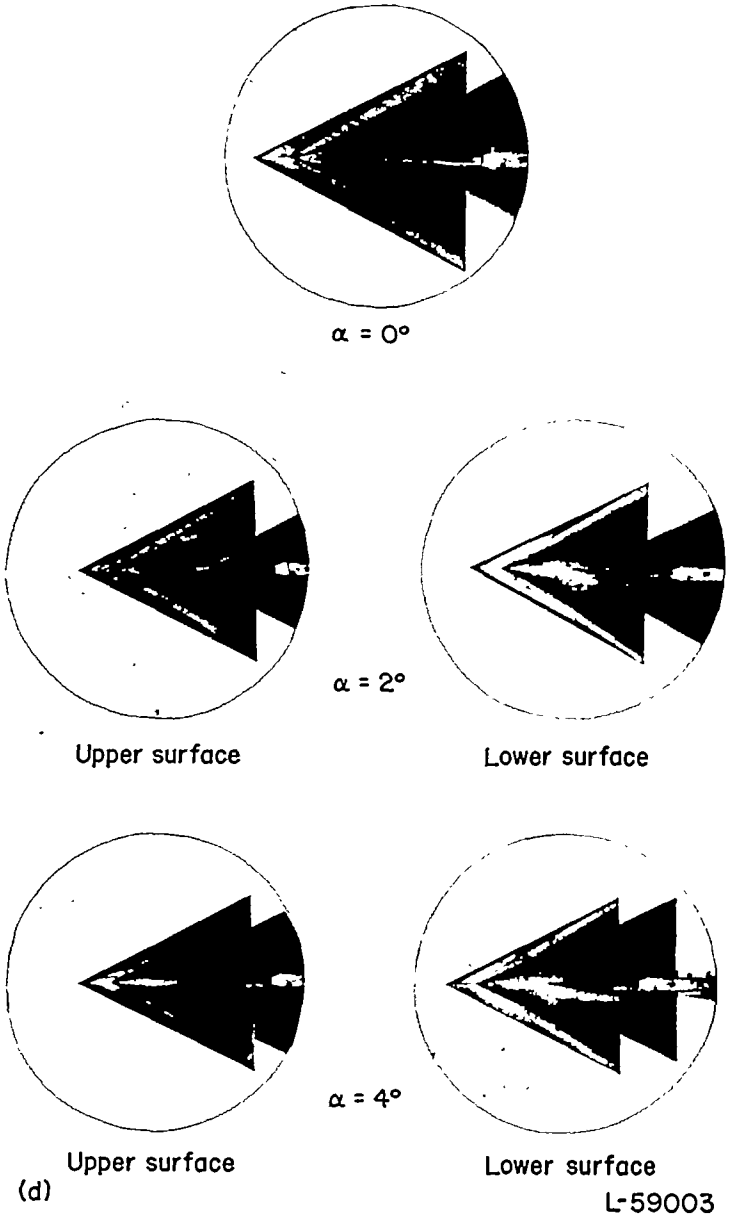

(d) Wedge-leading-edge wing 5.

FIGURE 20.—Concluded.

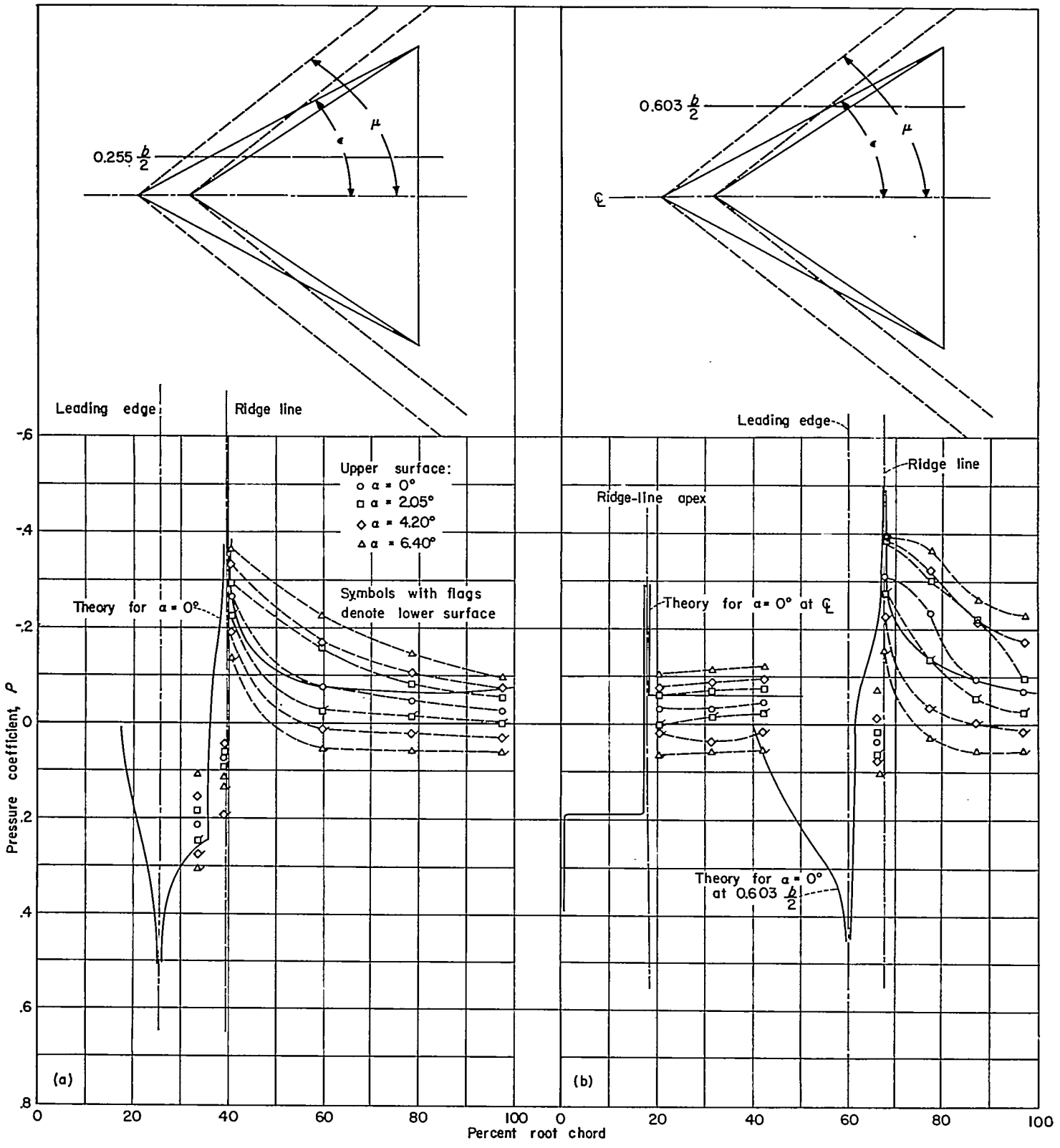

(a) 25.5 percent semispan. (b) 60.3 percent semispan and wing center line.

FIGURE 21.—Pressure distribution at varying angle of attack on wedge-leading-edge wing 5 at $M=1.62$. $\frac{\tan \epsilon}{\tan \mu}<1$.

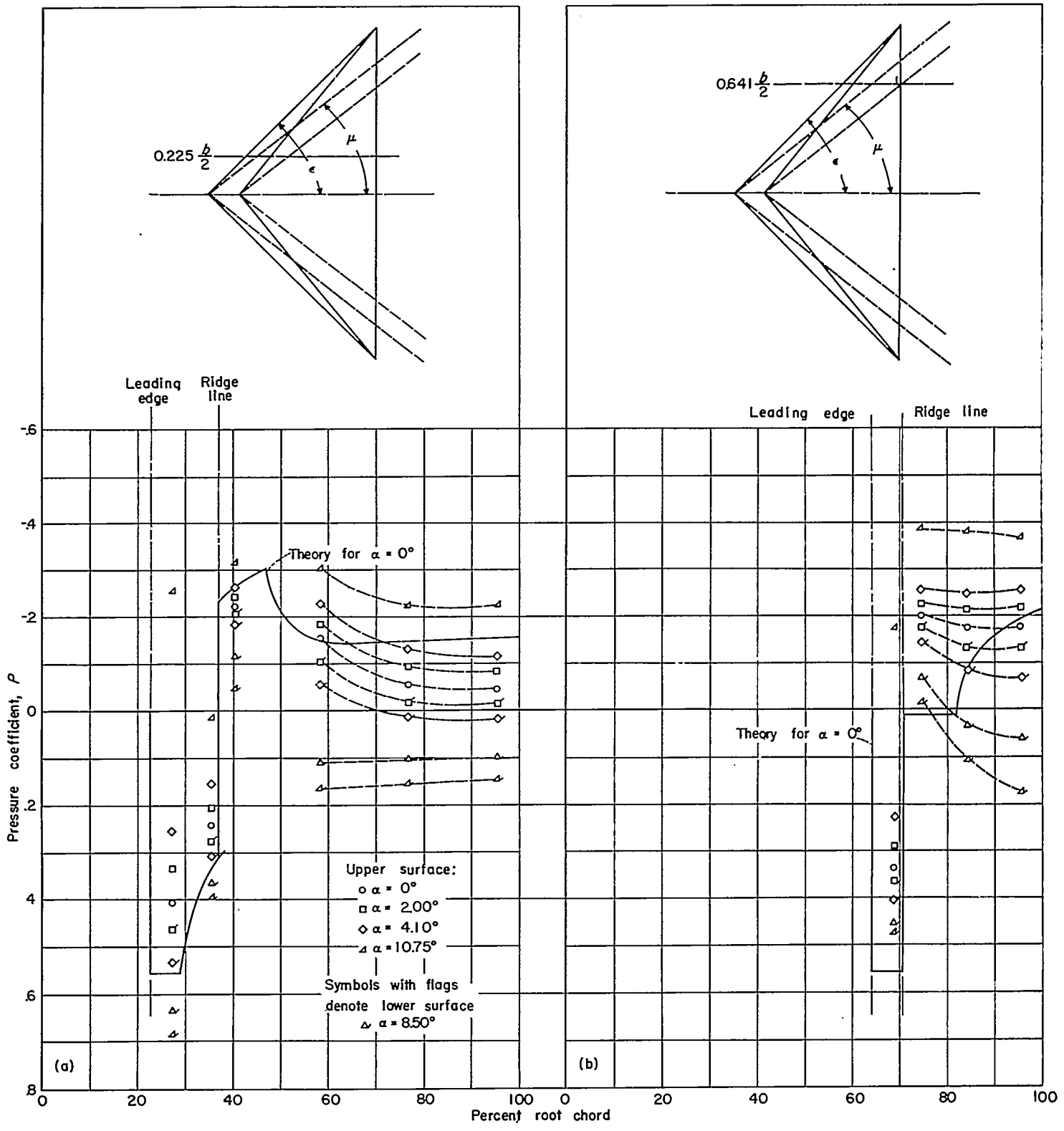

(a) 22.5 percent semispan. (b) 64.1 percent semispan.

FIGURE 22.—Pressure distribution at varying angle of attack on wedge-leading-edge wing 11 at $M=1.62$. $\frac{\tan \epsilon}{\tan \mu}>1$.

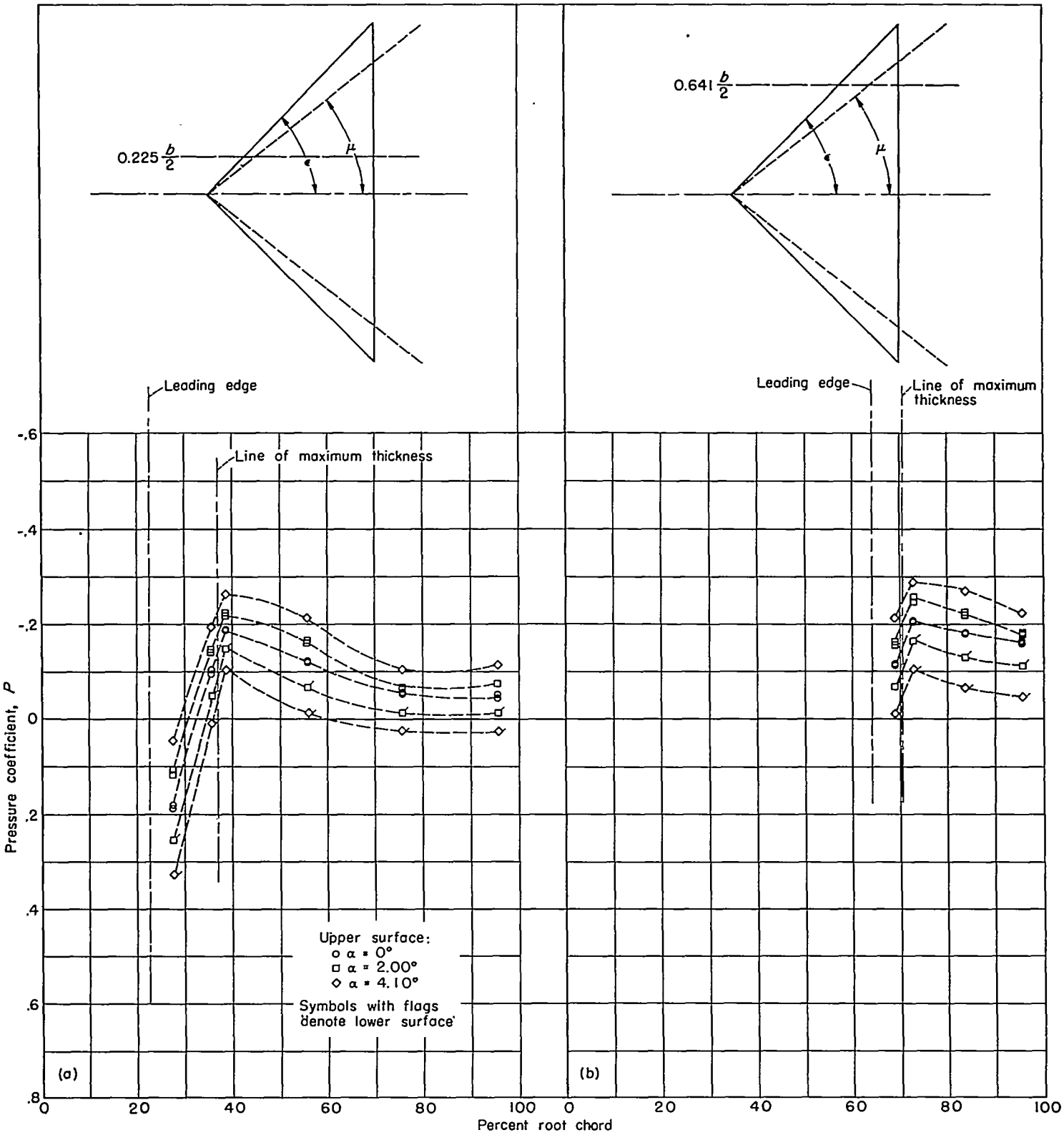

(a) 22.5 percent semispan. (b) 64.1 percent semispan.

FIGURE 23.—Pressure distribution at varying angle of attack on elliptical-leading-edge wing 11 at $M=1.62$. $\frac{\tan \epsilon}{\tan \mu}>1$.

APPENDIX A

CALCULATION OF PRESSURE DRAG

The equations for computation of the pressure drag of triangular wings are as follows:

When Mach line is behind both leading edge and ridge line,

$$C_D=\frac{2\tau^2}{\beta\pi(1-r^2)}\left\{\frac{1}{\sqrt{1-n^2}}\cos^{-1}n+\frac{1}{r\sqrt{1-r^2n^2}}\left[\frac{\pi}{2}+\sin^{-1}(rn)\right]\right\} \tag{A1}$$

When Mach line is ahead of leading edge but behind ridge line,

$$C_D=\frac{2\tau^2}{\beta\pi}\left[\frac{G_2(n,r)}{r(1-r)^2}+\frac{1}{r(1-r)}\left(\frac{\pi}{2}-\frac{\log n}{\sqrt{n^2-1}}-\sin^{-1}\frac{1}{n}\right)\right] \tag{A2}$$

where

$$G_2(n,r)=\frac{1-r}{1+r}\left[\frac{\log n}{\sqrt{n^2-1}}+\frac{r\cosh^{-1}n}{\sqrt{n^2-1}}+\frac{2}{\sqrt{1-r^2n^2}}\tan^{-1}\left(\frac{\sqrt{1-r^2n^2}}{n+\sqrt{n^2-1}-rn}\right)\right] \tag{A3}$$

When Mach line is ahead of both leading edge and ridge line,

$$C_D=\frac{2\tau^2}{\beta\pi}\left[\frac{G_2'}{r(1-r)^2}-\frac{F'}{(1-r)^2}+\frac{1}{r(1-r)}\left(\frac{\log nr}{\sqrt{r^2n^2-1}}-\frac{\log n}{\sqrt{n^2-1}}+\sin^{-1}\frac{1}{rn}-\sin^{-1}\frac{1}{n}\right)\right] \tag{A4}$$

where

$$G_2'=\frac{1-r}{1+r}\left\{\frac{\log n}{\sqrt{n^2-1}}+\frac{r\cosh^{-1}n}{\sqrt{n^2-1}}+\frac{1}{\sqrt{r^2n^2-1}}\log\left[1+\frac{2\sqrt{r^2n^2-1}}{n(1-r)+\sqrt{n^2-1}-\sqrt{r^2n^2-1}}\right]\right\} \tag{A5}$$

and

$$F'=\frac{1-r}{1+r}\left\{\frac{\log rn}{\sqrt{r^2n^2-1}}+\frac{1}{\sqrt{n^2-1}}\log\left[\frac{rn^2-1+\sqrt{(r^2n^2-1)(n^2-1)}}{n(1-r)}\right]\right\} \tag{A6}$$

$\beta=\sqrt{M_0^2-1}$

τ thickness ratio at root chord

r distance of ridge-line apex from trailing edge, expressed as percent of root chord

$n=\frac{\tan\mu}{\tan\epsilon}$

APPENDIX B

CALCULATION OF PRESSURE DISTRIBUTIONS

The method and equations for computation of the pressure distributions over triangular wings are as follows:

The wing is broken down into two infinite wedge wings, and by superposition of the conical-flow solutions, the pressure distribution is obtained for each wedge. Combining the solutions yields the pressure distribution for the composite wing. The flow solutions for the given conditions are as follows:

When leading edge is within Mach cone,

$$P=\frac{4\delta w_1}{\pi\beta\sqrt{1-w_1^2}}\tanh^{-1}\sqrt{\frac{1-w_1^2}{1-\left(\frac{\beta y}{x}\right)^2}} \qquad (0\leqq w\leqq w_1)$$

$$P=\frac{4\delta w_1}{\pi\beta\sqrt{1-w_1^2}}\tanh^{-1}\sqrt{\frac{1-\left(\frac{\beta y}{x}\right)^2}{1-w_1^2}} \qquad (w_1\leqq w\leqq 1)$$

When leading edge is outside Mach cone,

$$P=\frac{4\delta w_1}{\pi\beta\sqrt{w_1^2-1}}\tan^{-1}\sqrt{\frac{w_1^2-1}{1-\left(\frac{\beta y}{x}\right)^2}} \qquad (0\leqq w\leqq 1)$$

$$P=\frac{2\delta w_1}{\beta\sqrt{w_1^2-1}} \qquad (1\leqq w\leqq w_1)$$

where $w_1=\frac{\tan\epsilon}{\tan\mu}$; w, in like manner, represents the position of a radial line through the apex of the wedge being analyzed; δ, the deflection or wedge half-angle with the proper sign attached; y, the span ordinate of the given chordwise station; and x, the chordwise ordinate at the same station with reference to the apex of the particular wedge.

REFERENCES

1. Jones, Robert T.: Wing Plan Forms for High-Speed Flight. NACA Rep. 863, 1947. (Supersedes NACA TN 1033.)
2. Busemann, A.: Aerodynamic Lift at Supersonic Speeds. Rep. No. 2844, British A.R.C., Feb. 3, 1937. (From Luftfahrtforschung, Bd. 12, Nr. 6, Oct. 3, 1935, pp. 210–220.)
3. Jones, Robert T.: Properties of Low-Aspect-Ratio Pointed Wings at Speeds Below and Above the Speed of Sound. NACA Rep. 835, 1946. (Supersedes NACA TN 1032.)
4. Jones, Robert T.: Estimated Lift-Drag Ratios at Supersonic Speed. NACA TN 1350, 1947.
5. Brown, Clinton E.: Theoretical Lift and Drag of Thin Triangular Wings at Supersonic Speeds. NACA Rep. 839, 1946. (Supersedes NACA TN 1183.)
6. Stewart, H. J.: The Lift of a Delta Wing at Supersonic Speeds. Quarterly Appl. Math., vol. IV, no. 3, Oct. 1946, pp. 246–254.
7. Puckett, Allen E.: Supersonic Wave Drag of Thin Airfoils. Jour. Aero. Sci., vol. 13, no. 9, Sept. 1946, pp. 475–484.
8. Puckett, A. E., and Stewart, H. J.: Aerodynamic Performance of Delta Wings at Supersonic Speeds. Jour. Aero. Sci., vol. 14, no. 10, Oct. 1947, pp. 567–578.
9. Von Kármán, Theodore: Supersonic Aerodynamics—Principles and Applications. Jour. Aero. Sci., vol. 14, no. 7, July 1947, pp. 373–409.
10. Ellis, Macon C., Jr., and Hasel, Lowell E.: Preliminary Investigation at Supersonic Speeds of Triangular and Sweptback Wings. NACA TN 1955, 1949. (Supersedes NACA RM L6L17.)
11. Vincenti, Walter G., Nielsen, Jack N., and Matteson, Frederick H.: Investigation of Wing Characteristics at a Mach Number of 1.53. I—Triangular Wings of Aspect Ratio 2. NACA RM A7I10, 1947.
12. Gray, W. E.: A Simple Visual Method of Recording Boundary Layer Transposition (Liquid Film). TN No. Aero 1816, British R.A.E., Aug. 1946.
13. Hayes, W. D., Browne, S. H., and Lew, R. J.: Linearized Theory of Conical Supersonic Flow With Application to Triangular Wings. Rep. No. NA–46–818, North American Aviation, Inc., Sept. 30, 1946. (Revised June 26, 1947.)

TABLE I.—DIMENSIONS OF TRIANGULAR-WING MODELS

(a) 8-Percent-Thick Triangular-Wing Model

Wing	b, ft	c_r, ft	ϵ, deg	x, percent	y, percent	M.A.C., ft	Area, sq ft	Aspect ratio, A
1	0.175	0.499	9.93	18	8	0.333	0.0437	0.700
2	.323	.499	17.91	18	8	.333	.0805	1.292
3	.398	.493	21.96	18	8	.329	.0980	1.612
4	.402	.431	25.01	18	8	.287	.0867	1.869
5	.409	.386	27.92	18	8	.257	.0790	2.114
6	.413	.360	29.84	18	8	.240	.0743	2.301
*7	.423	.336	32.15	18	8	.224	.0711	2.518
8	.433	.307	35.21	18	8	.205	.0665	2.812
9	.436	.279	38.01	18	8	.186	.0607	3.130
10	.444	.265	39.92	18	8	.177	.0588	3.350
11	.463	.230	45.15	18	8	.153	.0532	4.023

* Remeasurement shows $y\approx 7.8$ percent.

(b) Flat-Plate Triangular-Wing Model

Wing	Sharp leading edge			Round leading edge (radius≈0.008 in.)		
	ϵ, deg	M.A.C., ft	t/c, percent	ϵ, deg	M.A.C., ft	t/c, percent
1	25.13	0.289	1.3	25.00	0.283	1.3
2	30.03	.233	1.6	30.47	.226	1.7
3	32.00	.219	1.7	31.93	.206	1.8
4	35.17	.204	1.8	35.17	.200	1.9

TABLE II.—SUMMARY OF RESULTS FOR 8-PERCENT-THICK TRIANGULAR WINGS

Wing	Wedge leading edge				Elliptical leading edge			
	$\left(\frac{dC_L}{d\alpha}\right)_{L=0}$	$\left(\frac{dC_m}{d\alpha}\right)_{L=0}$	$\left(\frac{L}{D}\right)_{max}$	$C_{D_{min}}$	$\left(\frac{dC_L}{d\alpha}\right)_{L=0}$	$\left(\frac{dC_m}{d\alpha}\right)_{L=0}$	$\left(\frac{L}{D}\right)_{max}$	$C_{D_{min}}$
$M=1.62$								
1	0.0232	−0.00075	5.0	0.0133	0.0221	−0.00004	5.3	0.0121
2	.0337	−.00113	5.3	.0184	.0347	−.00008	5.8	.0159
3	.0366	−.00133	5.1	.0220	.0393	−.00003	5.6	.0184
4	.0382	−.00127	5.0	.0255	.0407	−.00011	5.5	.0207
5	.0388	−.00118	4.8	.0288	.0423	.00013	5.3	.0233
6	.0388	−.00106	4.7	.0309	.0422	.00013	5.0	.0261
*7	.0384	−.00100	4.6	.0313	.0426	.00039	5.0	.0259
8	.0385	−.00081	4.4	.0352	.0421	.00047	4.6	.0300
9	.0387	−.00056	4.2	.0372	.0429	.00070	4.4	.0324
10	.0396	−.00054	4.2	.0388	.0431	.00075	4.4	.0337
11	.0416	.00007	4.1	.0433	.0449	.00146	4.1	.0399
$M=1.92$								
1	0.0216	−0.00078	5.2	0.0125	0.0215	−0.00036	5.3	0.0119
2	.0287	−.00013	4.9	.0186	.0298	−.00023	5.3	.0154
3	.0294	−.00095	4.7	.0219	.0317	−.00010	5.0	.0185
4	.0295	−.00083	4.4	.0256	.0328	−.00005	4.9	.0205
5	.0300	−.00056	4.3	.0277	.0335	.00029	4.6	.0228
6	.0296	−.00048	4.1	.0291	.0334	.00027	4.5	.0258
*7	.0299	−.00034	4.1	.0292	.0332	.00057	4.3	.0253
8	.0308	−.00018	4.0	.0333	.0330	.00073	4.0	.0293
9	.0316	.00000	3.8	.0342	.0337	.00077	3.9	.0323
10	.0324	.00010	3.9	.0355	.0340	.00110	3.8	.0331
11	.0346	.00057	3.7	.0396	.0353	.00180	3.5	.0397
$M=2.40$								
1	0.0189	−0.00070	4.7	0.0127	0.0192	−0.00009	5.2	0.0109
2	.0223	−.00058	4.4	.0179	.0236	.00008	4.8	.0148
3	.0225	−.00027	4.2	.0211	.0244	.00035	4.5	.0179
4	.0229	−.00003	4.1	.0238	.0246	.00047	4.3	.0196
5	.0237	.00009	4.0	.0260	.0247	.00055	4.0	.0224
6	.0243	.00016	3.8	.0272	.0249	.00059	3.8	.0248
*7	.0245	.00022	3.8	.0272	.0254	.00064	3.7	.0252
8	.0256	.00037	3.7	.0301	.0254	.00077	3.3	.0291
9	.0266	.00053	3.7	.0293	.0258	.00086	3.2	.0319
10	.0281	.00053	3.5	.0325	.0262	.00095	3.2	.0333
11	.0317	.00100	3.4	.0350	.0270	.00145	3.0	.0397

* See table I (a).

TABLE III.—SUMMARY OF RESULTS FOR THIN-PLATE TRIANGULAR WINGS AT $M=1.92$

Wing	Sharp leading edge					Round leading edge				
	$\left(\frac{dC_L}{d\alpha}\right)_{L=0}$	$\left(\frac{dC_m}{d\alpha}\right)_{L=0}$	$\left(\frac{L}{D}\right)_{max}$	$C_{D_{min}}$	R	$\left(\frac{dC_L}{d\alpha}\right)_{L=0}$	$\left(\frac{dC_m}{d\alpha}\right)_{L=0}$	$\left(\frac{L}{D}\right)_{max}$	$C_{D_{min}}$	R
1	0.0388	0.0022	8.00	0.0070	1.08×10^5	0.0379	0.0011	8.10	0.0071	1.00×10^5
2	.0387	.0014	7.80	.0079	.87	.0380	.0013	7.65	.0090	.85
3	.0386	.0017	7.80	.0083	.82	.0386	.0018	7.35	.0121	.77
4	.0395	.0019	7.85	.0092	.76	.0395	.0015	7.15	.0121	.75